ms-1

N65-30453

(ACCESSION NUMBER)   240

(PAGES)

(NASA CR OR TMX OR AD NUMBER)   CR 64186

(THRU)

(CODE)

(CATEGORY)   12

GPO PRICE $ _____

CFSTI PRICE(S) $ _____

Hard copy (HC) _____

Microfiche (MF) _____

ff 653 July 65

Fluid Power Controls Laboratory

School of Mechanical Engineering

OKLAHOMA STATE UNIVERSITY

Stillwater, Oklahoma

Annual Report No. 1

STUDY OF FLUID TRANSIENTS IN
CLOSED CONDUITS

Contract: NAS 8 11302

Annual Report No.: 1

Contractor: Oklahoma State University, Stillwater, Oklahoma

Segment Generating Report: School of Mechanical Engineering
Fluid Power and Controls Laboratory

STUDY OF FLUID TRANSIENTS IN CLOSED CONDUITS

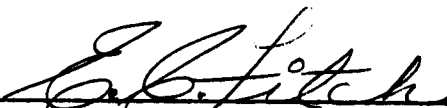
Contract: NAS 8 11302

Control Number: DCN-1-4-50-01153-01(IF)
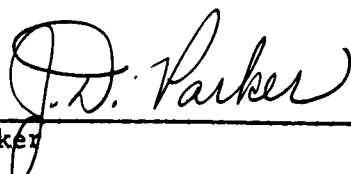CPB 02-1209-64

Date: 15 July, 1965

Prepared for: George C. Marshall Space Flight Center, Huntsville, Alabama

Prepared by: E. C. Fitch, Project Co-director
J. D. Parker, Project Co-director
C. R. Gerlach, Project Leader
H. C. Hewitt, Research Assistant
G. Maples, Research Assistant
E. Mitwally, Research Assistant
R. Stuntz, Research Assistant

Approved:

E. C. Fitch

J. D. Parker

ii

TABLE OF CONTENTS

LIST OF FIGURES

LIST OF TABLES

LIST OF SYMBOLS

a	Thermal diffusivity
$\dfrac{a_v}{a_1}$	Cavitation form parameter based on areas
A	$\begin{cases} \text{Constant at integration} \\ \text{Conduit cross-sectional area} \end{cases}$
B	Constant of integration
c	Speed of sound in fluid
c_o	Isentropic speed of sound in fluid
c_v	Specific heat, constant volume
C	Chord length
C_1	369 nT ft-#f
C_e	Electrically equivalent capacitance
C_p	Pressure coefficient
C_{P_1}	Specific heat of the liquid
$C_{P_{min_s}}$	Minimum pressure coefficient of a smooth surface
C_q	Conduit capacitance based on flow rate
C_v	Conduit capacitance based on velocity
C_w	Conduit capacitance based on weight flow rate
D	Conduit diameter
$\dfrac{D}{Dt}$	Substantial derivative
D_i	Conduit inside diameter
D_o	Conduit outside diameter

x

D^*	Critical bubble diameter
e_j	Voltage at point j
f	$\begin{cases} \text{Tube wall factor, Equation (2.44)} \\ \text{Parameter defined by Equation (6.53)} \end{cases}$
F_L	Froude's number
g	Acceleration due to gravity
h	$\begin{cases} \text{Height of roughness element} \\ \text{Tube wall thickness} \end{cases}$
$h(z,s)$	A function of integration
H	Boundary layer shape parameter
i	Imaginary unit, $\sqrt{-1}$
i_j	Electrical current at point j
I_q	Fluid inertance based on flow rate
I_v	Fluid inertance based on velocity
I_w	Fluid inertance based on weight flow rate
$J_o(x)$	Bessel function of order zero and argument x
$J_1(x)$	Bessel function of order one and argument x
k	$\begin{cases} \text{Coefficient of heat conduction} \\ \text{Parameter defined by Equation (6.25)} \end{cases}$
K	Cavitation number
K_o	Cavitation number evaluated at reference plane "o"
$\overline{K_o}$	Modified cavitation number, Equation (4.9)
K_d	Desinent cavitation number evaluated at plane of desinent cavitation
K_i	Incipient cavitation number evaluated at plane of incipient cavitation
K_{do}	Desinent cavitation number evaluated at reference plane "o"
K_{io}	Incipient cavitation number evaluated at reference plane "o"

K_{ro}	Incipient cavitation number of roughness element evaluated at reference plane "o"
L	Conduit length
L_1	Length or linear dimension
L_e	Electrically equivalent inductance
L_v	Heat of vaporization
n	$\begin{cases} \text{Number of moles of gas} \\ \text{Index number} \end{cases}$
N	Number of nuclei per unit volume of the fluid
$p = P(t)$	Fluid stream pressure, function of time
P_b	Back pressure
P_d	Stream pressure at plane of desinent cavitation
P_e	Exit pressure
P_g	Partial pressure of gas
P_i	Stream pressure at plane of incipient cavitation
P_v	Vapor pressure
P_{do}	Stream pressure for desinent cavitation evaluated at reference "o"
P_{io}	Stream pressure for incipient cavitation evaluated at reference "o"
$p*$	$(p-p_v)$ min.
P_{∞}	Pressure at a distance from a bubble
$P(s)$	Transformed pressure, function of s
$P_j(s)$	Transformed pressure at point j
P_e	Pecle't number
q	Fluid flow rate
$\dot{q}$	Heat generated per second per unit volume
q_b	Heat flux density across vapor - liquid interface

$\bar{q}$	Vector heat flow rate
$Q(x)$	Heat liberated at bubble radius
r	Radial coordinate position
$\mathbf{r}$	Unit vector in radial direction
r_o	Conduit inner radius
R	Bubble radius
$R(v)$	Conduit resistance
R_1	Resistance coefficient, Equation (2.16)
$\bar{R}$	Radius of centerline of elbow
R_e	$\begin{cases} \text{Reynolds number} \\ \text{Electrically equivalent resistance} \end{cases}$
$R*$	Critical bubble radius
s	Laplace variable
t	Time
$\bar{t}_{max.}$	Maximum thickness of hydrofoil
T	Temperature
T_o	Initial temperature
T_s	Saturation temperature at a given pressure
T_{rs}	Temperature of saturated vapor
$T_{\infty s}$	Saturation temperature away from the bubble
T_{ws}	Saturation temperature at the wall
T_∞	Temperature away from any bubbles
T_w	Wall temperature
ΔT	$T_\infty - T_s$
v	Axial velocity
v_c	Conduit wall velocity
v_ℓ	Specific volume of liquid

v_o	Steady flow velocity
v_r	Radial velocity
v_v	Specific volume of vapor
v_z	Axial velocity
$\bar{v}$	Vector velocity (see Figure 2.1)
$V(s)$	Transformed velocity
V	Stream velocity
$V_c(s)$	Transformed conduit wall velocity
V_o	Stream velocity at reference "o"
V_t	Stream velocity at throat
W	Weber number
x	Distance measured along hydrofoil centerline
z	Axial coordinate
Z_c	Characteristic impedance (see Equation 2.26)
Z_c'	Characteristic impedance (see Equation 6.37)
α	Air content
α/α_s	Relative air content
β	Parameter
$\bar{\beta}$	1.03 psi/ppm
β^*	$R/2\sqrt{at}$
Γ	Propagation constant
δ	Boundary layer thickness
δ^*	Displacement thickness
ε	Parameter defined by Equation (2.22)
θ	Momentum thickness
θ	Coordinate angle
$\boldsymbol{\theta}$	Unit vector in θ direction
χ	Bulk modulus of elasticity of fluid
μ	Absolute viscosity

ν	Kinematic viscosity
ξ	Parameter defined by Equation (2.20)
ρ	Mass density
ρ_L	Liquid mass density
ρ_0	Average mass density
ρ_v	Vapor mass density
σ	Surface tension
σ_0	Prandtl number
φ	Scalor field
φ_f	Scalor field related to body force, see Equation (6.45)
φ_1	Scalor field
$\hat{\varphi}_1$	Transformed φ_1
Φ	Dissipation function
$\bar{\psi}$	Vector field
$\bar{\psi}_1$	Vector field
ψ_1	Related to $\bar{\psi}_1$ by $\bar{\psi}_1 = \Theta \, \psi_1$
$\bar{\psi}_f$	Vector field related with body force, see Equation (6.45)
$\hat{\psi}_1$	Transformed ψ_1
ω	Angular frequency
∇	Vector operator del

CHAPTER I

Introduction

Since the turn of this century, transient flow behavior in closed conduits has been recognized as a necessary part of making accurate flow predictions in fluid systems. In response to application requirements in the past, the technological development of this subject area has been generally concerned with theory and techniques needed to predict flow behavior in product pipelines and potential lines associated with hydro-electric plants.

In the past few years, serious transient flow problems have been encountered in sophisticated fluid systems on aircraft and missiles that make pipeline flow predictions seem elementary. It is apparent from an appraisal of the current "state of the art" in this field and the requirements imposed by modern systems, that new theories and techniques must be developed. It has been discovered that methods used in the past severely limit the accuracy of predicting peak pressures and attenuation characteristics in current systems. Furthermore, the acceleration forces externally imposed on the entire fluid system and the obvious need to marginally design the system due to space and weight considerations necessitate a more complex theory.

The name "conduit dynamics " has been given to the area of study involving a closed conduit system, its fluid, and all associated forces. Only "token" interest has been generated in this relatively new field

to date as evidenced by the published literature. However, recent articles indicate that interest is growing among systems engineering people who possess an appreciation for the analysis of high performance systems.

This project has been concerned with the development of applicable theory and techniques for predicting transient flow behavior in single phase fluid systems. In addition, the properties and flow characteristics of cryogenic fluids which influence analytical simulation studies are being investigated. The research associated with this project has been relegated to two research teams. The first team is charged with the development of appropriate theory and techniques for establishing a conduit model. The second team has undertaken the investigation of cryogenic properties and flow characteristics. This report purports the project activities and efforts for the first year of the study.

Scope of Work

The original scope of work for this study may be broken down into four phases as follows:

A. Complete a comprehensive review of past literature.

B. Develop a mathematical model which describes the transients in fluid conduits and shows the effects of fluid inertance, fluid capacitance, and fluid resistance. Develop an analog model based on the mathematical model which will simulate the fluid transients in a cryogenic closed conduit.

C. Conduct an experimental study to verify the conduit simulation models. Make necessary modifications in the models to achieve appropriate agreement with laboratory data.

D. Study the effects of components, derive their associated transfer functions, and add this input to paragraph C above to obtain the effects of added components.

Summary of Accomplishments

The work which has been done to date toward the successful completion of the work objective as indicated in the scope may be summarized as follows:

A. An exhaustive survey of previous investigations has been completed for both the single-phase and two-phase areas of the study.

B. A detailed transfer function model for a viscous, two-dimensional, single-phase conduit has been derived and appears to be capable of extension to cover preliminary two-phase and cavitation studies. This model has been experimentally verified for the single-phase case.

C. A conduit model showing the effects of body forces and system vibration was derived.

D. An investigation of the nonlinear effects associated with conduit dynamics has been made using a linearized second-order equation of motion.

E. The design of a hydrodynamic tunnel capable of handling liquid nitrogen has been completed and construction is underway.

F. A theoretical investigation of the onset of cavitation has been started; however, the necessary boundary conditions must be determined experimentally.

G. A bubble observation chamber, suitable for studies with

    liquid nitrogen, has been designed and constructed.

H. An experimental investigation of the effect of an orifice

    in a fluid conduit has been carried out.

The following chapters of this report give a detailed account of
this work.

Recommendations for Future Investigations

    Although the work which will be accomplished in this first year
of study represents a significant contribution in the field of conduit
dynamics, we feel that, due to the experience and knowledge gained
during this period, we will be at a stage where we can undertake more
specific and practical problems of interest to NASA. Areas which
it is felt deserve further study and will be rewarding to the space
program include:

A. Study the formation and behavior of bubbles in conduit

    systems subject to vibrations.

B. Extend the concepts of the present conduit models to

    incorporate turbulence, bubbles and cavitation effects.

C. Continue the analytical and experimental investigation

    of the significance of the nonlinear effects in conduits

    and their components.

D. Investigate the effects of transient pressures on the

    cavitation properties of liquids in a static state. A

    comparison should be made with the results obtained from

    the hydrodynamic tunnel for the same liquid flowing through

    the same pressure transients.

CHAPTER II

Review of the Literature for Single-Phase
Conduit Systems

2.1 Definition of the Problem

The problems associated with the design or analysis of fluid

systems are challenging, particularly for systems involving unsteady

flows. A typical system may contain many components such as pumps,

valves, actuators, reservoirs, motors, etc., generally connected

together in some manner by fluid lines. A complete analysis of

such a system must involve not only the components but also the

fluid lines. This is particularly true for unsteady conditions

where the effects of the fluid lines have in some cases caused

otherwise well-designed systems to be inoperable.

In general, the area of study associated with the flow of fluids

through conduits is called "Conduit Dynamics." A rigorous application

of Conduit Dynamics to the study of a fluid line involves a complete

study of the fluid itself plus a study of the effect which the pipe

or conduit has upon the fluid. For example, in making computations

involving the effect of fluid compressibility we may make large

errors if we do not include the compressibility effect due to the

elasticity of the pipe walls. Conduit Dynamics includes fluid studies

which are associated with the two areas known as "water hammer" and

"surge".

The complete description of a fluid line in which the effects of compressibility, fluid inertia, viscosity, and heat transfer are important involves the simultaneous solution of the following equations:

1) Equations of Motion (Navier-Stokes equations)

2) Continuity equation

3) Energy equation

4) Equation of state of fluid

5) Dynamical equation of motion of tube or conduit

Also, application of the boundary and initial conditions is necessary in order that answers may be arrived at for particular cases of interest. An exact description, i.e., an exact solution of the governing equations, is nearly impossible. However, by means of various simplifying assumptions, it is possible to arrive at solutions which yield rather good quantitative descriptions of the system being analyzed. In many cases these simplifying assumptions are questionable. By means of the discussions which follow, an effort will be made to present, in an organized manner, the work which has been accomplished by previous investigators. Indications will be made, where possible, of the application and limitation of the ideas.

2.2 Lumped and Distributed Systems

The physical properties of all real systems are distributed with respect to time and space. The extent or influence of this distributive effect varies greatly, depending on the particular system being studied. For the case of the fluid systems which will concern us, this distributive effect may or may not need be considered. In general, those physical systems which are described by relations involving distributed

6

parameters are called distributed parameter systems. The dynamical

equations for distributed systems are generally partial differential

equations. Those systems which do not involve distributed parameters

are called lumped parameter systems. The dynamical equations for lumped

systems are generally ordinary differential equations. If we take a

distributed parameter system, average the effect of the distributed

parameter(s), and concentrate this average at some point, then we

say that we have "lumped" the system. The validity of approximating

a distributed system by a lumped system or systems depends upon the

operating conditions of the system and also upon the manner in which

the lumping is performed.

The distributed effects of fluid systems which will concern us

are those due to compressibility, inertia, and resistance. In the

literature, those studies which involve compressibility and inertia

are called "water hammer studies," while those involving mainly

inertia effects are called "surge studies."

2.3 Linear Distributed Models - No Conduit Wall Effects

For the purposes of this discussion, consider a fluid conduit

system to be describable in terms of a cylindrical coordinate system

as shown in Figure 2.1. Unless otherwise indicated we will assume

laminar, axisymmetric flow. Also, for brevity, we will use vector

notation where applicable (a summary of vector notation is given in

Appendix B or see reference 1).

As indicated in the introduction, a complete description of the

system involves solving the following equations.

A) The Navier-Stokes Equations [2, 3][*]

Assuming a fluid of constant viscosity, we may write

$$\rho \frac{D\bar{v}}{Dt} = -\nabla p + \mu \left\{ \frac{4}{3} \nabla(\nabla \cdot \bar{v}) - \nabla \times (\nabla \times \bar{v}) \right\} \qquad (2.1)$$

B) The Continuity Equation

$$\frac{\partial \rho}{\partial t} + \nabla \cdot (\rho \bar{v}) = 0 \qquad (2.2)$$

C) The Energy Equation

Assuming the fluid to have constant specific heat and viscosity, we have

$$\rho g \, C_v \, \frac{DT}{Dt} - \frac{DP}{Dt} = \mu \Phi - \nabla \cdot \bar{q} \qquad (2.3)$$

where Φ is the dissipation function [2] and $\bar{q}$ is the vector heat flow rate.

D) Equation of State of Fluid

The equation of state of a fluid is the functional relationship between its pressure, density and temperature (i.e., its state variables). For a liquid it is given by

$$d p = \chi \frac{d\rho}{\rho} \qquad (2.4)$$

where χ is the bulk modulus of elasticity of the fluid.

In this chapter we will be mainly concerned with those conduit models which are describable in terms of first-order or linearized governing equations. When this is done, the nonlinear convective inertia terms which appear in the substantial derivation D/D_t are removed. Also, where ρ appears alone it is replaced by an average

---

[*]Brackets denote references at end of report.

density ρ_0 . We will also neglect temperature effects unless it is otherwise specified. Under these stipulations the governing relations become,

$$\rho_0 \frac{\partial \bar{v}}{\partial t} = -\nabla p + \mu \left\{ \frac{4}{3} \nabla (\nabla \cdot \bar{v}) - \nabla (\nabla \times \bar{v}) \right\} \tag{2.5}$$

for the first-order equation of motion,

$$\frac{\partial \rho}{\partial t} + \rho_0 \nabla \cdot \bar{v} = 0 \tag{2.6}$$

for the continuity equation, and

$$d p = \chi \frac{d \rho}{\rho_0} \tag{2.7}$$

for the liquid equation of state. The quantities $\bar{v}$ and p now represent small perturbations from some steady condition. We must also restrict ourselves to perturbations about a mean or net velocity, $v_0 \ll c_0$. These restrictions are important to remember. In Section 2.7 we will discuss briefly the effect of violation of these assumptions.
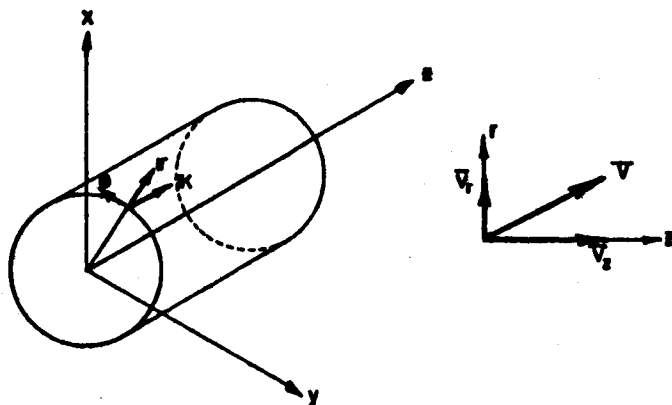
Figure 2.1 Coordinate System

Frictionless Model

The starting point for studies of conduit dynamics is the
one-dimensional wave equation which was first derived by d'Alembert
in about 1750 in connection with his studies of vibrating strings.
Joukowsky [4] and Allievi [5] are generally credited as first
associating wave phenomena with water hammer problems in order
that studies of the wave equation could be used in explaining
pressure transients in conduits. The wave equation for a
compressible liquid is derivable from Equations (2.5), (2.6),
and (2.7) if one assumes that the viscous effects are negligible.
The result is

$$\frac{\partial^2 v}{\partial t^2} = c_0^2 \nabla^2 v , \tag{2.8}$$

where c_0 is the isentropic speed of sound in the fluid and is
given, for a fluid, by

$$c_0 = \sqrt{\frac{\gamma}{\rho_0}} . \tag{2.9}$$

v represents the fluid disturbance velocity in the direction of
propagation. Solutions to Equation (2.8) predict sinusoidal
pressure and velocity disturbances propagating unattenuated with
respect to space and time with a velocity c_0. If Equation (2.8)
is solved for the case of a suddenly closed valve on one end of
a line with a constant pressure reservoir at the other end, Figure
2.2a, then the disturbance pressure will be of the form

$$P(t) = \rho_0 c_0 v_0 \left(\frac{4}{\pi}\right) \sum_{n=1}^{\infty} \left(\frac{1}{2n-1}\right) \sin\left\{\frac{\pi c_0}{2L}(2n-1)t\right\} , \tag{2.10}$$
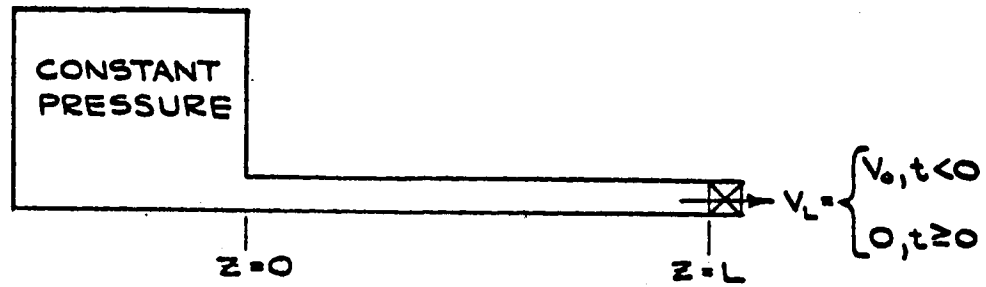
(a) Conduit with Suddenly Closed Valve at One End, Reservoir Other End
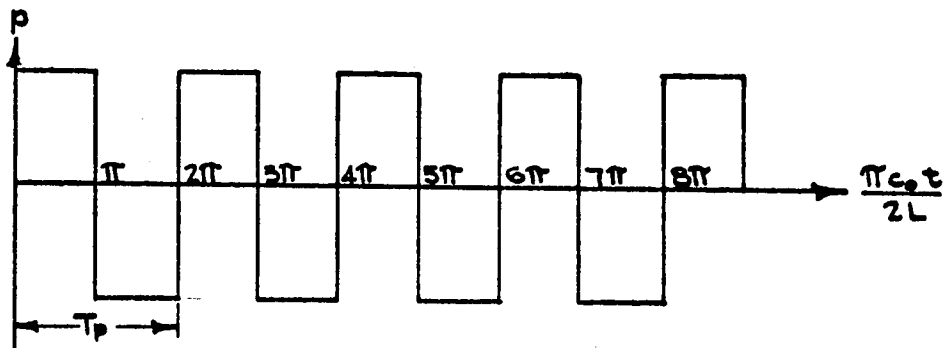
(b) Square Wave Pressure Variation at Suddenly Closed Valve
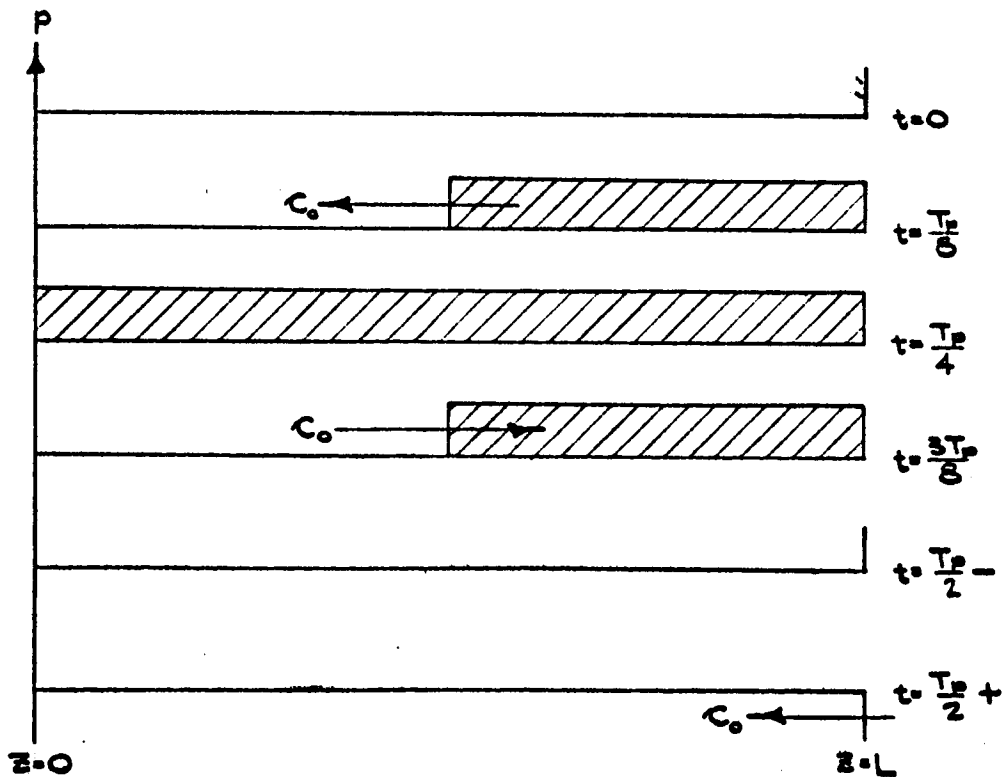
(c) Pressure History of Waves in Conduit for One Half Period

Figure 2.2 Suddenly Closed Valve - Classical Water Hammer Problem

where v_0 is the initial mean velocity in the pipe before flow
stoppage. Equation (2.10) is the mathematical expression for a
square wave with period ($4L/c_0$), see Figure 2.2b. Now examine
the physical chain of events which result in this pressure square
wave. At the instant of valve closure the fluid at $z = L$ is
instantly stopped and the kinetic energy of the fluid is converted
instantaneously (no friction) to potential energy (pressure). This
positive pressure wave propagates toward $z = 0$ with velocity c_0
and reflects back to $z = L$ with zero pressure, see Figure 2.2c.
The pressure wave then becomes negative and propagates again to
$z = 0$ where it reflects with zero pressure back again to $z = L$,
thus completing one cycle of the pressure wave.

It is evident from this discussion that the conduit of Figure
2.2 has a characteristic "natural" frequency of oscillation fc = $c_0/4L$.
A critical analysis of Equation (2.10), however, shows that this
particular disturbance actually consists of an infinite number of
discrete characteristic frequencies fc = $c_0(2n-1)/4L$. In general,
we may say that a conduit will have an infinite number of characteristic
frequencies, whose values depend not only upon c_0 and L but also
upon the end conditions for the conduit. When we excite this system
with some form of time variant non-sinusoidal disturbance, the system
response will be the sum of the response of each characteristic
frequency. The extent to which a given characteristic frequency
will be "excited" depends on the type of disturbance. In general,
the "sharper" the disturbance, the greater will be the extent to
which the high frequency terms are excited. It is important to

realize that the above results are very idealized and include neither the effects of friction or of pipe wall elasticity (these topics will be discussed later on). The results, however, indicate the upper limit of amplitude for a given disturbance. Extensive treatments of the application of this simple theory to practical problems may be found in references $\begin{bmatrix} 6, & 7, & 24 \end{bmatrix}$. These applications, in general, involve a graphical or numerical solution of the wave equation.

Friction Effects

When researchers $\begin{bmatrix} e.g., & 12 \end{bmatrix}$ performed experiments on models demonstrating water hammer they found considerable discrepancy between the simple plane wave theory and actual results. They found that when sudden flow changes were effected, the resulting pressure transients changed shape with time similar to the diagram in Figure 2.3.
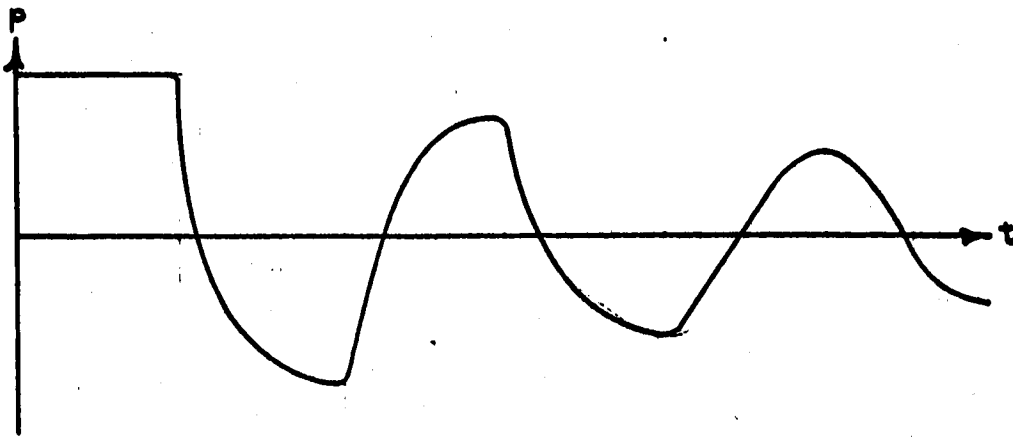
Figure 2.3 Actual Pressure vs. Time Plot for Suddenly Closed Valve

We see that, in the actual case, the sharp corners of the pressure trace are being "rounded off" and the amplitude is decaying with time. This phenomena results from dispersive and dissipative effects which are a consequence of viscosity, pipe wall effects, etc. In general, they result from friction effects. It is interesting to note that the greatest dispersion and dissipation occur on the high frequency terms which are those terms responsible for the sharp corners of the pressure trace. To account for all dispersive and dissipative effects would require an exact solution of the governing equations. However, past researchers have obtained useful results by means of approximate solutions.

Plane Wave Viscous Model

It was demonstrated by Stokes that plane or unbounded waves do not satisfy the simple one-dimensional wave equation, but rather, due to viscosity, must satisfy

$$\frac{\partial^2 v}{\partial t^2} = c_o^2 \frac{\partial^2 v}{\partial z^2} + \frac{4}{3} \nu \frac{\partial^3 v}{\partial z^2 \partial t} \tag{2.11}$$

Equation (2.11) may be obtained from Equations (2.5), (2.6), and (2.7) by assuming one-dimensional effects only. Solutions to Equation (2.11) may be represented by

$$v = v_o \, e^{\pm \gamma z + i \omega t} \tag{2.12}$$

where γ is a complex constant called the propagation constant or propagation factor and is given, in general by

$$\gamma = \gamma_r + i \gamma_c \tag{2.13}$$

14

The quantity γ_r is the spatial attenuation factor since the term $e^{\pm \gamma_r z}$ represents the spatial decay or attenuation of the wave. The quantity ω/γ_c is called the phase velocity and is the actual velocity of propagation of the disturbance. In general, the phase velocity does not equal c_o. The value of γ for the solution given in Equation (2.9) is

$$\gamma = \frac{i\omega}{c_o \sqrt{1 + \frac{4}{3} \frac{i\omega \nu}{c_o^2}}} \tag{2.14}$$

ω represents the angular frequency of the disturbance.

Solutions to Equation (2.11) have been obtained by some reseachers [8] in an effort to account for dispersion and dissipation effects in water hammer. These solutions, however, greatly underestimate the viscous effect because Equation (2.11) accounts for shear only in the direction of propagation (the z direction). Much greater viscous effects are acting in the radial direction due to the fact that the fluid velocity must go to zero at the pipe wall. We must conclude then that solutions to Equation (2.11) will not adequately describe the viscous effects in conduit dynamics.

Linear Resistance Model

The approach that a great number of researchers [6, 7, 9, 10, 11, 12, 13, 14] have used is to modify Equation (2.5) by substituting in place of the viscosity dependent terms a friction term which is proportional to the velocity. The resulting equation of motion is

$$\frac{\partial v}{\partial t} = -\frac{1}{\rho_o} \frac{\partial p}{\partial z} - R_1 v. \tag{2.15}$$

R_1 is a resistance or friction coefficient often given by the laminar flow resistance value, or

$$R_1 = \frac{8\nu}{r_0^2} \qquad (2.16)$$

r_0 being the pipe radius. When Equation (2.15) is solved simultaneously with the continuity equation and the equation of state, we obtain the same solution as in Equation (2.12) except γ now has the value

$$\gamma = \frac{i\omega}{c_0} \sqrt{\frac{R_1}{i\omega} + 1} \ . \qquad (2.17)$$

If the solution to Equation (2.15) is obtained for the case of a suddenly closed valve, the pressure versus time plot at the valve will look similar to Figure 2.4.
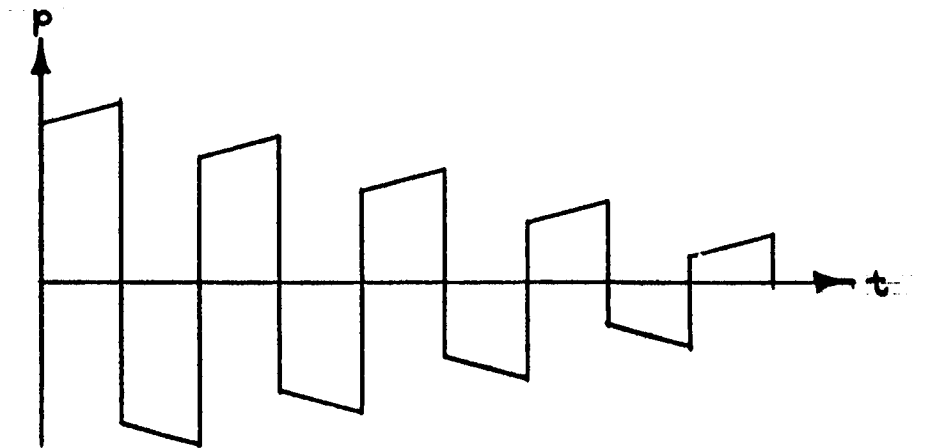
Figure 2.4 Pressure for Suddenly Closed Valve from Linear Friction Model

Although this linear friction model does not give the exact answer, especially over a wide frequency range, it has good utility when experimental values of R_1 may be determined and when the frequency range is limited.

Two-Dimensional Viscous Model-Longitudinal Mode Only

A model reported in the literature [17, 18] which more exactly describes the first-order viscous effects for the longitudinal mode of vibration _only_ is a result of the solution of the following reduced form of the equation of motion

$$\rho_0 \frac{\partial v}{\partial t} = - \frac{\partial p}{\partial z} + \mu \left\{ \frac{\partial^2 v}{\partial r^2} + \frac{1}{r} \frac{\partial v}{\partial r} \right\}.$$

(2.18)

The resulting propagation factor is

$$\gamma = \frac{\left(\frac{i\omega}{c_0} \right)}{\left\{ 1 - \frac{2 J_1 (\zeta r_0)}{\zeta r_0 J_0 (\zeta r_0)} \right\}^{1/2}}$$

(2.19)

where

$$\zeta^2 = - \frac{i\omega}{\nu}$$

(2.20)

and where $J_1(\zeta r_0)$ and $J_0(\zeta r_0)$ are, respectively, the first and zeroth order Bessel functions [19] of the argument ζr_0. Brown [17] has obtained the pressure history for the case of a suddenly closed valve using the solution to Equation (2.18). His results have much the same general shape as that of the experimental results of other authors, but the results are inconclusive since no supporting experimental results were included with the theoretical predictions. We can conclude, however, that Equation (2.18) is a better representation of the true physical situation than the models previously discussed. From the standpoint of frequency response chracteristics as reported by Oldenberger and Goodson [10], this theory follows very closely the experimental results. Brown [17] and two other authors [15, 16] have solved Equation (2.18) for a fluid in which the heat transfer

may not be neglected, thus it must be solved simultaneously with the
energy, continuity and state equations. This results in a propagation
factor

$$\gamma = \frac{i\omega}{c_o} \left\{ \frac{1 + (\gamma-1)\frac{2 J_1(\epsilon r_o)}{\epsilon r_o J_0(\epsilon r_o)}}{1 - \frac{2 J_1(\zeta r_o)}{\zeta r_o J_0(\zeta r_o)}} \right\} \qquad (2.21)$$

where now

$$\epsilon^2 = - \frac{i\omega}{\nu} \sigma_o \qquad (2.22)$$

and σ_o is the Prandtl number [2] and γ is the ratio of specific
heats for the fluid. This model has not been experimentally verified
by researchers so its validity must be regarded, at this time, as
undetermined.

Exact Linear Model

A model based on the exact solution of Equations (2.5), (2.6),
and (2.7) was presented in Interim Report No. 64-1. This model pre-
dicts an infinite number of discrete modes of propagation instead
of only one mode as the previously discussed models predict. In a
given situation, the fundamental or longitudinal mode usually pre-
dominates but there may be some circumstances under which neglecting
the higher modes leads to errors in the analysis. This more elaborate
model needs to be verified experimentally before any definite con-
clusions can be reached. It is interesting to note that the zeroth
mode propagation factor for this model coincides with that given by
Equation (2.19) for the simpler model which has been proven experi-
mentally to give good results in predicting the frequency response
for this mode.

Discussions of analytical and experimental investigations of the higher modes of propagation in connection with inviscid flow or wave propagation are extensive throughout the acoustics literature [27, 28, 29, etc.]. To the best knowledge of the writer, however, an exact treatment of these higher modes with respect to _viscous_ propagation is nonexistent in the literature except for the presentation in Interim Report No. 64-1 (see also Chapter VI of this report).

2.4 Fluid Transmission Line Concept - Transfer Equations

So far we have been discussing only time domain solutions to our equations. If we were to begin the exact study of a fluid system in which several components were involved, then the time domain approach would be exceedingly difficult and we would probably get completely lost in the mathematics. A useful and simple approach when dealing with the frequency analysis of fluid conduits (or any fluid component) is that of the fluid transmission line [7, 10, 20]. Consider the fluid line to be representable as shown in Figure 2.5 as a four-terminal system. If we solve the system equations for
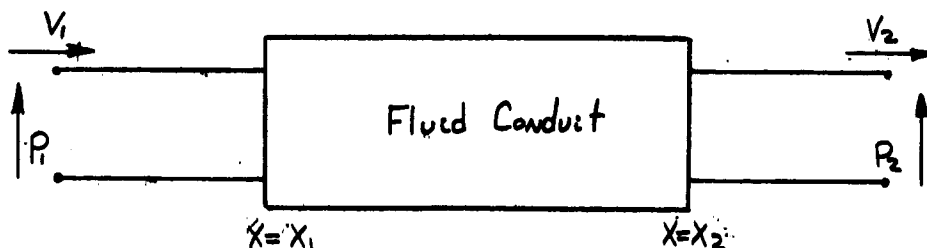
Figure 2.5 Four-Terminal Representation of Fluid Conduit

our conduit in the Laplace transform domain then we obtain a rather simple set of equations relating the four transformed variables, thus

$$P_2(s) = P_1(s) \cosh \gamma L - Z_c V_1(s) \sinh \gamma L \tag{2.23}$$

and

$$V_2(s) = V_1(s) \cosh \gamma L - \frac{P_1(s)}{Z_c} \sinh \gamma L \tag{2.24}$$

In Equations (2.23) and (2.24), $V_1(s)$, $V_2(s)$, $P_1(s)$, and $P_2(s)$ represent the Laplace transform of the respective time functions and s is the Laplace variable. Also,

$$L = X_2 - X_1 \tag{2.25}$$

and

$$Z_c = \frac{\rho_0 c_0^2 \gamma}{S} \tag{2.26}$$

Z_c is called the characteristic impedance of the conduit. The γ which appears in Equations (2.23), (2.24) and (2.26) is identical with previous γ's except that here $i\omega = s$, the Laplace variable. The value of γ, of course, depends upon the model. It is important to note that this form of the transfer equations is the same for all of the previous models discussed, only the value of γ varies. The transfer equations for the four-terminal representation of Figure 2.5 will change, in general, when there is motion of the pipe wall and when we include the higher modes of propagation. Note also that the fluid velocities represented here are average values, that is, they have been integrated over the cross-section; thus they are only dependent on time and the axial coordinate.

20

The utility of valid transfer equations in the frequency analysis
of a conduit system cannot be over-emphasized. If four-terminal trans-
fer equations can be written for each element of a fluid system, then
the total system performance may be analyzed by combining the equations
into a new set of transfer equations which represent the entire system.
Suppose, for example, that we have two components of a fluid system
arranged in series as shown in Figure 2.6.
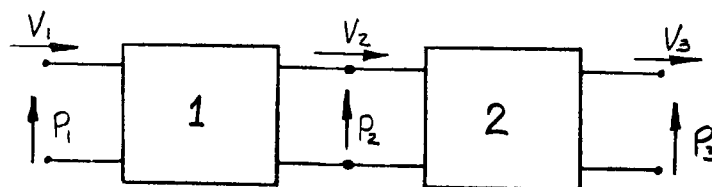
Figure 2.6 Series Arrangement of Two-Fluid Components

Suppose that the transfer equations for element 1 may be expressed
in the form

$$P_2(s) = A_1(s) \, P_1(s) + B_1(s) \, V_1(s) \qquad (2.27)$$

and

$$V_2(s) = C_1(s) \, P_1(s) + D_1(s) \, V_1(s). \qquad (2.28)$$

Writing Equation (2.28) in matrix form gives

$$\begin{bmatrix} P_2 \\ V_2 \end{bmatrix} = \begin{bmatrix} A_1 & B_1 \\ C_1 & D_1 \end{bmatrix} \cdot \begin{bmatrix} P_1 \\ V_1 \end{bmatrix} \qquad (2.29)$$

21

In a similar manner we may write for element 2,

$$\begin{bmatrix} P_3 \\ V_3 \end{bmatrix} = \begin{bmatrix} A_2 & B_2 \\ C_2 & D_2 \end{bmatrix} \cdot \begin{bmatrix} P_2 \\ V_2 \end{bmatrix} \qquad . \qquad (2.30)$$

Substitution of (2.29) into (2.30) yields

$$\begin{bmatrix} P_3 \\ V_3 \end{bmatrix} = \begin{bmatrix} A_2 & B_2 \\ C_2 & D_2 \end{bmatrix} \cdot \begin{bmatrix} A_1 & B_1 \\ C_1 & D_1 \end{bmatrix} \cdot \begin{bmatrix} P_1 \\ V_1 \end{bmatrix} \qquad (2.31)$$

or, by matrix multiplication

$$\begin{bmatrix} P_3 \\ V_3 \end{bmatrix} = \begin{bmatrix} (A_1 A_2 + B_2 C_1) & (A_2 B_1 + B_2 D_1) \\ (A_1 C_2 + C_1 D_2) & (B_1 C_2 + D_1 D_2) \end{bmatrix} \cdot \begin{bmatrix} P_1 \\ V_1 \end{bmatrix} \qquad , \qquad (2.32)$$

We might for convenience write

$$\begin{bmatrix} P_3 \\ V_3 \end{bmatrix} = \begin{bmatrix} A_3 & B_3 \\ C_3 & D_3 \end{bmatrix} \cdot \begin{bmatrix} P_1 \\ V_1 \end{bmatrix} \qquad (2.33)$$

so that, effectively we have combined elements 1 and 2 into a new

element 3. We may represent the new element as shown in Figure 2.7.
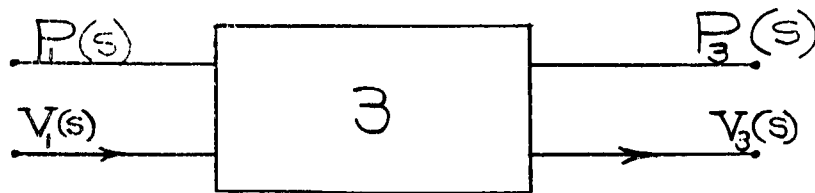
Figure 2.7 Combined Series Elements

Methods similar to this have been employed to great advantage in
the analysis of noise transmission in complex fluid systems which
involve series and parallel elements [22]. The matrix theory for
four-terminal elements has been worked out by Pipes [23] for various
types of arrangements of the elements.

22

In general, the matrix method approach is _ideally_ suited to frequency analysis studies of a conduit system. It allows very complex systems to be analyzed easily with a digital computer.

2.5 Lumped Models

Up to now we have been discussing distributed parameter models of conduit systems. We found such models to be expressible in terms of transfer relations which lend themselves well to frequency analysis. In general, these distributed models are difficult to deal with in the time domain. This is a major handicap for many technically interesting problems such as problems involving conduit systems which contain valves closing or opening arbitrarily with time. In cases such as this we may want only the time response of the system. In terms of the distributed parameter models, this means that the transfer relations for the system of interest must be transformed from the Laplace domain back into the time domain, or that some numerical or graphical procedure must be used to solve the system describing equations. The transformation of the transfer relations is very formidable; on the other hand, the graphical or numerical procedures are rather simple ways to analyze a system but lack the degree of generality usually desired in system analysis. Due to these drawbacks in the application of the distributed parameter models, lumped parameter approximations are often used in conduit system analysis. These models also have drawbacks which much be kept in mind. The major restriction which must be imposed on the lumped model of a distributed system is that it is valid only at low frequency. The method has been found to be valid, in most instances, only if the frequencies involved are not

greater than about one-eighth of the first critical frequency of the
lumped element. The exception to this restriction would be a system
which has sufficient damping so that compressibility may be neglected.
Now examine some typical ways in which conduit systems are lumped;
first, we need to consider the basic lumped elements, i.e., inertance,
capacitance and resistance [7, 20, 25].

Fluid Inertance

Consider the fluid line shown in Figure 2.8. We will assume that
only the pressure and inertia forces are important and that compressi-
bility may be neglected.
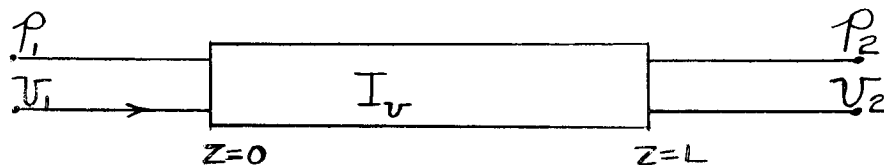
Figure 2.8 Lumped Model Inertance Element

Writing the equation of motion for this case gives

$$P_1 - P_2 = \rho_0 L \frac{dv}{dt} = I_v \frac{dv}{dt} \qquad (2.34a)$$

where $v_1 = v_2 = v$ since the flow is incompressible. The quantity
$\rho_0 L$ represents a fluid inertance. Before proceeding, it should be
noted that Equation (2.34a) is often found in various other forms
in the literature. It may be found also as

$$P_1 - P_2 = \frac{\rho_0 L}{A} \frac{dq}{dt} = I_q \frac{dq}{dt} \qquad (2.34b)$$

where q is the flow rate and A is the cross-sectional area. For
this case the fluid inertance is $\rho_0 L/A$. Another form of Equation
(2.34a) is

$$P_1 - P_2 = \frac{L}{Ag} \frac{dw}{dt} = I_w \frac{dw}{dt} \qquad (2.34c)$$

24

where w is the weight flow rate. Notice that the inertance, I, is not the same in each case. Notice also that these equations are valid only for constant area lines.

Fluid Capacitance

Now consider a fluid line in which only compressibility effects are important, i.e., inertia or inertance effects and resistance effects are unimportant. With respect to Figure 2.9, applying the
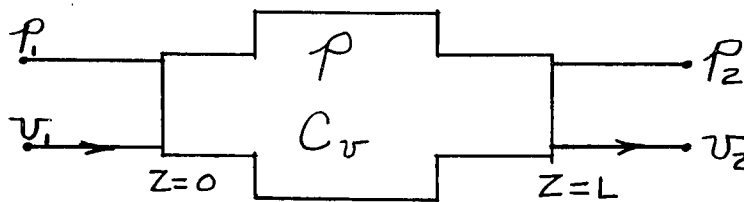
Figure 2.9 Lumped Model Capacitance Element

continuity and state equations we have, since $p_1 = p_f = p$

$$\upsilon_1 - \upsilon_2 = \frac{\mathcal{L}}{\chi} \frac{dp}{dt} = C_\upsilon \frac{dp}{dt} .$$ (2.35a)

Again, as was true for Equation (2.34) we could have just as well have written Equation (2.35) in terms of q or w, but the value of C would also have been different, thus

$$q_1 - q_2 = \frac{AL}{\chi} \frac{dp}{dt} = C_q \frac{dp}{dt}$$ (2.35b)

and also

$$w_1 - w_2 = \frac{\rho_0 g AL}{\chi} \frac{dp}{dt} = C_w \frac{dp}{dt} .$$ (2.35c)

Fluid Resistance

Because of the large number of parameters which may effect the fluid resistance, it becomes more difficult in this case to write

25

a valid theoretical relationship which holds for a wide range of flow and pressure variations. The usual approach, therefore, is to treat fluid resistance semi-empirically by defining the pressure drop due to resistance between points 1 and 2 of a lumped resistive element as

$$P_1 - P_2 = R(v) \, v \tag{2.36}$$
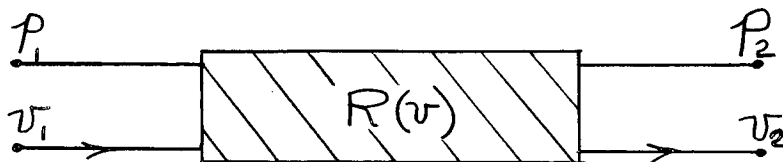
Figure 2.10 Lumped Model Resistive Element

where $v_1 = v_2 = v$ and $R(v)$ is an experimentally determined function of velocity. Of course if the pressure and velocity are steady, then $R(v)$ is well known from information contained in standard fluid mechanics textbooks. For the case of oscillating flow only (no net flow), we can get a good value for the resistance coefficient by considering a low frequency approximation of the two-dimensional viscous distributed parameter model. This will be shown later in this section.

Fundamental Lumped Model

If we now combine our three basic elements together, we have the fundamental representation of a lumped line. If we combine Equations (2.34a) and (2.36) and consider also Equation (2.35a), then we may
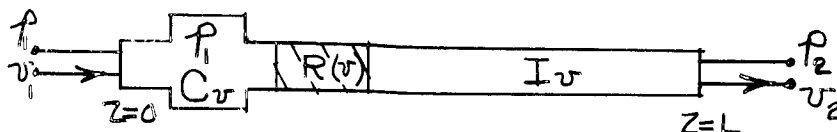
write for the fundamental representation

$$P_1 - P_2 = I_v \frac{dv_2}{dt} + R(v) v_2 \qquad (2.37)$$

and

$$v_1 - v_2 = C_v \frac{dP_1}{dt}. \qquad (2.38)$$

Now take the Laplace transformation of (2.37) and (2.38), thus

$$P_1(s) - P_2(s) = s I_v V_2(s) + R(v) V_2(s) \qquad (2.39)$$

and

$$V_1(s) - V_2(s) = s C_v P_1(s). \qquad (2.40)$$

Writing these last two equations in our standard transfer form gives,

$$P_2(s) = P_1(s) \left\{ 1 + s C_v [s I_v + R(v)] \right\} - V_1(s) \left\{ s I_v + R(v) \right\} \qquad (2.41)$$

and

$$V_2(s) = V_1(s) - s C_v P_1(s). \qquad (2.42)$$

In Chapter VI we will further discuss these last two relations with reference to the exact or distributed parameter models.

There are many possible ways of representing a conduit with lumped elements other than the representation of Figure 2.11.

Equivalent Electrical Circuits

One motivation for using lumped models, other than simplicity, is that they readily yield to simulation on an analog computer. Using a pressure-voltage analogy the electrical equivalent of the

fundamental lumped model becomes that shown in Figure 2.12. The values
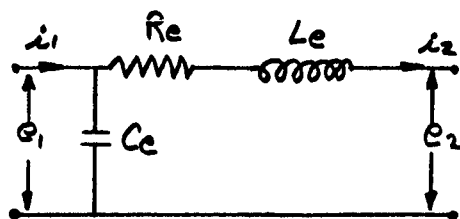
Figure 2.12 Electrical Analogy for Fundamental Lumped
Conduit with Friction

of Re, Le and Ce depend upon what is made to be the analog of electrical

current. Table 2.1 shows the analogous quantities for three possible

analogs. Other circuits which are often used in an effort to improve

Electrical Quantity	Voltage e	Current i	Resistance Re	Inductance Le	Capacitance Ce
Analogous	p	v	$R(v)$	$\rho_0 L$	L/γ
Conduit System	p	q	$\dfrac{R(v)}{A}$	$\dfrac{\rho_0 L}{A}$	AL/γ
Quantity	p	w	$\dfrac{R(v)}{\rho_0 Ag}$	$\dfrac{L}{Ag}$	$\dfrac{\rho_0 gAL}{\gamma}$

Table 2.1 Electrical Analogs

the accuracy of representation are shown in Figure 2.13.

Method for Improving Lumped Model

We stated previously that a lumped model generally is valid only

if the frequencies involved are not greater than about one-eighth of

the first critical frequency of the lumped element. We can conveniently

get around this restriction by using several "lumps" to simulate a

conduit. Suppose, for example, that the highest frequency encountered

28

π Representation   T Representation
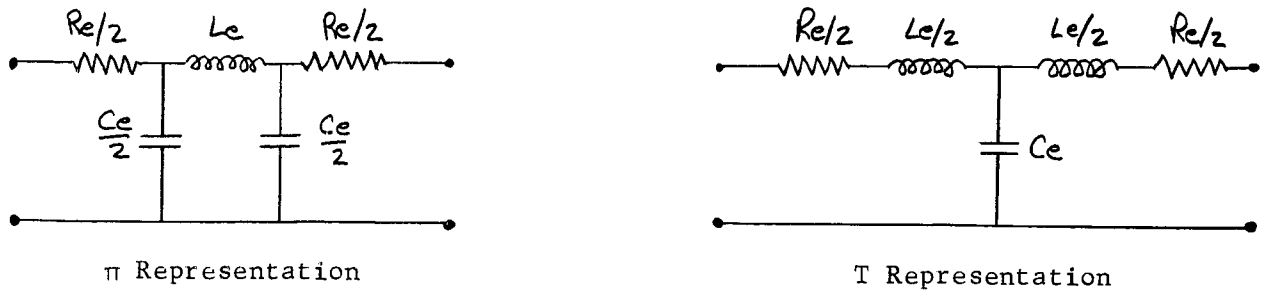
Figure 2.13   Variations of Electrical Analogs

is about ten times too high for valid lumping; then, if we use ten

electrically equivalent circuits in series (after reducing Re, Le and

Ce by a factor of ten) we are able to circumvent the original restriction.

Figure 2.14 shows the electrical analog for an n-segmented lumped model.
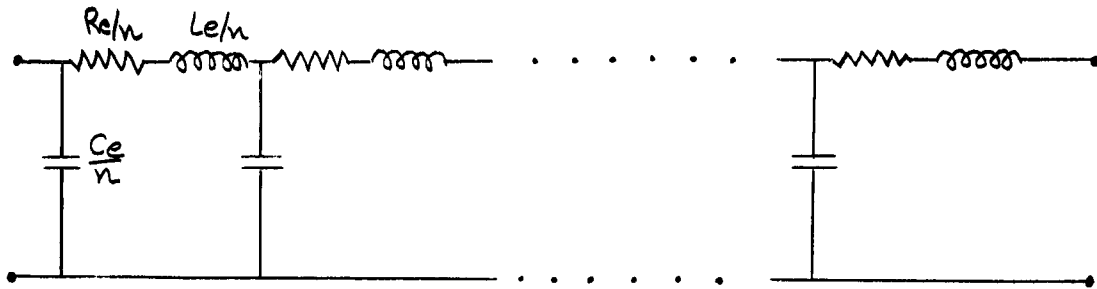
Figure 2.14   Analog for n-Segmented Lumped Conduit with Friction

In practice it has been found that this model does lead to greater

accuracy but that the number of segments required becomes very great when

the frequencies involved go beyond about the second critical value. Another

method of lumping, invented to overcome this difficulty, is discussed below.

Tapered Models

The representation of lossless fluid lines by a tapered lumped model is the subject of a patent by Paynter [26]. The analog of an n-segmented tapered representation as presented in the patent is shown in Figure 2.15. The values of the ψ's and ϕ's is dependent on the value of n and are given in Table 2.2 for values of n up to 5.
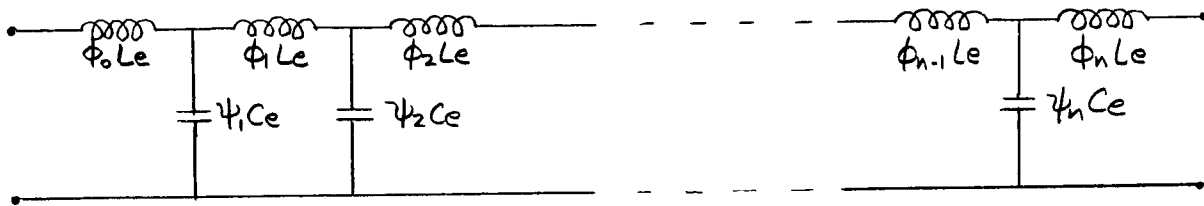
Figure 2.15   Tapered Lossless Analog

n→	0	1	2	3	4	5
ϕ_0	1.000	.250	.142	.099	.075	.061
ψ_1		.541	.289	.199	.152	.122
ϕ_1		.750	.311	.205	.154	.124
ψ_2			.367	.218	.159	.127
ϕ_2			.547	.244	.168	.131
ψ_3				.295	.182	.137
ϕ_3				.452	.209	.146
ψ_4					.257	.160
ϕ_4					.394	.185
ψ_5						.229

Table 2.2   Values of ϕ's and ψ's

It has been found that this tapered representation gives good results for any number of critical frequencies and the number of "lumps" or segments needed for an accurate representation up to a given frequency is equal to

$$N_c + 1$$

where N_c is the number of critical frequencies below the desired cutoff frequency.

2.6 Conduit Wall Effects

Thus far in our developments we have been overlooking the effects which the conduit wall may have upon the fluid dynamics. Depending upon the operating parameters of the system being analyzed, accounting for the effects of the wall may be very simply achieved or, on the other hand, may require an extensive mathematic treatment in order to get reasonable answers. Fortunately, most problems with which we will be concerned can be handled with the simple treatment. Problems demanding a complex analysis usually occur only when dealing with extremely high operating frequencies.

Simplified Analysis

Korteweg in 1878 showed that wave propagation was dependent upon both the elasticity of the fluid and of the conduit wall and that the resultant propagation velocity must be equal to or less than c_o. It has been shown (see, for example, Reference 7) that the actual sound velocity is

$$c = \frac{c_o}{\sqrt{1 + \chi f / E_t}} \qquad (2.43)$$

where E_t is Young's modulus for the tube material and f is given by

$$f = \begin{cases} D_o/h & \text{thin-walled tube} \\ 2\left(\dfrac{D_o^2 + D_i^2}{D_o^2 - D_i^2}\right) & \text{thick-walled tube} \end{cases} \qquad (2.44)$$

31

In Equation (2.44) D_o represents the conduit outside diameter and D_i represents the inside diameter. All that is required in the simplified analysis is that we replace c_o with the c of Equation (2.43) in our analysis.

More Exact Analysis

There have been a large number of papers written pertaining to the effect of conduit wall elasticity on the transmission character-istics of fluid within the conduit. Basically, conduits may be divided into two types with regard to the elastic characteristics of their walls: elastic flexible and elastic stiff. For a conduit with elastic flexible walls we assume that pressure variations within the conduit can cause radial deformations which do not cause corresponding axial disturbances in the conduit wall, i.e., all disturbances in the wall are localized and cannot propagate axially along the conduit wall. For elastic stiff walls, on the other hand, disturbances can propagate axially along the pipe wall. Some of the authors who have made contributions on the effects of conduit elasticity are Lamb [27], Jacobi [28], Morgan [29], Lin and Morgan [30] and Skalak [31]. None of these authors have treated exactly a viscous fluid in this connection. An exact treatment of both flexible and stiff walls for a viscous fluid is outlined in Chapter VI.

In general, the relations expressing the propagation velocity variation with frequency have trends as shown sketched in Figure 2.16. Notice that only one mode transmits for all frequencies for the case of an elastic flexible wall, whereas two modes transmit at all frequencies for an elastic stiff wall. Note also that the limiting value for small

32
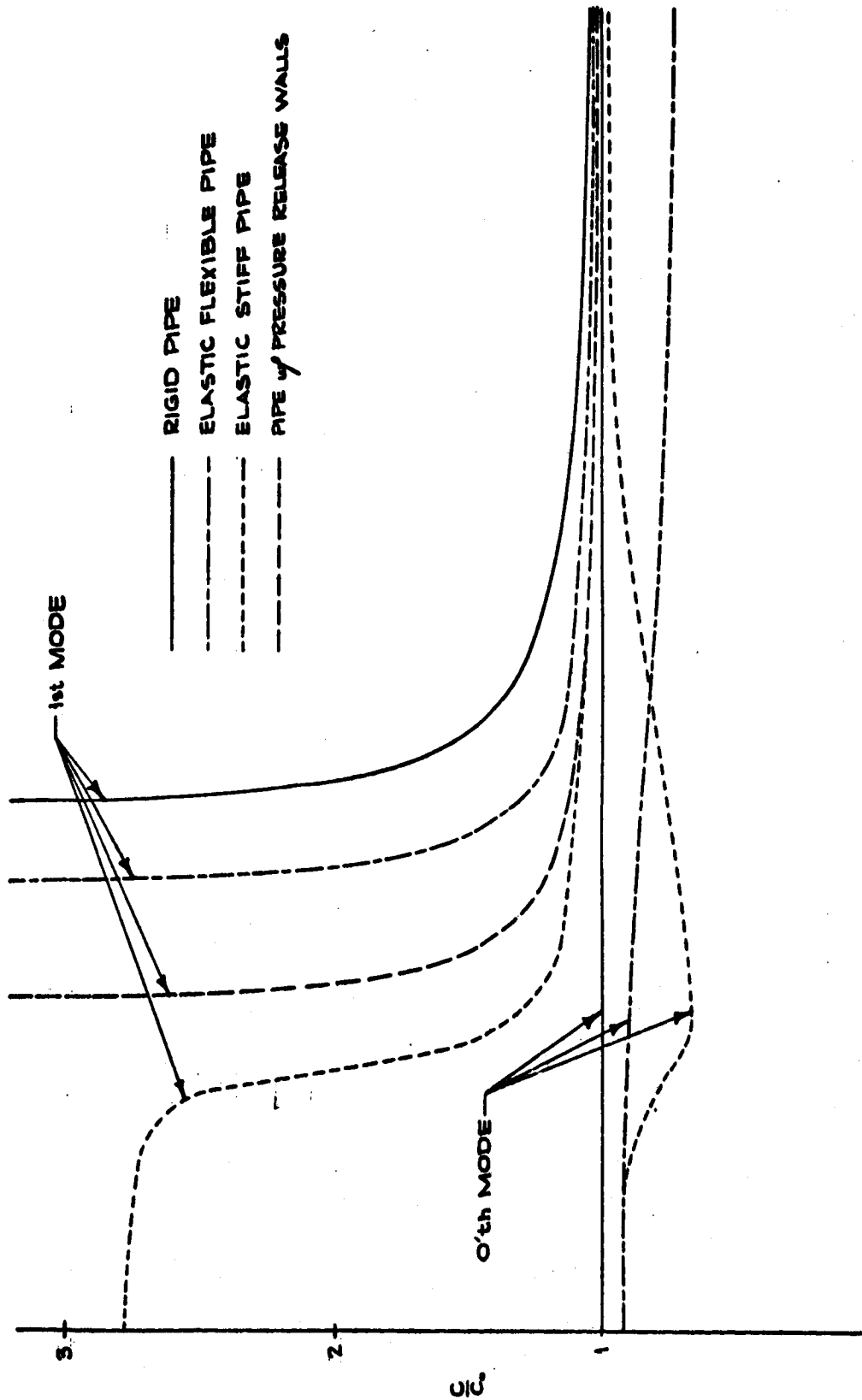
Figure 2.16 Propagation Velocity vs. Frequency
for Nonviscous Fluid

33

frequency in both cases approaches the same value, c/c_o. This is the same value as predicted by the simplified analysis from Equation (2.43). We see then that the simplified analysis is exact for low frequencies for the zeroth mode (nonviscous fluid only).

2.7 Nonlinear Effects

Thus far in our discussion we have been limited to problems involving small perturbations about some steady flow condition where the steady velocity component is much less than c_o. The reason for imposing these restrictions stems from the fact that, in the previous developments, the nonlinear terms of the equations of motion were neglected. Consider again the exact form of the Navier-Stokes equations (for a constant viscosity fluid) given by Equation (21.), or

$$\rho \frac{D\bar{v}}{Dt} = -\nabla p + \mu \left\{ \frac{4}{3} \nabla (\nabla \cdot \bar{v}) - \nabla \times (\nabla \times \bar{v}) \right\}. \qquad (2.1)$$

The difficult nonlinear terms are contained in the substantial derivative, $D\bar{v}/Dt$. For the velocity component in the z direction, we have (assuming axisymmetric flow),

$$\frac{Dv_z}{Dt} \equiv \frac{\partial v_z}{\partial t} + v_r \frac{\partial v_z}{\partial r} + v_z \frac{\partial v_z}{\partial z}. \qquad (2.45)$$

There seem to be two main conditions, with respect to problems of conduit dynamics, under which we must account to some degree for the nonlinear terms of the equations of motion. These conditions are:

1) Case where there is a large steady flow component but small unsteady components.

34

2) Case where the unsteady terms are large and the steady flow

terms may or may not be large.

We will now discuss each case in more detail.

Case 1

We assume in this case that we may write for the velocity

$$v_z = v_{z_0} + v_{z_1} \tag{2.46}$$

where v_{z_0} is the steady flow term, i.e. independent of time, and

v_{z_1} is the time variant perturbation or disturbance velocity. We

assume also that $|v_{z_1}| \ll |v_{z_0}|$. Based upon these assumptions

we may approximate Equation (2.45) by (after neglecting the small

order terms)

$$\frac{Dv_z}{Dt} \approx \frac{\partial v_{z_1}}{\partial t} + v_{z_0} \frac{\partial v_{z_1}}{\partial z} \tag{2.47}$$

Since v_{z_0} will be a known quantity as a result of solving the steady-

state hydrodynamical equations, this means Equation (2.47) is linear;

thus, we have linearized the substantial derivative for this case.

Regetz [32] utilized a linearization such as this to enable an

analytical description of the response characteristics of hydraulic

lines with a net flow. Regetz' analytical work is for nonviscous flow.

Considerable work has been done along these same lines by one

of the project members and is reported in Chapter VI.

Case 2

If the unsteady perturbations are of sufficiently large magnitude,

then a linearization procedure will not work and one has to contend

with the nonlinear equations. This area of study needs much work before

35

generally applicable methods of solution are available. In many cases the method of characteristics [33] may be used if we do not have to contend with viscosity.

2.8 Component Effects

There are many types of components commonly associated with fluid conduits which affect the transmission characteristics of the system. The most basic of these is the orifice and is the one to which we will devote our attention.

With respect to conduit dynamics applications, only a small amount of literature is available that specifically concerns the nonsteady flow of a liquid through a circular orifice. The problem has not been one of general interest since highly powered and slowly responding systems can, in general, be analyzed with the aid of the steady state orifice equation modified by appropriate correction factors. More interest is being shown in the subject as systems become more complex.

In the field of acoustics, however, the problem of nonsteady flow through an orifice is fundamental. It will be shown that some of the concepts and expressions from this field are applicable to hydraulic problems. Indeed, the bulk of the literature surveyed is from acoustic sources.

A treatment of the unsteady flow of a liquid through an orifice in a conduit is due to Goodson [34]. In this method the describing partial differential equations are reduced by integration to a linear ordinary differential equation in time relating flow, pressure drop and area of the orifice. Now follow his development.

We will assume the following conditions to hold:

(1) The conduit length is much greater than its diameter so that wave effects associated with the orifice may be neglected.

(2) Tube wall effects are negligible in the vicinity of the orifice.

(3) Viscous effects are negligible.

(4) Density changes are small.

If we average the equation of motion, Equation (2.1), across the cross-section, considering the above conditions, we then may write

$$\frac{\partial q}{\partial t} + \frac{\partial [q\, v_m]}{\partial z} + \frac{A}{\rho_o} \frac{\partial p}{\partial z} = 0 \tag{2.48}$$

for the one-dimensional equation of motion, and

$$\frac{\partial [\rho A]}{\partial t} + \rho_o \frac{\partial q}{\partial z} = 0 \tag{2.49}$$

for the continuity relation. Here, $q = q(z,t)$ is the flow rate; $v_m = v_m(z,t)$ is the average axial velocity over the cross-section; and $A = A(z,t)$ is the orifice area. We now define an effective length ℓ_o of the orifice, as shown in Figure 2.17, to account for the effect of
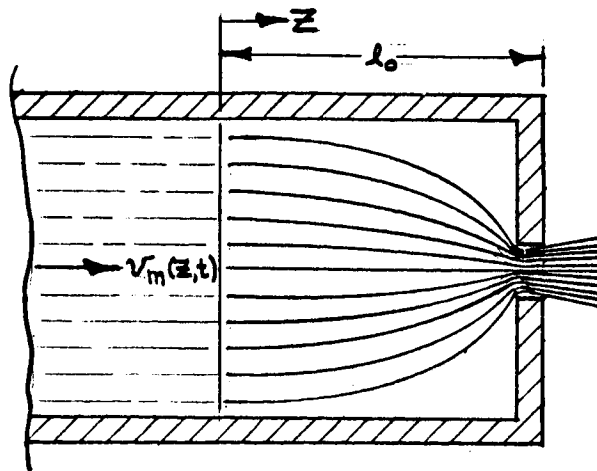
Figure 2.17 Flow Patterns Near Orifice

37

the orifice on the flow patterns in the vicinity of the orifice. Goodson has simultaneously integrated Equation (2.48) and (2.49) from 0 to ℓ_0 which results in an ordinary differential equation relating flow rate and pressure drop in terms of a time variant area for the case of a compressible liquid. For many purposes the compressibility effects may be neglected which much simplifies the resulting differential equation to

$$b_1 \frac{dq(0)}{dt} + b_2 \, q(0)^2 = \frac{\Delta p(t)}{\rho_0} \tag{2.50}$$

where $q(0)$ is the flow rate at $z = 0$ and $\Delta p(t)$ is the pressure drop across the orifice. Also,

$$b_1 = \int_0^{\ell_0} \frac{dz}{A(z,t)} \tag{2.51}$$

and

$$b_2 = \int_0^{\ell_0} \frac{dz}{A(z,t)} \cdot \frac{\partial}{\partial z}\left(\frac{1}{A(z,t)}\right) . \tag{2.52}$$

We can express Equation (2.50) in a more convenient form by letting $q = q_0 + q_1$ where q_0 is a steady flow term and q_1 is the perturbed flow. We then have, assuming q_1 is small,

$$b_1 \frac{dq_1}{dt} + 2 b_2 \, q_0 q_1 = \Delta p_1(t) \tag{2.53}$$

where $p = p_0 + p_1$ and p_0 is the steady pressure and p_1 is the perturbed pressure. No experimental evidence is presented by Goodson specifically verifying this orifice model. This model is interesting from the standpoint of accounting for the nonlinear characteristics of orifices and also in allowing the orifice area to be variable in time.

Notice that, in view of the discussion of Section 2.5, Equation (2.53) demonstrates the pressure drop to be composed of an inertance

term plus a resistive term; thus we may rewrite Equation (2.53) in the form

$$I_{\xi} \frac{dq_1}{dt} + R(q) \, q_1 = \Delta P(t).$$

(2.54)

I_q is the inertance for the orifice and $R(q)$ is the resistance.

Thurston and Martin [35] investigated the acoustic impedance of a small orifice in a thin plate for liquids driven by a high frequency, low amplitude driver. The results are shown in Figure 2.18.

———— WATER
– – – – 10 CENTISTOKE FLUID
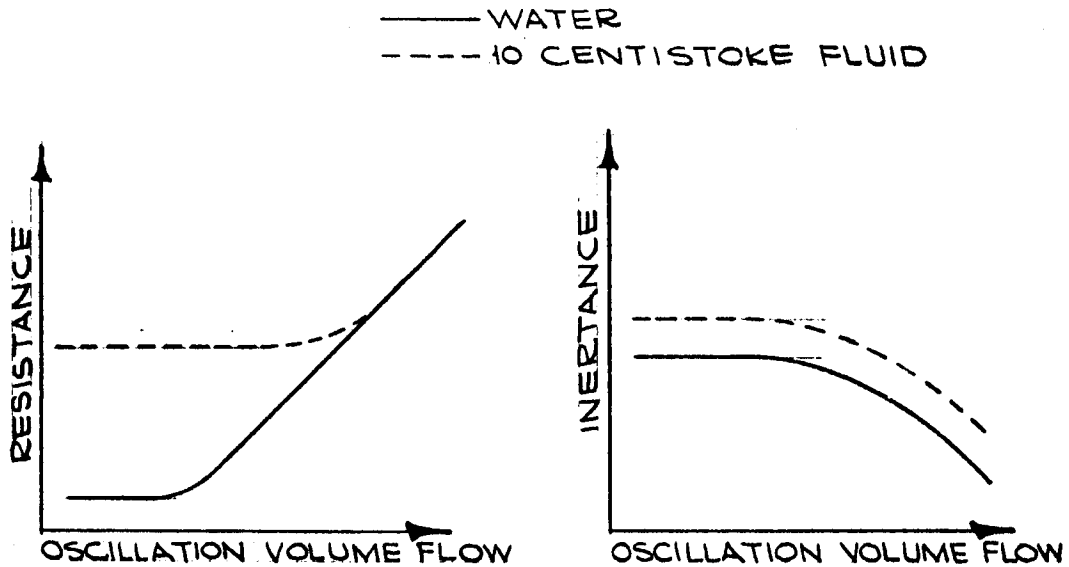
Figure 2.18 Inertance and Resistance Versus Volume Flow
for Oscillating Flow Through Orifice

The region in which resistant and impedance are not a function of volume flow is defined as the linear region, and where they are not independent of volume flow it is called the nonlinear region. These investigators reported distortions in the sinusoidal form of the differential pressure across the orifice as the nonlinear region was penetrated.

39

The end correction factor for an orifice is defined as the length which must be added to the real length of the orifice in order to render correct the calculation of resistance and inertance using the exact solution for the per-unit-length values for an incompressible fluid being driven periodically in a tube of infinite length. The concept is due to Rayleigh [36] who arrives at the range of end correction values

$$\frac{\pi}{4} d < \delta < \frac{8d}{3\pi}$$

from total work calculations. Some investigators select values from this range while others modify it. Goodson incorporates the end correction factor in his choice of ℓ_o. Thurston and Martin relate resistance and inertance to end correction factors by the expressions,

$$R = \left(\frac{R}{R_o}\right) \frac{8\pi\mu}{A^2} (\lambda + \delta_R)$$

(2.55)

and

$$I = \left(\frac{I}{I_o}\right) \frac{4\rho}{3A} (\ell + \delta_L)$$

(2.56)

where, R/R_o and I/I_o are functions of $A(\rho\omega/\mu)^{\frac{1}{2}}$.

Thurston, Hargrove, and Cook [37] present a more comprehensive study of low amplitude flows through small orifices by the use of more advanced instrumentation.

If the instantaneous volume flow through an orifice is

$$q = q_o \sin \omega t$$

the total pressure differential across the orifice is a function of the odd frequency harmonics and may be expressed as

$$\Delta P = \sum_{n}^{\infty} P_n \sin(n\omega t + \phi_n) \quad, \; n = 1, 3, 5, \cdots$$

where

$$P_1 \sin(\omega t + \phi_1) = I q_0 \omega \cos \omega t + R q_0 \cos \omega t$$

Experimental data is presented in terms of these parameters.

The effect of adding a steady flow component to the sinusoidal volume flow input can be described by

$$q = q_s + q_0 \sin \omega t$$

Since the differential pressure is a function of all frequency harmonics,

$$\Delta P = \Delta P_0 + \Delta P_a = \sum_{n=1}^{\infty} P_n \sin(n\omega t + \phi_n), \; n = 1, 2, 3, \cdots$$

where, ΔP_a is the increase in the steady flow pressure when the sinusoidal flow is added, and ΔP_o is the pressure differential resulting from q_s.

Thurston et. al. define the differential pressure across the orifice as,

$$\Delta P = P_L + P_{NL}$$

where,

P_L = Linear pressure contributions, and

P_{NL} = Nonlinear pressure contributions.

In the linear region Thurston's statement of the pressure flow equation is,

$$\Delta P_L = R q + I \frac{dq}{dt}$$

41

where, R and I are approximately constant for small volume flow rates as defined by Equations (2.54) and (2.55) and applying $\delta = \frac{8d}{3\pi}$. At higher volume flow rates the nonlinear pressure drop is generated by the convective acceleration of the fluid entering the orifice. The energy associated with this component of pressure drop is not recovered downstream of the orifice since it goes into the formation of vorticies and maintains circulations. Hence,

$$P_{NL} = \pm \frac{\sigma \rho \, \mathcal{V}_m^2}{2}$$

where,

$$\sigma \mathcal{V}_m^2 = \overline{\mathcal{V}^2}.$$

The authors also present semi-empirical data to show the dependence of the pressure flow equation (8.e., the dependence of σ and δ) on the parameters, orifice diameter, velocity, frequency, orifice length, and kinematic viscosity. The equation is most directly influenced by particle velocity.

Wood [38] states that the zero frequency limit of resistance for periodic flow should be equal to the resistance for steady-state flow for the linear region of operation. He presents steady flow data for orifices which show that at low values of volume flow, resistance is independent of volume flow. Appropriate values of periodic flow fall on the curves as shown in Figure 2.19.

The value of Reynolds number at which the nonlinear region begins is, in general, very close to ten. It is also significant to note that the values for periodic flow do not seem to correspond to this transition point. Wood points out that for a knife edged orifice the entire effective length of the orifice is due to the end correction.

42

$\dfrac{R}{\mu}$

△ PERIODIC FLOW
○ STEADY FLOW

10

N_R
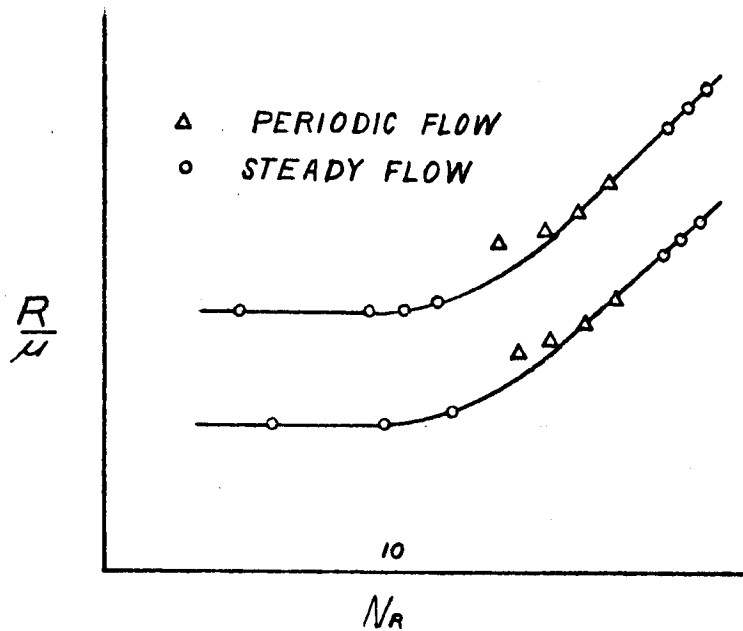
Figure 2.19 Resistance/Viscosity Versus Reynolds Number

An early development of a formula for the nonlinear acoustic re-
sistance of an orifice is due to Sivian [39]. His expression is based
on the consideration of the kinetic energy of the fluid in the orifice
for the steady flow of air. The plot of resistance versus particle
velocity was verified experimentally by Thurston et.al. [37].

Papers by Thurston and Wood [40] and Ingard and Labate [41] are
of general interest because the present evidence that for small sinus-
oidal fluid motions the relationship between volume flow and differential
pressure can be characterized by constant values of resistance and inert-
ance. These references lend further credence to the concept of the linear
region.

The problem of the description of an orifice of appreciable length
has been regarded as difficult by some investigators [37]. Karal [42]
considers the orifice to be a circular constriction between two segments

43

of a circular conduit. He analytically derives a correction which can be added to the analogous acoustical inductance of a tube of circular cross section and interpreted physically as an increase in the effective length of the tube.

Bolt, Labate, and Ingard [43] empirically measured a correction factor and a theoretically derived term which includes tube wall effects. Thurston and Wood [40] empirically determined an end correction factor and separated the impedance of the orifice from that of the tube.

The classic expressions from which many of the above references have been derived are due to Crandall [44]. Bergeron [24] presents a practical graphical treatment for unsteady flow through an orifice and for the case in which orifice area is a function of time; however, his approach requires complete time domain characteristics and is not applicable to the problem considered herein.

CHAPTER III

Discussion of Two-Phase Flow

3.1 Introduction

The term "two-phase flow" covers a large field. In general, two-phase flow refers to the fluid flow of concurrent and counter-current mixtures of any two of the three phases - gas, liquid, and solid. The field of two-phase flow can be further subdivided into two-component and one-component flow. One-component flow is complicated by mass exchange between phases.

The flows of gas-liquid systems have external and internal bounding surfaces. The external bounding surfaces are usually considered to be fixed with respect to time; however, the internal interfaces between the flowing media are generally variable in space and time. Interactions of forces and thermal interactions (for nonisothermal flows) arise at these interfaces. These interactions fundamentally affect the changes in the fields of flow velocities, pressures, temperatures, and thermal and diffusion fluxes transferring from one point of space to another point separated from the first by an interface.

The existence of twice as many flow and property variables indicates that even the simplest physical model will produce complex relationships. The simplest of models has not been adequate. However, with the aid of high speed digital computers and recent

45

developments in numerical techniques, the solution of a two-phase problem does not seem impossible.

This chapter will be limited to a discussion of one component, liquid-vapor, two-phase flow. This is the type of flow which would normally be of concern in the flow of a cryogenic fluid through conduits.

3.2 Discussion of Two-Phase Single-Component Flow

The amount of material published on the subject of two-phase flow has increased tremendously over the past decade. According to Reference [47], over 400 publications on two-phase gas-liquid flow phenomena appeared during the year 1963. These publications do not include the subjects of atomization, cavitation, and condensation. With such a large number of publications appearing each year on this subject, it is difficult to thoroughly review all of the material. Several recent documents have attempted to compile a list of important publications on the subject of two-phase flow, References [48], [49], [50], [51]. It has been said that it may soon be necessary to have a bibliography on two-phase flow bibliographics.

Basically, the analytical treatment of two-phase flow is no different from that of single-phase flow. The fundamental concepts of conservation of mass, conservation of momentum, and the first and second laws of thermodynamics hold for two-phase flow as they do for single-phase flow. These basic laws may be expressed in differential form leading to the differential equations of conservation of mass, conservation of momentum and conservation of energy. A difficulty

46

arises in the solution of these equations however since the differential equations must be written for each phase and solved simultaneously. The difficulty is in attempting to write the necessary boundary and initial conditions for these equations. The complexities involved in such an approach have limited the usefulness of this method. A number of simplifying assumptions have been put forward in the literature to permit some accomplishments in predicting two-phase flow behavior.

Perhaps the most common assumption that has been made is the recognition of distinct flow patterns that exist in two-phase flow. A study of these individual flow patterns or flow regimes has allowed some simplifications to be made in the analysis of each regime. There is some disagreement in the description of the various flow regimes. However, most attempts at describing the flow patterns begin with distinguishing the flow as either horizontal or vertical. In horizontal flow the flow patterns normally described in the literature include spray or mist flow, annular flow, slug flow, wavey flow, stratified flow, plug flow, and bubble flow. (The flow patterns are listed in order of decreasing gas or vapor to liquid flow rate). In vertical flow the patterns are usually described as mist flow, spray-annular flow, annular flow, slug, churn, or plug flow and bubble or froth flow. A number of flow regime maps have been given in the literature for a prediction of the conditions under which the various flow regimes exist. Several of these flow regime maps are given in Reference [47].

Since the area of study involved in this contract include situations where only a small amount of vapor formation will be permitted,

the bubble or froth flow regime was considered to be the most important regime for intense study. This placed a limit upon the amount of literature which had to be carefully reviewed and permitted a narrowing down of the techniques of solution of the two-phase problem. Bubble or froth flow lends itself to certain mathematical treatment not useful in many of the other two-phase flow regimes. The assumptions of isotropic and homogeneous behavior are fairly realistic ones for the bubble flow regime.

The most important information needed for any bubble flow study is that on the behavior of the individual bubbles. An adequate description of bubble formation and growth is needed in order to complete the description of the behavior of two-phase flow involving the bubble or froth flow regime. Bubble formation and bubble dynamics has long been of interest to persons studying the phenomena of boiling heat transfer. Much of the current literature being studied and utilized has come from this field.

Another important fact that has been realized during the course of the investigation is that the presence of the bubbles in the liquid has a very outstanding effect on the velocity of sound. At mass ratios of vapor to liquid which exist in the bubble flow regime, the effect on the sonic velocity is considerable. This can be seen in Figure 3.1 and Figure 3.2 taken from Reference [52]. The speed of sound has been shown in Interim Report 64-1 to be an important parameter in certain single-phase flow problems. It would be expected that similar effects would carry over into the two-phase flow problems. Ability to estimate the sonic velocity of various mixtures of vapor

and liquid must be acquired before any great degree of success can be accomplished in this area.

The prediction of pressure drop in steady two-phase flow is not too difficult using rather well-established methods, first developed in Reference [53]. The transient two-phase flow problem, however, has been given only a minimum amount of study. A very recent survey on the problem of flow oscillations in two-phase systems is given in Reference [54]. It is felt that some of this material will be useful in the continuing study of transient two-phase systems.
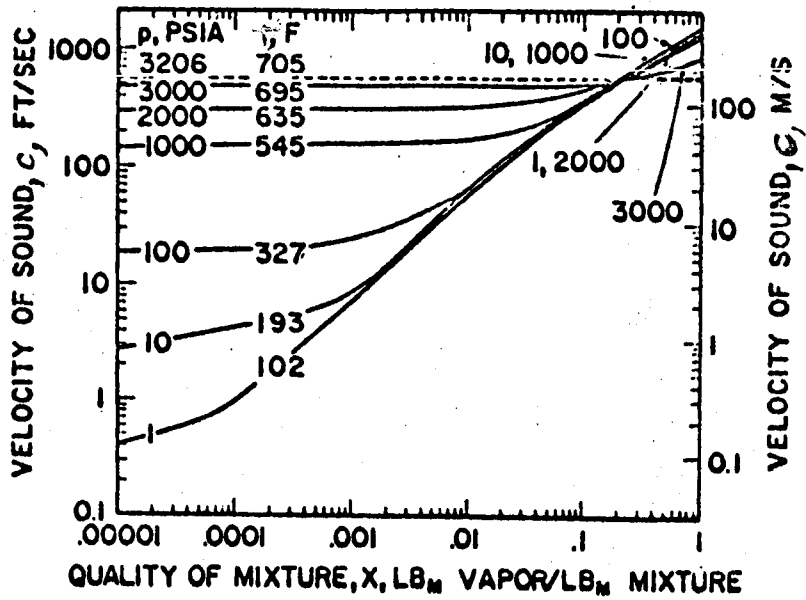
Figure 3.1   Velocity of Sound in Steam-Water Mixtures as a
Function of Mixture Quality
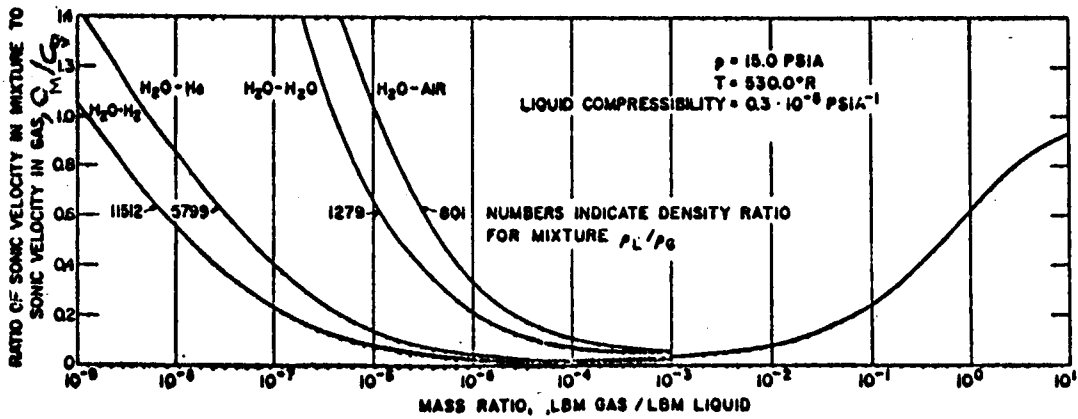
Figure 3.2   Ratio of Adiabatic Sonic Velocity in Mixture to Sonic
Velocity in Gas Phase Versus the Ratio of Mass of Gas
to Mass of Liquid for Several Gas-Liquid Combinations

CHAPTER IV

Review of the Literature on the Formation of Two-Phase
Flow As Caused by Pressure Drop (Cavitation)

4.1 Introduction

Cavitation is the formation and subsequent collapse of cavities in a liquid when the local static pressure at some point decreases to or below the vapor pressure and then increases as the fluid progresses downstream. This can easily occur when a fluid, near its saturation pressure, is flowing through conduits which are equipped with components. Whenever cavitation occurs the complexity of the flow problem is increased several times because of the formation of two-phase flow. Two-phase flow is often undesirable not only because of the increased complexity of the flow problem but also because of the unsteadiness often caused by its formation. Therefore, before a complete analysis of two-phase single component flow through conduits can be attempted, we must be able to predict the conditions at which two-phase flow starts and the conditions under which these cavities will collapse.

The literature on cavitation has grown to great proportions since studies began in the late nineteeenth century. This is due to the large number of variables involved and to the wide range of the aspects of cavitation any one of which may happen to be of prime interest to investigators in different fields. The

literature reviewed on cavitation will be directed toward vaporous cavitation as might be expected to occur in fluids flowing through conduits.

In order to clearly bring out the problem to be discussed it is necessary to distinguish between two broad types of cavitation. Vaporous cavitation is the sudden expansion of a vapor bubble due to vaporization of the liquid at the bubble wall whereas gaseous cavitation is the relatively slow expansion of a gas bubble due to diffusion. Strasberg [55] showed that the critical pressure needed for vaporous cavitation would be equal to or less than the vapor pressure whereas gaseous cavitation could occur at pressures above the vapor pressure.

Vaporous Cavitation, a phenomenon caused by a decrease in the stream pressure, may occur as a result of any one or combination of: (1) friction in the conduit, (2) decreasing the flow area, (3) centrifugal effects (flow in bends), (4) vibration and etc. However, pressure alone does not specify the conditions under which a flowing fluid will cavitate. It might be said that pressures below the vapor pressure is a necessary condition for vaporous cavitation; however, this is not sufficient because of other variables.

4.2 Variables Affecting Cavitation

The variables which affect the onset of cavitation may be divided into four major groups. These groups together with the individual group variables are:

I. Fluid Properties

1. Vapor pressure
2. Surface tension
3. Wettability of liquid
4. Viscosity
5. Thermal conductivity
6. Mass diffusion coefficient
7. Pressure

II. Foreign Variables

1. Dissolved gases
2. Undissolved gases
3. Impurities (solids, dissolved solids, etc.)

III. Conduit Variables

1. Surface roughness
2. Material of conduit

IV. Dynamic Variables

1. Turbulence level
2. Pressure distribution
3. Velocity
4. Vibration

Because of the large number of varibles involved, the efforts to find similarity or scaling laws encompassing all of these variables has not been successful.

The problem of determining the conditions under which a fluid will cavitate is not impossible because of the relatively minor role most of these variables play and the dominant role of a few. Vapor pressure is the most important single variable because it gives an indication of the pressure necessary to cause cavitation. Several investigators have considered the nuclei present in the fluid and conduit as an important variable. The role of the nuclei in producing cavitation will be discussed in a following section.

4.3 Incipient and Desinent Cavitation

Incipient cavitation is defined as that phenomena which occurs when the stream pressure progresses from a condition of no cavitation to one supporting cavitation. It marks the onset of cavitation. Desinent cavitation, on the other hand, identifies the condition

when the stream passes from a condition supporting cavitation to one wherein there is no cavitation. It defines the cessation of cavitation. Many investigators in the past called both the beginning and the cessation "incipient" cavitation. Holl [56] in 1960 named these two different occurrences of cavitation.

For incipient cavitation there will correspond a particular value of p called the "inception pressure" p_i, whereas for desinent cavitation there is the "desinence presure" p_d. From these definitions there follows the incipient-cavitation number K_{i_o} and desinent-cavitation number K_{d_o} defined by

$$K_{i_o} = \frac{p_{i_o} - p_v}{\frac{1}{2} \rho_o V_o^2}$$

(4.1)

and

$$K_{d_o} = \frac{p_{d_o} - p_v}{\frac{1}{2} \rho_o V_o^2} .$$

(4.2)

The subscript "o" designates a reference state which is usually taken upstream of the minimum pressure section.

The experimental investigation by Lehman and Young [57] and Kermeen [58] indicate that the desinence pressure, p_d, is greater than or equal to the inception pressure, p_i. The pressure difference $p_d - p_i$ is often referred to as the "cavitation hysteresis." Thus, for the same vapor pressure, we can write the following relation between Equations (4.1) and (4.2),

$$K_{d_o} \geq K_{i_o} .$$

(4.3)

For a given flow condition K_{d_o} appears to be the upper limit for K_{i_o}. Holl [56] pointed out that investigators, in the past, called desinent cavitation as incipient cavitation because of its repeatable nature. However, in some cases, there is no difference between incipient and desinent cavitation except in the definitions.

4.4 The Inception of Cavitation

A. Nuclei Theory for Cavitation Inception

It is now the generally accepted view that the inception of cavitation in ordinary liquids is associated with the growth of nuclei containing vapor, undissolved gas, or both, which are present either within the liquid or in crevices on bounding walls. On the basis of physical arguments made by Eisenberg [59], it is unlikely that completely dissolved gases can play a dominant role in inception, although in certain cases such dissolved gases may become important during the inception process. The work of Harvey, McElroy and Whiteley [60] is of particular importantce in this connection, having demonstrated that water, saturated with air, when "denucleated" by prior application of large pressures exhibited very high fracture strength. Thus, the presence of such nuclei is taken to account for cavitation onset at pressures of the order of vapor pressure.

Cavitation inception is a dynamic phenomenon; however, the basic principles can be revealed by a static analysis. For static equilibrium the following equation, for a spherical bubble, must be satisfied:

$$P_v + P_g = P + \frac{2\sigma}{R} .$$

(4.4)

55

For a constant weight of a perfect gas at constant temperature $p_g =$ $\frac{C_1}{R^3}$, where C_1 is proportional to the number of molecules or weight of the gas and R refers to the radius of the sphere. Hence, Equation (4.4) becomes

$$p - p_v = \frac{C_1}{R^3} - \frac{2\sigma}{R} .$$

$$(4.5)$$

The minimum value of $p - p_v = p*$ occurs at a radius

$$R = R^* = \left(\frac{3C_1}{2\sigma}\right)^{1/2}$$

or

$$(p - p_v)_{min} = -\frac{4\sigma}{3R^*} .$$

$$(4.6)$$

In this relation the negative sign indicates that the critical fluid pressure is actually below the vapor pressure. If the pressure is decreased slightly from the condition of $(p - p_v)_{min} = p*$ at $R = R^*$, the bubble becomes unstable and tends to grow without bound. At pressures greater than the critical pressure, the bubble is stable and assumes an equilibrium radius satisfying Equation (4.4). The relation between $p - p_v$ and diameter for different values of C_1 and assuming a surface tension value of 0.005 lbs. per ft. for 68 F water are shown in Figure 4.1. The corresponding relation between pressure and critical diameter is shown in Figure 4.2.

It may be observed from Equation (4.6) that the critical radius for a bubble containing only vapor ($C_1 = 0$) is zero and consequently the fluid pressure must be infinitely negative in order to cavitate such a bubble. This requirement for infinite pressure to cause
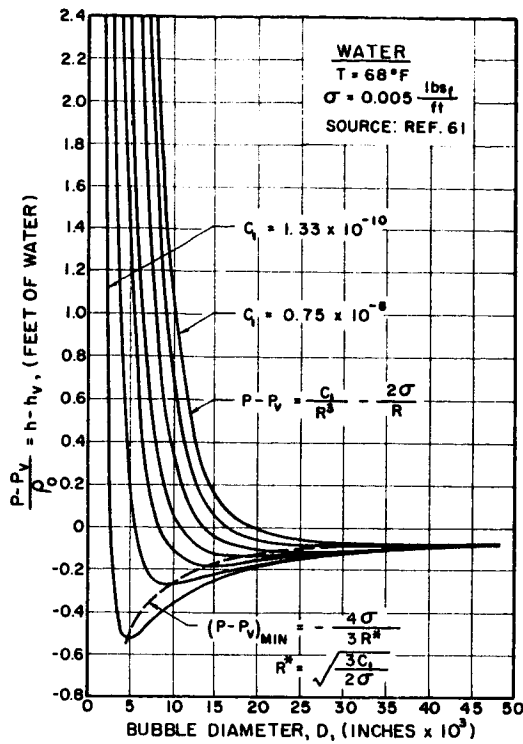
Figure 4.1   Pressure as a Function Bubble Size
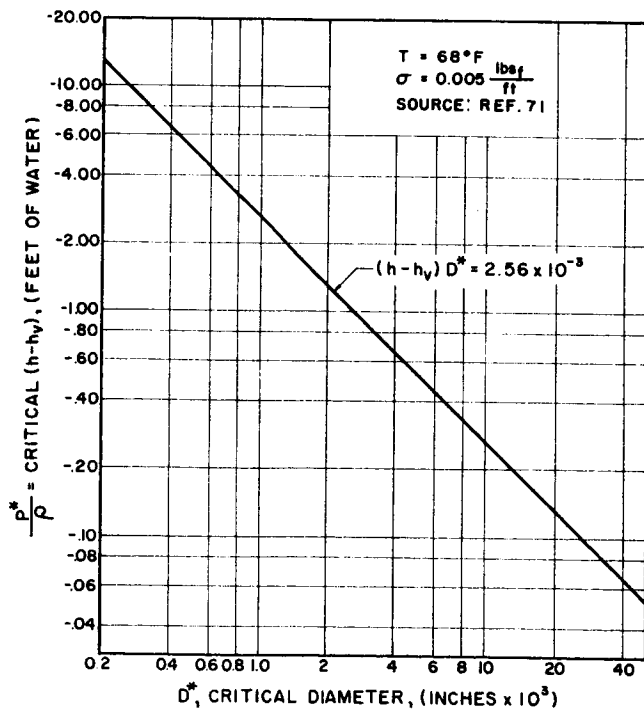
Figure 4.2   Pressure Required to Cause Instability
of Critical-Size Gas Nuclei

instability of a vapor bubble must be modified when the bubble radius approaches molecular size and the continuum theory becomes invalid.

The previous analysis has considered only the static stability of the cavitation nuclei. It appears reasonable to expect that if nuclei are subjected to transient pressure reductions the critical pressure for instability might be considerably less than the value given by Equation (4.6). Noltingk and Neppiras [62], [63] were able to show, in the majority of cases, that the critical pressure predicted by the static analysis is not significantly altered by the duration of the transient. The investigations performed by Noltingk and Neppiras revealed that the pressure need only stay at the critical pressure for a time slightly greater than the natural period of oscillation of the bubble. For a bubble diameter of 0.001 inches, the pressure need remain at the critical value for approximately 10 microseconds. On the other hand, cavitation experiments conducted at high velocities on small scale models with short low pressure regions (flow through venturi type nozzles) can be misleading if it is assumed that dynamic effects do not influence the critical nuclei size and pressure.

B. Sources of Nuclei

In the previous section a spherical gas bubble was assumed as the nuclei for cavitation. Such nuclei do exist near the surface of agitated liquids as continuously entrained air bubbles. However, at greater depths, or in a confined fluid, it appears that the gas should dissolve in the fluid. The partial pressure of the gas within the bubble is higher than the surrounding fluid pressure because of surface

tension and thus some gas should diffuse into the liquid. The loss of gas decreases the size of the bubble, and thus increases the surface tension pressure which increases the gas partial pressure and increases the rate of diffusion into the liquid, and so forth. From Equation (4.6) we have seen that stable spherical vapor nuclei cannot exist. Consequently, some nuclei source other than free gas bubbles must be postulated in order to explain the cavitation that is observed in fluids in which free gas bubbles of the required size for instability are not observed.

When new glass which has been cleaned with acid is immersed in water, the water tends to fill all the microscopic cracks and crevices. Such a surface is often referred to as hydrophyllic. Schweitzer and Szebehely $\left[64\right]$ ran some gas evolution test by placing the fluid to be tested in steel and lucite containers. No precaution was made to chemically clean the containers. With water they were unable to produce any appreciable supersaturation without observing bubble formation. However, with petroleum hydrocarbons, which wet both steel and lucite, they observed considerable supersaturations (100 percent) without bubble release, provided the liquid was kept in a static state. Thus, this illustrates that the properties of the liquid are important when studying cavitation.

A material in which water does not tend to fill microscopic cracks and crevices is classified as hydrophobic. This type of material includes almost everything and thus gas volumes are easily contained in the crevices of foreign particles entrained

in the fluid or in the crevices of the boundary material itself. It

is presently believed that the nuclei needed for the cavitation pro-

cess (other than free gas bubbles) are located in the crevices and

cracks of such hydrophobic materials. Harvey, McElroy, and Whiteley

[60] were able to show that in a crevice of a hydrophobic material

it is possible to have contact angles between the liquid, solid,

and gas, such that the surface tension pressure is considerably

reduced and tends to decrease rather than increase the cavity

pressure. Under these circumstances, it is possible to postulate

an equilibrium condition in which gas neither diffuses into or out

of the gas trapped in the crevice, and it is these microscopic gas

volumes that are currently believed to be the nuclei needed for

cavitation inception.

Knapp [65] explained the difference between a pure liquid's

ability to cavitate and a liquid that cavitates as soon as the

pressure drops below the vapor pressure in terms of "weak spots."

The findings of Knapp agreed with those of Harvey et.al. [60] in

that weak spots which initiate cavitation usually occur on solid

surfaces in contact with liquids. Knapp observed that normal

cleaning methods were inadequate to remove weak spots from metal

surfaces. This is probably due to the presence of innumerable

cracks in the metal surface.

In summary, there are three distinct sources of nuclei. Each

source is capable of causing the phenomena of cavitation. These

are:

1. The free undissolved gas bubble, usually macroscopic in size.

2. The nuclei that exist in the crevices of foreign particles.

3. The nuclei that exist in the boundary material. Kermeen, McGraw and Parkin [66] were able to take pictures of this source of nuclei during a cavitation study.

The interpretation of cavitation tests, in which cavitation is actually produced in the test facility, is effected by the nuclei present. To properly extrapolate such test results to the prediction of prototype cavitation, the relevant scaling factors must be considered.

C. Cavitation Scale Effects

If the occurrence of cavitation were uncluttered by the appearance of scale effects, the experimental study of cavitation would be fairly easy. The test of a given shape over a range of K_o values would give the desired information. An indication of such an idealized cavitation behavior is presented with the aid of Figure 4.3.

The streamlines and pressure coefficient, for potential flow past a simple shape, are shown in Figure 4.3(a) and 4.3(b) respectively. At some point on the body, the minimum pressure occurs. The absolute value of this pressure is dependent only on the relative flow velocity, V_o, the reference pressure, p_o, and the exact shape of the body. This minimum pressure value for the given body is thus uniquely characterized by $C_{p_{min}}$, the minimum value of the conventional pressure coefficient in which

61

$$C_p = \frac{P - P_o}{\frac{1}{2} \rho_o V_o^2} \quad . \qquad\qquad (4.7)$$

In the idealized situation, no cavitation test would be required because the value of K_o at which cavitation would first appear is simply $-C_{p_{min}}$. If the pressure could be measured at the proper location, $C_{p_{min}}$ could be found by a noncavitating test with water, or even air, as the test medium. However, as a result of scale effects, cavitation tests are required.

The manner in which a cavitation test would verify the K_{i_o} prediction, in the idealized cavitation situation, is shown in Figure 4.3(c). A cavitation test is normally conducted with the initial operation of the test facility at a high K_o value, for which there is no possibility of cavitation. The operating K_o

(a) FLOW PAST A BODY

(b) PRESSURE VARIATION ON BODY

(c) DIRECTION OF TEST

SOURCE: REF. 67
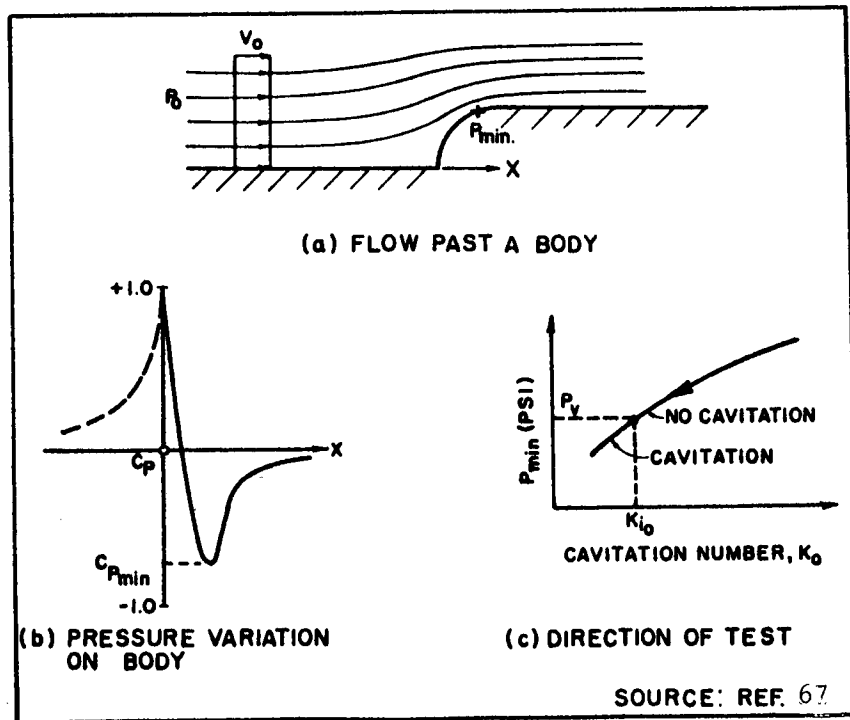
Figure 4.3   Body Flow Dynamics and Idealized Cavitation Test Behavior

62

value is then reduced, either by raising V_o or lowering p_o, with

an associated decrease in the absolute pressure p_{min}, until the

value $p_{min} = p_v$ is reached. The reduction of K_o below the in-

ception value (K_{i_o}) has no further effect on p_{min}, which remains

equal to p_v. However, the nature of cavitation is changed as K_o

is reduced below K_{i_o}. At the inception point, the cavitation con-

sists of small bubbles that quickly collapse with tremendous noise

as they proceed into regions of higher pressure. At K_o values

below K_{i_o}, larger cavities may form which change the flow and force

relations for the object or conduit.

Unfortunately, little is known about how the conditions, at

the beginning of a cavity, change with the degree of cavitation.

Thus, a detailed study of this could provide useful information.

From this discussion of the idealized cavitation occurrence

situation scale effects may be defined as any flow phenomena which

will cause deviations from the idealized occurrence. Thus, if

the pressure distribution over the body varies with the nature

of the flow, this represents one kind of scale effect. If

cavitation does not always start when p_v is reached, then another

type of scale effect is represented. The pressure distribution on

a body is affected by such factors as fluid viscosity, surface

roughness and etc. The pressure at which cavitation occurs depends

on such factors as nuclei present, surface tension, pressure dis-

tribution and etc.

Holl and Wislicenus [68] pointed out that the idealized

similarity relation of cavitation $(K_o = P_o - P_v / \frac{1}{2} \rho_o V_o^2)$ is based

on certain assumptions. These are:

1. All pressure differences in the flow are proportional to ρV^2.

2. Geometric similarity includes surface irregularities of the flow boundaries.

3. The vapor pressure in the flow field is constant and the pressure at which cavitation takes place is the equilibrium vapor pressure.

4. Cavitation takes place instantaneously whenever the vapor pressure is reached.

The correct similarity relations, which are needed to describe cavitation, are unknown. However, Holl and Wislicenus [68] listed several similarity relations which may help describe cavitation. These are given in Table 1. The classical relation, included in Table 1, must always be satisfied together with the requirement of geometric and kinematic similarity.

4.5 The Investigations of Cavitation Inception

In the following sections we will discuss the experimental and theoretical investigations of cavitation inception for unseparated flow past streamlined bodies, separated flow past non-streamlined bodies, and flow through venturi type nozzles, orifices, and tubes.

A. Unseparated Flow Past Streamlined Bodies

A streamlined body is a body in which the curvatures are sufficiently mild to permit nearly ideal flow (that is, flow without boundary layer separation). The pressure distribution on this body, as obtained from potential flow theory, would be expected to be in

64

TABLE 4-1 [68]

	No.	Forces And Characteristics	General Similarity Requirements	Similarity Requirements For Same Fluid Properties	Probable Effects On K of Change in V and L_1 Only
Ideal Flow	1	Inertia Forces Only (Classical Theory)	$K = \dfrac{p - p_v}{\frac{1}{2}\rho V^2} = $ Const.	$p - p_v$ proportional to V^2	No Effects $K = $ Const.
Hydrodynamic Scale Effects On The Fluid Pressure	2	Viscosity And Inertia Forces	Reynolds' Law of Similarity $R_e = VL_1/\nu = $ Const.	$VL_1 = $ Const.	K increases With VL_1
	3	Gravity And Inertia Forces	Froude's Law of Similarity $F_L = V/\sqrt{gL_1} = $ Const.	$V/\sqrt{gL_1} = $ Const.	Vertical Differences In Cavitation Decrease With Increasing $V/\sqrt{L_1}$
	4	Elastic And Inertia Forces (Compressibility)	Law of Constant Mach Number $M = V/c = $ Const.	$V = $ Const.	Not Predictable. Probably Effective Only With Extensive Cavitation
	5	Effects of Surface Irregularities	$h/\delta = $ Const. for $R_e = $ Const.: $h/L_1 = $ Const.	SAME	K increases With h/L_1. K decreases with increasing L_1 if h increases slower than L_1.
Thermodynamic Scale Effects	6	Effects of Vapor Pressure	$p_v/p = $ Const.	$p = $ Const. Therefore $V = $ Const.	K increases with V
	7	Effects of Vaporization And Heat Transfer	$\dfrac{1}{p}\,\dfrac{\partial p_v}{\partial T}\,\dfrac{a_v}{a_l}\,\dfrac{V_l}{V_v}\,\dfrac{L_v}{c_{p_l}}$ $P_e^A = $ Const. Peclet Number, $P_e = \dfrac{c_{p_l} VL_1}{V_l\,k}$	$VL_1 = $ Const.	K decreases with increasing VL_1
			(6) and (7) may be neglected if p_v/p is very small (e.g. for Cold Water)		
Molecular And Other Microscopic Scale Effects	8	Surface Tension And Inertia Forces	Law of Constant Weber Number $W = \rho V^2 L_1/\sigma = $ Const.	$V^2 L_1 = $ Const.	K increases with $V^2 L_1$
	9	Number of Nuclei	$\sqrt{N} \cdot L_1 = $ Const. (Only if nearly all nuclei form centers of cavitation)	$L_1 = $ Const.	K increases with L_1 (for N = Const.)

Table 4.1 Cavitation Similarity Relations

good agreement with experimental measurements if the boundary layer displacement thickness is small compared with the body diameter. This condition is usually met if the Reynolds number is sufficiently high to produce a fully developed turbulent boundary layer. [69]

Knapp and Hollander [70] made a high-speed photographic (20,000 pictures per second) study of the formation and collapse of individual bubbles during the flow of water past a 1.5 caliber Ogive-Nosed body. The life of the bubble from the instant it was large enough to be detected until the completion of its first collapse was only about 0.003 seconds. The formation period required about three fourths of this time, leaving one fourth for the collapse period. The conditions of the water tunnel were: V_o = 40 fps, p_v = 0.40 psia, and p_o = 4 psia.

In many of the pictures taken, it was obvious that the collapse of one bubble had a major effect on the collapse of its neighbor. Furthermore, as the severity of the cavitation was increased, the bubble concentration built up very rapidly, so that rarely if ever could a single bubble be seen to form and collapse without interference.

Kermeen, McGraw, and Parkin [66] investigated several geometrically similar hemispherical and 1.5-caliber Ogive-Nosed bodies for cavitation inception at various water tunnel speeds. The results of this investigation are shown in Figure 4.4. Figure 4.4 illustrates that the measured incipient cavitation numbers were less than $|C_{p_{min}}|$ and depended on both the model size and the test velocity. However, the data indicates that the incipient cavitation number does approach

$\left|C_{P_{min}}\right|$ for large size bodies and high tunnel speeds. It is suggested that the scale effects shown in Figure 4.4 are primarily caused by the low concentration of nuclei and the small nuclei sizes present in the test water. [71] The curves shown in Figure 4.4 are average curves drawn through the data.
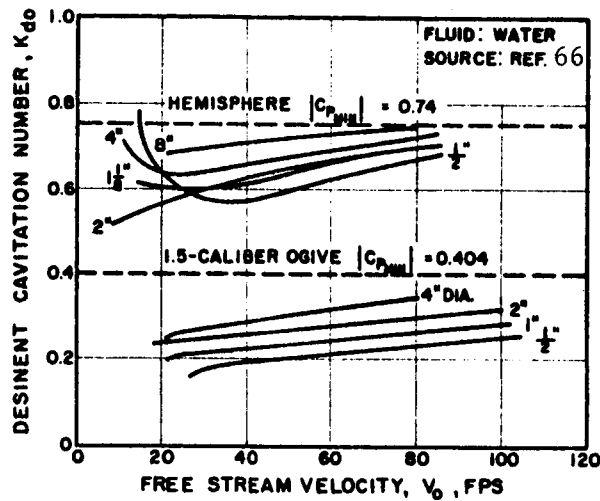
Figure 4.4   Incipient Cavitation Number as a Function of Free-Stream
Velocity for Bodies With Hemispherical
Noses and 1.5-Caliber Ogive Noses

Figure 4.5 shows how the desinent cavitation number varies with the Reynolds number for the flow of water past Joukowski hydrofoils. For a given size the desinent cavitation number increases with the Reynolds number. Furthermore, for a given Reynolds number, the desinent cavitation number decreases with increasing size. On the other hand, the NACA 16012 hydrofoil data shown in Figure 4.6 differ markedly from the trend shown in Figures 4.4 and 4.5. In Figure 4.6 the cavitation number decreases for a given size with

increasing Reynolds number (with increasing velocity) and increases

for a given Reynolds number with increasing size. This unique

behavior goes together with the flat pressure distribution of these

profiles at 0-degree angle of attack (see Figure 4.7) in contrast

to the peaked minimum pressure of other streamlined bodies treated.

Calehuff and Wislicenus [74] reported that cavitation on the profiles

with flat pressure distribution had the form of traveling bubbles,

whereas with peaked under-pressures cavitation appeared to be attached

to the surface.

In Figures 4.5 and 4.6 the scale effects can be seen. Also, the

effect of pressure distribution on the inception of cavitation is

shown to have an important influence.
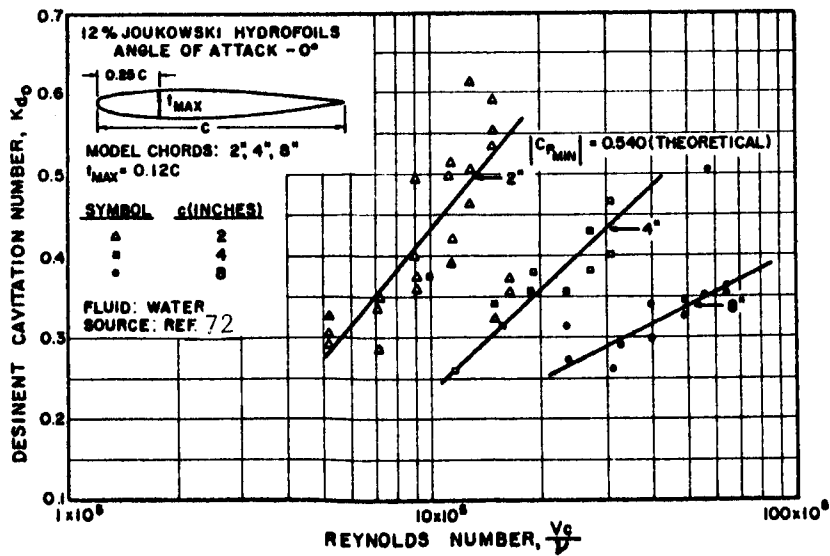
Figure 4.5   Desinent Cavitation Number as a Function of Reynolds
Number for Water Flowing Past
Joukowski Hydrofoils
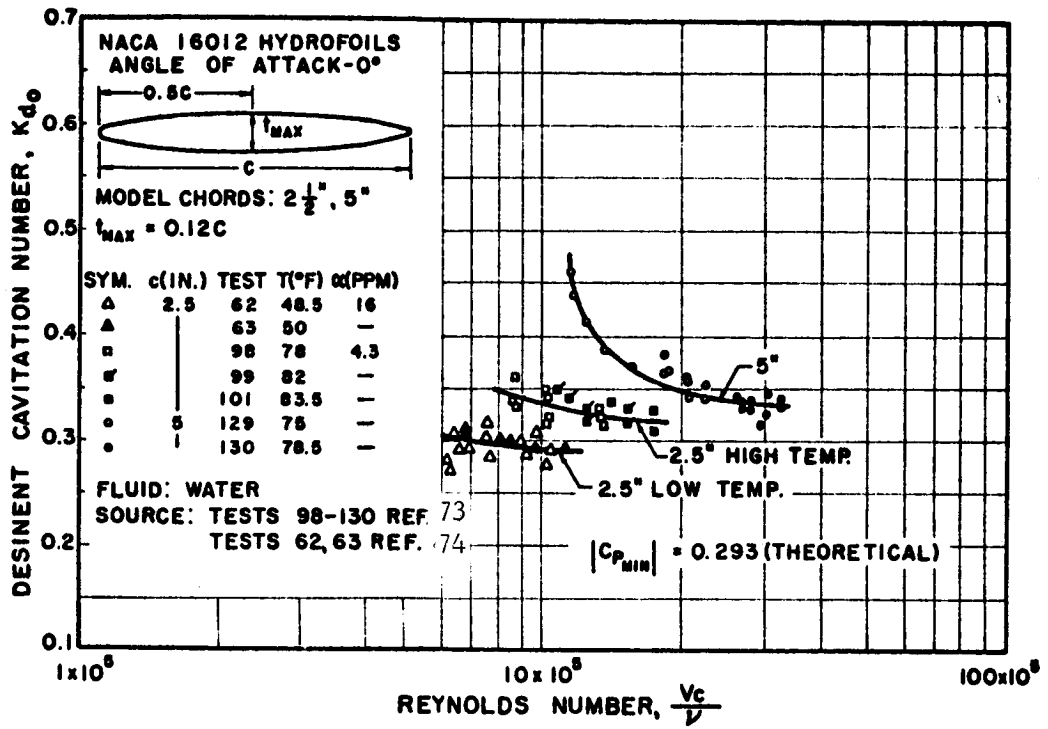
Figure 4.6 Desinent Cavitation Number as a Function of Reynolds
Number for Water Flowing Past NACA 16012 Hydrofoils
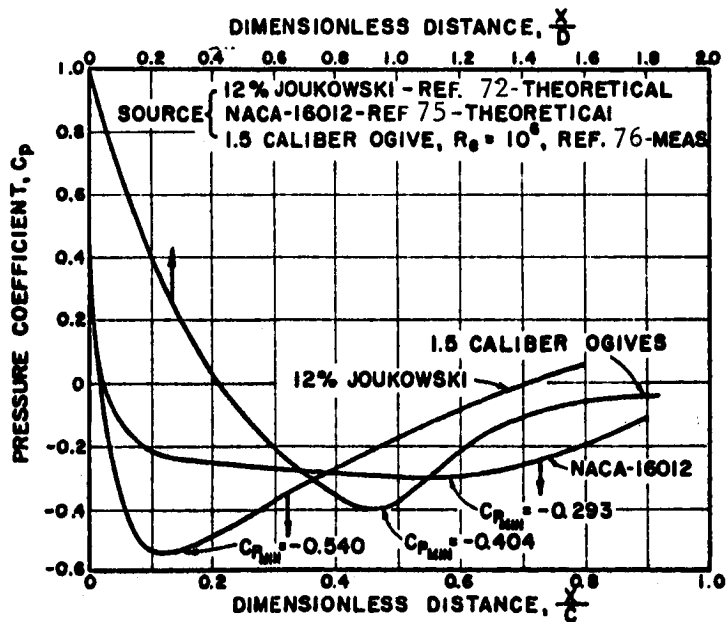
Figure 4.7 Pressure Distributions for Streamlined Bodies

The type of flow in the boundary-layer has an important effect on the inception of cavitation. Daily and Johnson [71] investigated the effects of a turbulent boundary-layer on the inception of cavitation for the flow of water through a two-dimensional nozzle. The flow in the boundary-layer was rotational and the minimum pressure did not occur on the wall (for large body curvatures) but slightly away from it in the center of the eddies that compose the boundary-layer. Thus cavitation can actually begin at values of K_o that are slightly greater than $|C_{p_{min}}|$ because of the additional pressure reduction caused by turbulence. However, Daily and Johnson pointed out that the boundary layer turbulence effect is small and can usually be neglected at the high velocities that are normally encountered in hydraulic structures where cavitation is expected.

The effect of air content on the occurrence of cavitation, for water flowing past hydrofoils, was investigated by Holl [56]. These hydrofoils were tested at various angles of attach. Figure 4.8 shows the results of these tests.

Holl [56] observed that two types of desinent cavitation could be determined. As the pressure was increased causing the cavitation to disappear, a pressure was reached where the cavitation disappeared uniformly across the span. This was referred to as areal cavitation. However, it was observed that several cavitation bubbles still clung to the surface and continued to do so up to very high ambient pressures. These spots of cavitation were manifest on the NACA 16012 hydrofoils at angles of attack above the critical angle.

NACA 16012 HYDROFOILS

TEST	61	133
CORD, INCHES	2.5	5
ANGLE OF ATTACK	2.5°	2°
α, PPM	17.3	7.3
TEMPERATURE, F	74.8	74.8
SPOTS OF CAVITATION	+	□
AREAL CAVITATION	●	○
β, PSI/PPM	1.03	1.03

FLUID: WATER
SOURCE: REF. 56

$K_{d_0} = 0.45 + \dfrac{\alpha\beta}{\frac{1}{2}\rho_0 V_0^2}$

C = 2.5"
θ = 2.5°

$K_{d_0} = 0.4 + \dfrac{\alpha\beta}{\frac{1}{2}\rho_0 V_0^2}$

$|C_{p_{min}}| = 0.8$
CORD = 2.5 in.

C = 5"
θ = 2°

$|C_{p_{min}}| = 0.6$
CORD = 5 in.

AREAL CAVITATION

C = 2.5"
θ = 2.5°

(Y-axis: DESINENT CAVITATION NUMBER, K_{d_0}, from 0.2 to 2.0)
(X-axis: FREE STREAM VELOCITY, V_0, FPS, from 0 to 140)

Figure 4.8 Two Types of Cavitation on 2.5-in. and 5-in.
NACA 16012 Hydrofoils

The critical angle of attack is that angle at which the change of $|C_{p_{min}}|$ with angle becomes very large. The critical angle of attack for the NACA 16012 hydrofoils is about 1.5 degrees. [75]

Oshima [77] developed a relation, from boundary-layer gas-nuclei interaction considerations, which allows predicting the Reynolds number variation in K_{i_0} for flow past axially symmetric bodies. Calculations of the turbulent boundary-layer growth on the test bodies were combined with the suggestions of Daily and Johnson [71], concerning nuclei growth and turbulence effects to predict the scaling of cavitation inception as observed on the axisymmetric bodies referred to previously. Oshima's formula appears to correspond closely with some selected experimental data. However, before definite conclusions can be formed about this work, additional experimental investigations (with liquids other than water) are necessary.

71

Knapp [78], in 1952, derived a formula which is similar to Oshima's formula. However, Oshima was able to show that Knapp's formula is a special case of his theory.

The inception of cavitation on isolated surface irregularities imbedded in a turbulent boundary layer was investigated experimentally and theoretically by Holl [79] and [73]. Holl was able to show how the effect of a small roughness element (of height, h) on a smooth surface may greatly increase the inception cavitation number (see Figure 4.9). In terms of the inception cavitation number, K_{r_o}, of
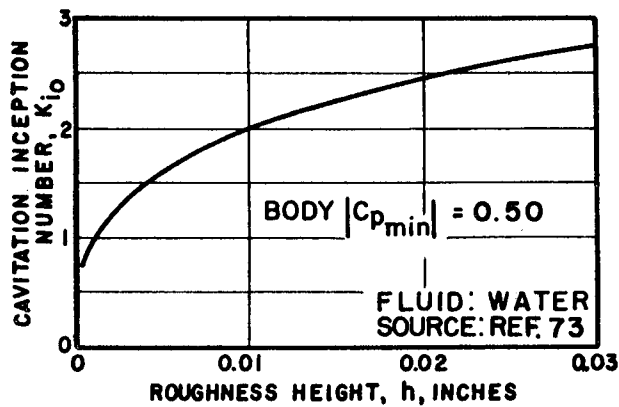
Figure 4.9 Calculation Effect of Relative-Roughness
for a Particular Flow

the roughness element and the pressure coefficient of the smooth body, the inception cavitation number of the roughened body is

$$K_{io} = -C_p + (1-C_p)K_{r_o} .$$

(4.8)

The roughness is most detrimental when placed at the minimum pressure-point of the parent body, that is, when $C_p = C_{p_{min}}$.

Holl [79] determined how K_{r_0} varied with the ratio of the height of a roughness element, h, to the boundary-layer thickness, δ, for different velocity-profile shapes and two different shapes of roughness elements. The velocity-profile shape was expressed by the boundary-layer shape parameter $H = \dfrac{\delta^*}{\theta}$, where δ* is the displacement thickness and θ the momentum thickness. Two families of cylindrical roughness elements having constant cross section were studied. One family had a circular-arc cross section. The other family had a triangular cross section. The results of this study are shown in Figure 4.10.
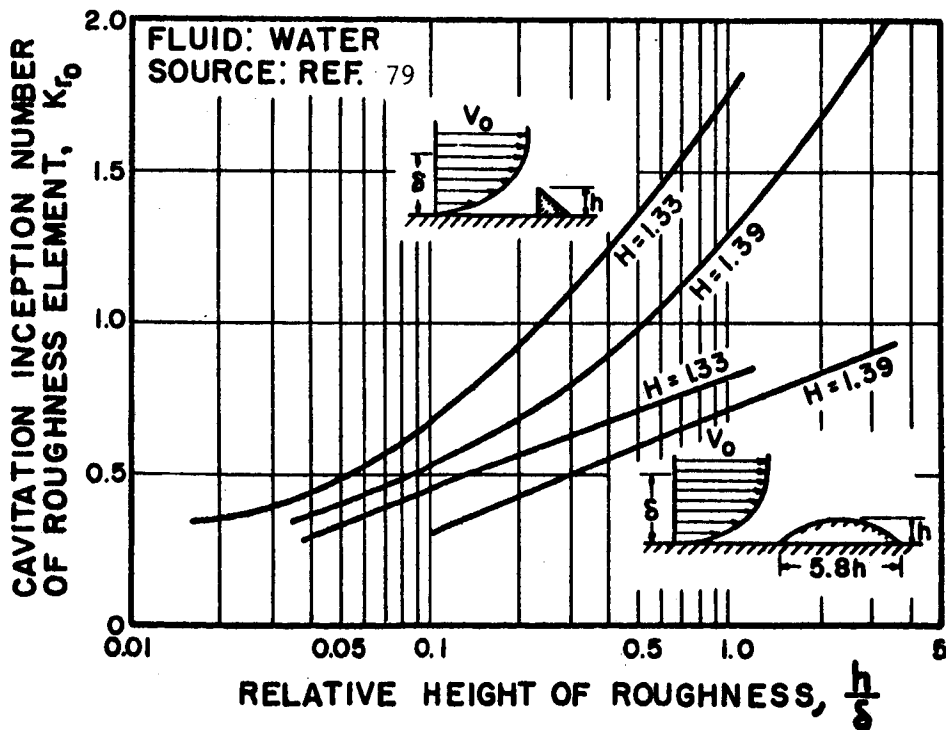
Figure 4.10   Cavitation Inception on Roughness Elements
in Boundary-Layer Flows

The seriousness of roughness effects in producing cavitation
inception scale effects is illustrated by the following example.
[79] Consider a body with $C_{p_{min}}$ = -0.50 of such proportions and
tested at such a speed (V_o = 50 fps) that δ = 0.048 in. As
Figure 4.9 shows, the effects for the sharp roughness of Figure
4.10 (and a fairly-normal turbulent boundary layer of H = 1.33)
are considerable. A 102% (K_{i_o} - $|C_{p_{min}}|$ / $|C_{p_{min_s}}|$ x 100) increase
in K_{i_o} occurs for a 0.001 in. high roughness and much larger
effects are easily possible.

B. Separated Flows Past Non-Streamlined Bodies

If the flow past a body is decelerated too rapidly, the
boundary-layer separates and the pressure distribution along the
boundary is no longer a true indication of the minimum pressure
in the field. Unfortunately, there is no exact method of obtaining
the minimum pressure coefficient in the flow field in terms of the
measured boundary pressure. Nevertheless, some experimental studies
of cavitation inception have been reported.

Most of the available test data pertain to sharp-edged disks
(Figure 4.11) and zero caliber ogives, i.e. cylinders with a flat
cutoff end facing the flow (Figure 4.12). The most striking
difference, as compared to the behavior of streamlined bodies, lies
in the magnitude of the changes in the desinent cavitation number,
which varies by a factor of two for a change in Reynolds number
by a factor of ten. This appears to be at least twice the largest
change observed with most of the streamlined bodies (excepting the
Joukowski hydrofoil data shown in Figure 4.5). Furthermore, the

74
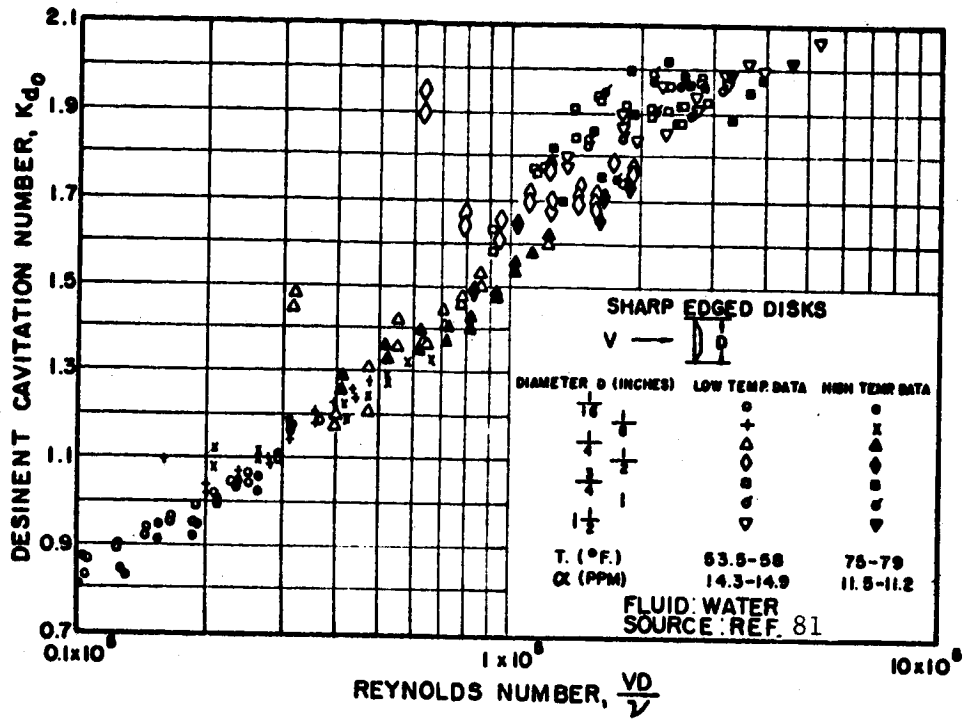
Figure 4.11 Desinent Cavitation Number as a Function of Reynolds Number for Water Flowing Past Sharp-Edged Disks
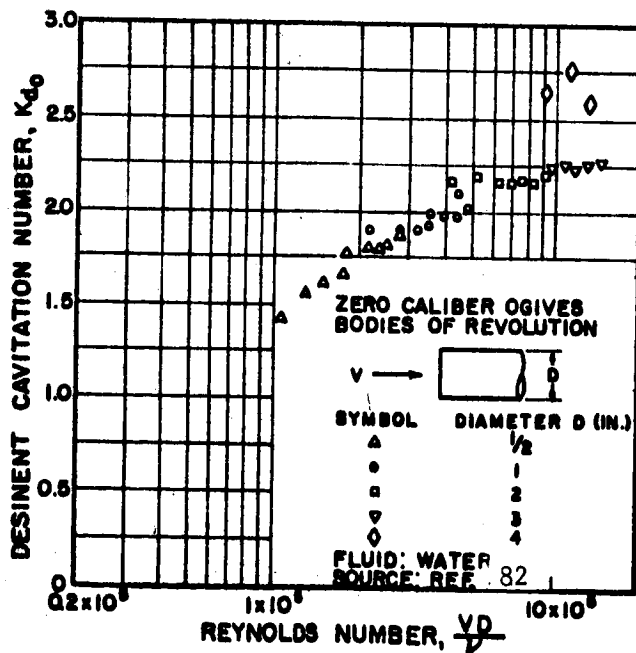
Figure 4.12 Desinent Cavitation Number as a Function of Reynolds Number for Water Flowing Past Zero-Caliber Ogives

cavitation number of bluff bodies (i.e., separated flow) continues

to increase with increasing Reynolds number. In this respect the

test points of the zero-caliber ogives (Figure 4.12) seem to continue

the sharp disk data (Figure 4.11) without a break or indication of

leveling off.

C. Flow in Venturi-Type Nozzles

The venturi-type nozzle has proved to be an effective

shape for studying cavitation. This is due to the fact that a

wide range of flow conditions are easily obtained. Thus, studies

can be made for various degrees of cavitation under different

pressure distributions.

In the experiments cited above (Kermeen, McGraw, and Parkin

[66]), no consistent effect of air content, varied between 7 and

13 ppm, could be detected. This disagrees with the observations

of Numachi and Kurokawa [83], McCormick [80], Crump [84], [85], and

others. Crump [84] found a significant dependence of inception on

total air content in experiments with a venturi nozzle having a

diffuser angle of 5°. He reports that in fully aerated fresh water,

cavitation first appeared at the boundary in the form of a small

vapor cavity. In deaerated fresh water, Crump found that cavitation

first appeared in the form of individual bubbles which do not neces-

sarily form at the boundary. Under these conditions, bubbles formed

and disappeared downstream under ambient tensions as high as four

atmospheres. Furthermore, he found that higher tensions were re-

quired as the velocity was increased.

76
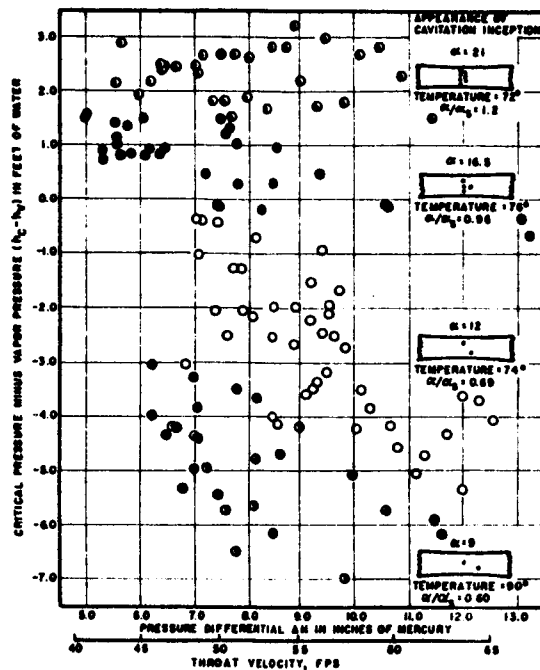
Figure 4.13 Critical Pressures for the Inception of
Cavitation in Fresh Water of Varying Air Content

Figure 4.13 shows that in the undersaturated liquid it was
possible to obtain tensions as the relative air content α/α_s
was reduced. Results in a nozzle with an abrupt expansion,
however, show opposite trends in the pressures required for
inception; [85] although here, too, tensions were obtained.
Comparable results for sea water are shown in Figure 4.14; in
this case, bursts of cavitation were observed at pressures well
above vapor pressure. While the trends in these experiments were
fairly definitive, the very large scatter of results is indicative
of the need for understanding the behavior and distribution of
nuclei; i.e, the mechanisms by which nuclei are stabilized and
the characterization of nuclei content; e.g., a "spectrum," or
description of number and distribution in size. [97]

77
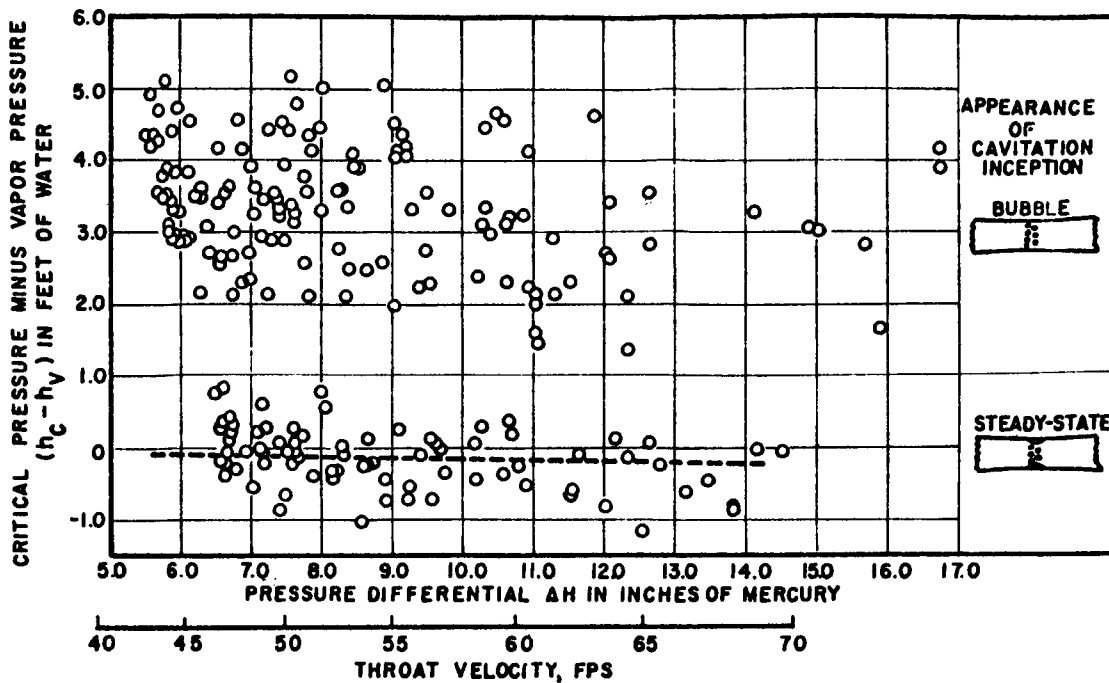
Figure 4.14 Critical Pressures for the Inception of Cavitation
in Sea Water

Williams and McNutly [86] investigated the effect of an additive
(sodium nitrate dissolved in distilled water) on cavitation inception.
The incipient cavitation number was found to increase (cavitation
to become easier) with an increase in the percentage (from 0 to 0.4%
by weight) of dissolved sodium nitrate.

The flow of liquid nitrogen through a venturi test section has
been investigated by Ruggeri and Gelder [88]. Just prior to incipient
cavitation, the minimum local wall pressure was significantly less
than the vapor pressure corresponding to the stream liquid temperature.
This pressure difference was called effective liquid tension. The
temperatures and pressures measured within regions of well-developed
cavitation were in thermodynamic equilibrium but were less than the
temperature and the saturation vapor pressure of the approaching

78

stream. These differences increased with both stream velocity and extent of cavitation.

Figures 4.15 and 4.16 show comparisons of cavitation tests of Nitrogen, Water, Freon-114, and Ethylene glycol (References [88], [87], [89], and [90]) in the same venturi test section. Nitrogen sustained more effective tension than the other liquids tested. This indicates a possibility that temperature influences the nuclei within the liquid and test section.

The effective tensions for all liquids studied increased with increasing flow velocity. The effective tensions for Freon-114 increased appreciably as the temperature was increased from 0° to 80^oF. The effective tensions for Ethylene glycol were practically independent of the temperature level for the range studied. For water in the 40° to 80^oF range, effective liquid tension was practically independent of temperature but increased appreciably as the temperature was increased to 120^oF.
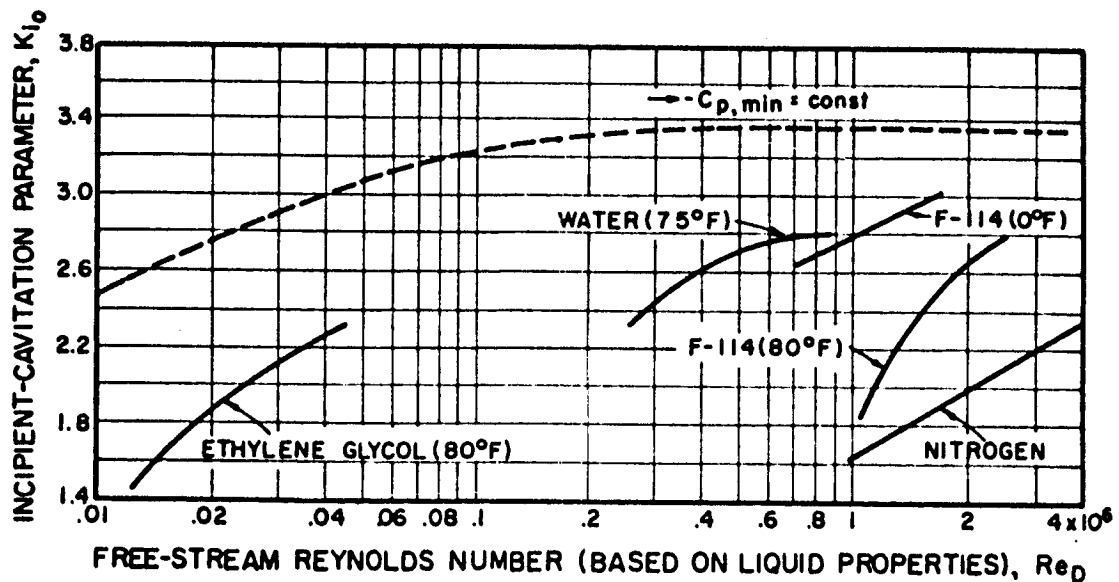
Figure 4.15 Comparison of Incipient Cavitation Number for Nigrogen, Water, Freon-114, Ethylene Glycol Flowing Through Same Venturi Model

79
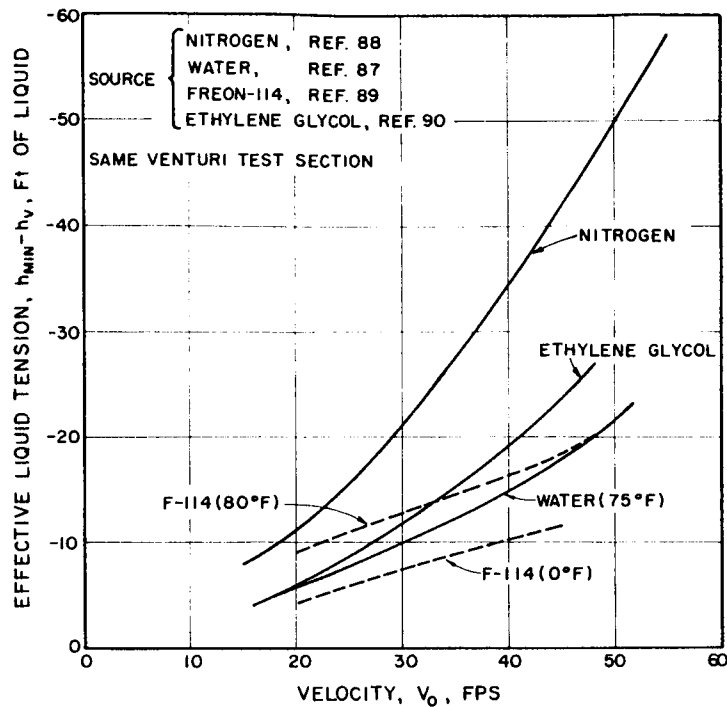
Figure 4.16 Comparison of Effective Liquid Tension Based on Visible Incipient Cavitation for Nitrogen, Water, Freon-114, and Ethylene Glycol Flowing Through Same Venturi Model

Lehman and Young [57] investigated the pressures and cavitation numbers, near the location where incipient and desinent cavitation occurred, for water flowing through different convergent-divergent test sections. The results of this investigation are shown in Figures 4.17 and 4.18. The cavitation pressures measured near the plane of incipient and desinent cavitation were generally higher for the tests made using an abrupt contour test section. The curves shown in Figure 4.17 disagree with what might be expected.

Hammitt [91] made an investigation similar to the investigation made by Lehman and Young [57]. Hammitt observed no difference between the incipient and desinent cavitation numbers while studying the flow of water through a smoothly changing internal contour nozzle. This corresponds closely with the investigation made by Lehman and

80
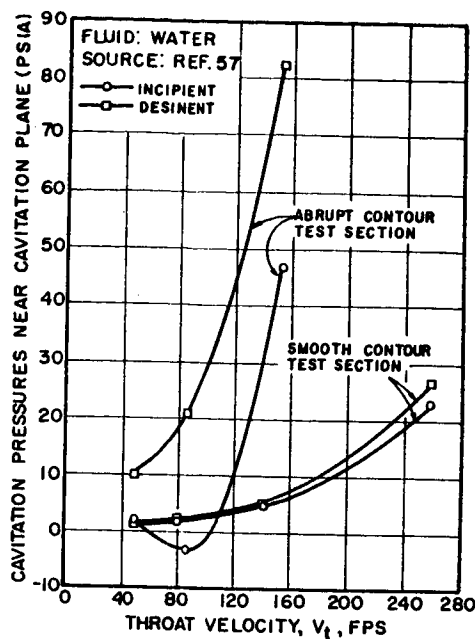
Figure 4.17   Cavitation Pressures Near Cavitation Planes As a Function
of Stream Velocity at the Throat of a Venturi
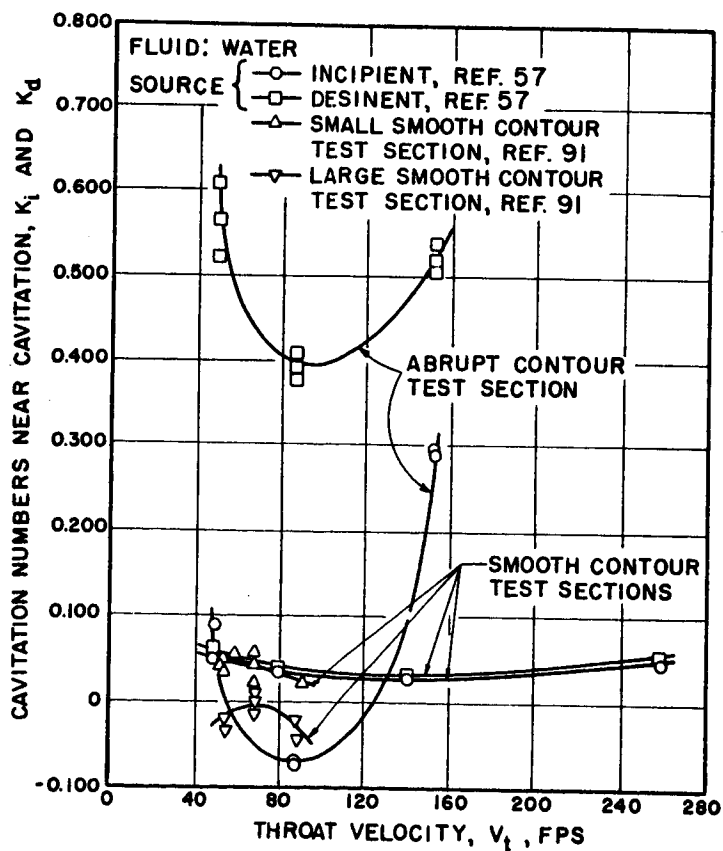
Figure 4.18   Comparison of Cavitation Numbers for Water
Flowing Through Abrupt- and Smooth-Contour
Venturi Type, Test Sections

81

Young on a similar shape nozzle. However, the abrupt contour tested by Lehman and Young indicates that the conditions at the plane of cavitation are a function of the pressure distribution prior to cavitation.

D. Flow Through Orifices

The jets flowing from orifices into filled conduits (sudden enlargements) represent cases of extreme separation where, in addition to expansion and diffusion of the main jet, there is the generation of secondary flow and countless small eddies and vortices. The pressures within the eddies will be appreciably below that of the surrounding fluid, particularly when the velocity of orifice efflux is high. These low pressures can quite easily reach the vapor pressure of the fluid and there exists the possibility of cavitation.

The effect of cavitation on the discharge coefficient of orifices has received some attention [93], [94]. However, only the investigation of the flow of pure fluids through orifices will be reported at this time.

Jacobs and Martin [92] investigated the flow of water, liquid hydrogen, and liquid nitrogen through sharp-edged orifices. They were unable to produce cavitation as long as pure liquid entered the orifices. With liquid nitrogen, the pressures at the venae contractae were as much as 170 inches of liquid below the vapor pressure, while with liquid hydrogen the pressures at the venae contractae were as much as 192 inches of liquid below the vapor pressure. These were the lowest pressures attainable with their apparatus.

Jacobs and Martin observed that the only way cavitation could be produced was to have two-phase flow entering the orifices. In many tests even when two-phase flow entered the orifices, cavitation symptoms were not evident.

E. Flow Through Conduits

Mikol and Dudley [95] investigated the conditions at which cavitation inception occurs for the flow of Freon-12 through small bore copper and glass tubes. The point of inception of cavitation was observed to move by discrete jumps rather than in a continuous manner as operating conditions were changed. This was probably due to the gradual and uniform pressure gradient in the tube. In venturi test the inception site is fixed within rather close limits by the nonuniform and sharper pressure gradients imposed by the geometry. No such shift has been reported in any venturi test.

Mikol and Dudley observed that the tube material had the most important influence on the incipient cavitation number. The incipient cavitation number for the glass tube was nearly twice that for the copper tube. This result is in agreement with the nucleation theory expectation that a metal surface should provide many more nucleation sites than a glass surface.

Fauske and Min [96] investigated the flow of slightly sub-cooled Freon-11 through apertures and short tubes. They used a modified cavitation number to establish a criterion for determining single-phase or two-phase flow regimes in short tubes. The modified cavitation number is:

$$\bar{K}_o = \frac{2g \, \Delta P}{P_o V_o^2} \left(\frac{L_1}{D}\right) , \qquad\qquad (4.9)$$

where ΔP is the pressure difference, $p_o - p_e$ for two-phase flow

or $p_o - p_b$ for single-phase flow. Figure 4.19 indicates that

for modified cavitation number below 10 the fluid exhibits completely

metastable single-phase flow. When the modified cavitation number

exceeds 14, two-phase flow exists. In the range of $\bar{K}_o$ between

10 and 14, unstable transitional flow occurs.
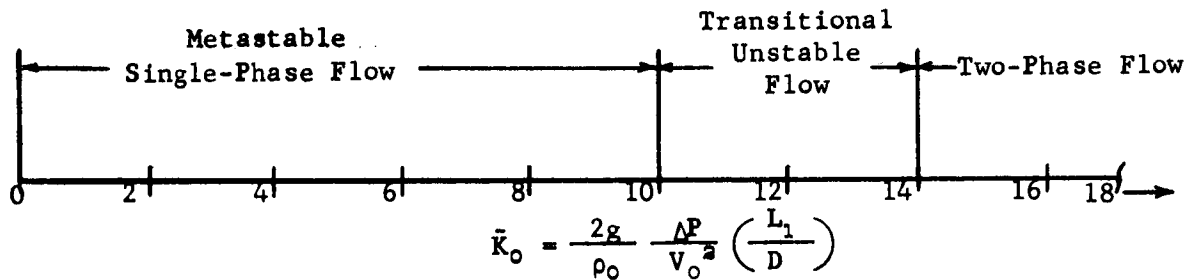
Figure 4.19 Correlation Number Determining the
Occurrence of Single- and Two-Phase Flow Regimes. [96]

4.6 Conclusions

The preceding discussions are primarily an attempt to point

out some of the knowns and unknowns about cavitation. For a

constant cavitation number, both the time of exposure to the

region of pressure below the vapor pressure (underpressure)

and the amount of this underpressure, are functions of velocity.

It may not be unreasonable to assume that the gross cavitation

pattern is largely controlled by the nucleation process. It

is conceivable that the nucleation process may depend upon time

of exposure to underpressure and absolute value of this under-

pressure in such a way that the effects are not cancelled for

constant cavitation number. With systematic experimental studies of different liquids flowing through various pressure distributions, it may be possible to obtain a reasonably correct Ki_o value or trend for an arbitrary body and liquid by means of some relations between underpressure and relaxation time (time fluid remains at pressures below the vapor pressure before cavitation occurs). Also, a method is needed to accurately predict the conditions at the position where cavitation starts for limited and profuse cavitation.

In the literature reviewed there is a total absence of experiments related to the cavitation phenomenon for flow in bends. Most of the conduits in hydraulic machinery where cavitation occurs are curved. There are no clear ideas as to what actually takes place under such conditions. What portion of the flow is actually vaporized is of interest. Also, it would be interesting to see how compound liquids (petroleum oils) behave under cavitating conditions.

CHAPTER V

Previous Investigations on Bubble Dynamics

5.1 Introduction

Bubble dynamics is the study of bubble growth and collapse. The primary variables affecting the growth and collapse are — the type of liquid around the bubble, the temperature and pressure fields in the liquid and inside the bubble, and the type of gas inside the bubble. In this report only the single component, liquid-vapor phase will be considered.

A knowledge of bubble dynamics is useful in the correlation of heat transfer data in the boiling regime and in the prediction of cavitation in a flowing system. The cavitation problem is presented in detail in another section of this report. The application of bubble dynamics to heat transfer correlations is reviewed at the end of this chapter.

The theories on bubble dynamics are considered in three main groups: 1. growth in a superheated liquid, 2. collapse in a subcooled liquid, 3. growth in a non-uniform temperature field.

Since experimental verification of the theories on bubble dynamics has been limited to the asymptotic growth phase, the theories are considered for this phase only.

5.2 Bubble Growth in a Superheated Liquid

Rayleigh [98] developed the equation governing the motion of the bubble wall in growth and collapse of a bubble:

$$R\ddot{R} + \frac{3}{2}\dot{R}^2 = -\frac{p_\infty - p_v}{\rho_L} \tag{5.1}$$

It is possible to solve this equation for constant vapor pressure, p_v, by numerical methods and by repeated application of gamma function solutions. However, when a vapor bubble grows, the latent heat of vaporization must be supplied at the liquid-vapor interface by the liquid around the bubble. The resultant drop in liquid temperature reduces the growth rate of the bubble. A vapor bubble in a superheated liquid can be expected to grow without bound as long as there is superheat in the liquid to provide latent heat of vaporization.

The pressure in the bubble is not a constant since the temperature at the liquid-vapor interface may vary. The vapor pressure is taken, in all cases, to be the saturation pressure associated with the temperature at the bubble wall.

There have been several methods applied to the analytical solution of the bubble dynamics problem. Some assumptions identical in all approaches are:

1. The bubble is spherical in shape.

2. The pressure field in the liquid is known.

3. The temperature field in the liquid is known.

4. The surface tension pressure is $2\,\frac{\sigma}{R}$.

5. The liquid and vapor are pure.

6. Fluid motion is irrotational.

7. Viscosity effects are neglected.

8. The liquid is incompressible.

9. Thermal conductivities and specific heats are constant over this temperature range.

10. Bubble wall velocity equals liquid velocity at the wall.

11. Bubble wall velocity is small compared to sonic velocity in the liquid.

12. The vapor pressure and temperature are uniform inside the bubble.

13. The vapor inertia is neglected.

Where these assumptions are applied to the continuity equation and the equation of motion, a differential equation for the radius of the vapor bubble is determined:

$$R\ddot{R} + \frac{3}{2}\dot{R}^2 = \frac{P_v(T) - P_\infty}{\rho_L} - \frac{2\sigma}{\rho_L R}. \tag{5.2}$$

Equation (5.2) is the starting point for all analytical solutions. Variations in the theories result basically from the way in which the bubble wall temperature (and therefore vapor pressure) is determined.

A. Plesset-Zwick Approach

Zwick [99] solves Equation (5.2) using the liquid temperature, determined from the energy Equation (5.3), to find the vapor pressure.

$$\rho_L C_{P_L} \left\{ \frac{\partial T}{\partial t} + \vec{V} \cdot \nabla T \right\} = k \nabla^2 T + \dot{q} \tag{5.3}$$

He used boundary conditions on Equation (5.3) as follows:

$$R^2 k \frac{\partial T}{\partial r}\Big|_{r = R(t)} = \frac{L_v}{3} \frac{d}{dt} \left\{ R^3 \rho_v(T) \right\} \tag{5.4}$$

and

$$T(r,0) = T_0 . \tag{5.5}$$

The mathematics of solving Equations (5.2), (5.3), (5.4) and (5.5) together is presented and the bubble radius is given for four phases of bubble growth. The phases are arbitrarily selected by Zwick and are called: delay period, early phase, intermediate phase, and asymptotic phase. The phase classification depends upon which physical variables may be neglected for a given range of values. Zwick uses the physical properties of water to explain which terms may be neglected.

Plesset and Zwick [100] give an alternate solution to Equation (5.3). They consider the temperature change in the liquid to be concentrated in a thin boundary layer around the bubble and treat the problem as a nonsteady heat diffusion problem. Then in reference [101] they use the temperature distribution of reference [100] to solve the bubble dynamics problem. They use the relationship

$$\frac{P_v(T) - P_\infty}{P_L} = A(T - 100) \tag{5.6}$$

where A is a constant and T from reference [100]

$$T = T_0 - \frac{\bar{D}}{K}\eta(t) - \left(\frac{\bar{D}}{\pi}\right)^{1/2}\int_0^t \frac{R^2(x)\left(\frac{\partial T}{\partial r}\right)_{r=R(x)}}{\left\{\int_x^t R^4(y)dy\right\}^{1/2}} dx . \tag{5.7}$$

$\eta(t)$ is the heat source per unit volume and $\bar{D} = k/\rho C$.

Plesset and Zwick [102] give the asymptotic solution for a vapor bubble in a superheated liquid. The solution is the same as the one given in reference [101], but this analytical approach is compared with experimental data. The bubble growth rate is proportional to the square root of time:

89

$$R = R_0 \left(\frac{2}{\pi \mu}\right)\left(\frac{\kappa t}{3}\right)^{1/2} \qquad (5.8)$$

Plesset [103] discusses the validity of some of the assumptions made in the analytical solution given. He gives expressions to be used in assessing the error resulting from assuming that the vapor pressure is uniform and that the wall velocity is the liquid velocity. These expressions give a very good feel for the order of magnitude of the terms involved.

B. Forster - Zuber Approach

Forster [104] gives a mathematical solution to Equation (5.3) with no heat generation (i.e., $\dot{q} = 0$). He assumes that the motion of the bubble wall, $R = R(t)$, is a known function. The boundary conditions are either constant temperature or vanishing heat flux. He obtains an approximate solution of the original problem by solving

$$dT = \frac{dQ(x)}{4\pi \sqrt{\pi a}\ R^2(\xi)\sqrt{t-x'}} \left\{ 1 - \sqrt{\pi}\ \frac{\sqrt{a(t-x)}}{R(\xi)}\ exp\left[\frac{a(t-x)}{R^2(\xi)}\right] erf\left[\frac{\sqrt{a(t-x)}}{R(\xi)}\right]\right\}$$

where $R(\xi)$ is an appropriate mean value $= \sqrt{R(x)\ R(t)}$. He explains that the second term in this equation vanishes at $x = t$; and, when dT becomes small, neglecting the second term will result in small error. Therefore this term is neglected and the resultant solution is

$$T(t) = \frac{L_v\ \rho_v}{C_{p\ell}\ \rho_L\ (\pi a)^{1/2}} \int_0^t \frac{R^2(x)\ \dot{R}(x)\ dx}{R(x)\ R(t)\sqrt{t-x}} \qquad (5.9)$$

Forster and Zuber [105] solve Equation (5.2) by using the Clausius-Clapeyron relation

$$P_v - P_\infty = \frac{L_v}{T(\upsilon_v - \upsilon_L)}\ (T_{vs} - T_{\infty s}) \qquad (5.10)$$

90

Then $T_{vs} - T_{\infty g}$ is found from the solution of (5.9). In addition, when $R > R_o$ the terms $R\ddot{R} + \frac{3}{2}\dot{R}^2 + \frac{2\sigma}{\rho_L L_v R}$ may be neglected when compared to $(P_v - P_\infty)/\rho_L$. These terms are the hydrodynamic terms. For a growing vapor bubble in a superheated liquid the solution of Equation (5.2) with (5.9) and (5.10) need be completed only for a time interval from zero to one millisecond and then the hydrodynamic terms may be neglected. This solution also gives the bubble growth rate proportional to the square root of time.

Zuber [106] considers the problem of bubble dynamics in both a superheated and a subcooled liquid. He starts with a heat balance

$$\bar{h}(T_o - T_s) = L_v \rho_v \frac{dR}{dt} \tag{5.11}$$

for a uniformly superheated liquid. The heat transfer coefficient, $\bar{h}$, was determined from the one-dimensional transient heat conduction problem.

$$a\frac{\partial^2 T}{\partial z^2} = \frac{\partial T}{\partial t} \tag{5.12}$$

Then,

$$\bar{h}(T_o - T_s) = k\left(\frac{\partial T}{\partial z}\right)_{z=0} \approx \frac{k(T_o - T_s)}{\sqrt{\pi(at)}} \tag{5.13}$$

The solution of Equations (5.11) and (5.13) agrees satisfactorily with experiment.

C. Birkhoff, Margulies, and Horning

The above authors in reference [107] assume the solution of Equation (5.3) to be of the form:

$$T(r,t) = f(s) \tag{5.14}$$

where

$$s = r/(at)^{1/2} \tag{5.15}$$

This implies that the bubble growth rate is $K_1 (\alpha t)^{\frac{1}{2}}$. K_1 is a dimensionless parameter. Equation (5.3) with (5.14) and (5.15) gives

$$f''(s) + \left\{ s - \frac{2}{s} - \frac{(\rho_L - \rho_v) K_1^2}{\rho_L s^2} \right\} f'(s) = 0 \tag{5.16}$$

This solution to Equation (5.3) is then of the form

$$T(r,t) = A - B \cdot F_K(s) \tag{5.17}$$

A and B are constants and $F_K(S)$ is defined:

$$F_K(s) = \int_s^\infty x^{-2} \exp \left\{ -\frac{x^2}{4} - \frac{K_1^3 (\rho_L - \rho_v)}{2 x \rho_L} \right\} dx. \tag{5.18}$$

For one particular range of the dimensionless parameter, K_1, this solution gives the result

$$R = \left(\frac{12}{\pi} \right)^{1/2} \frac{\rho_L C_{p\ell}}{\rho_L L} (T_{ws} - T_\infty)(at)^{1/2} \tag{5.19}$$

This is the asymptotic growth rated equation determined by Plesset and Zwick for a uniformly superheated liquid. However, other ranges of K_1 give other asymptotic solutions.

D. Bankoff and Mikesell

Reference [108] considers Equation (5.2) where p_v and p_∞ are constant (the Rayleigh solution) and compares it with experiment. Then the authors solves the same equation allowing p_∞ to vary the

92

way it would in cavitating flow. The analytical solution of Equation
(5.2) with p_v constant is used to fit the experimental data.

E. Scriven Approach

Scriven [109] considers the growing vapor bubble in an infinite
medium of uniform superheat. He considers the growth to be controlled
entirely by the transport of heat and matter across the bubble boundary.
He states that the solutions presented above are valid only over re-
stricted ranges of pressure and superheat. His solution is exact under
the assumptions made and is adequate for all but the earliest stages
of bubble growth. He lists assumptions which are substantially those
of the beginning of this section. He arrives with Equations (5.2) and
(5.3) by considering the continuity equation, equation of motion, and
energy equation. The exact solution to Equations (5.2) and (5.3) results
from neglecting the hydrodynamic terms. His exact solution reduces ap-
proximately to those of Forster-Zuber and Plesset-Zwick, depending upon
the growth constant, $\beta*$. Where $\beta*$ is defined

$$R = 2\beta* \sqrt{at} .$$

(5.20)

Figure 5.1 is a comparison of Scriver's solution and the approximate
solutions:

$$R = \sqrt{\frac{2\Delta T \, K t}{\rho_v \left[L_v + (C_{p\ell} - C_{pv}) \Delta T \right]}} \; , \quad \beta* \longrightarrow 0$$

(5.21)

$$R = \left(\frac{12}{\pi} \right)^{1/2} \frac{\Delta T \sqrt{\rho_\ell C_{p\ell} K t}}{\left[L_v + (C_{p\ell} - C_{pv}) \Delta T \right]} \; , \quad \beta* >> 0$$

(5.22)
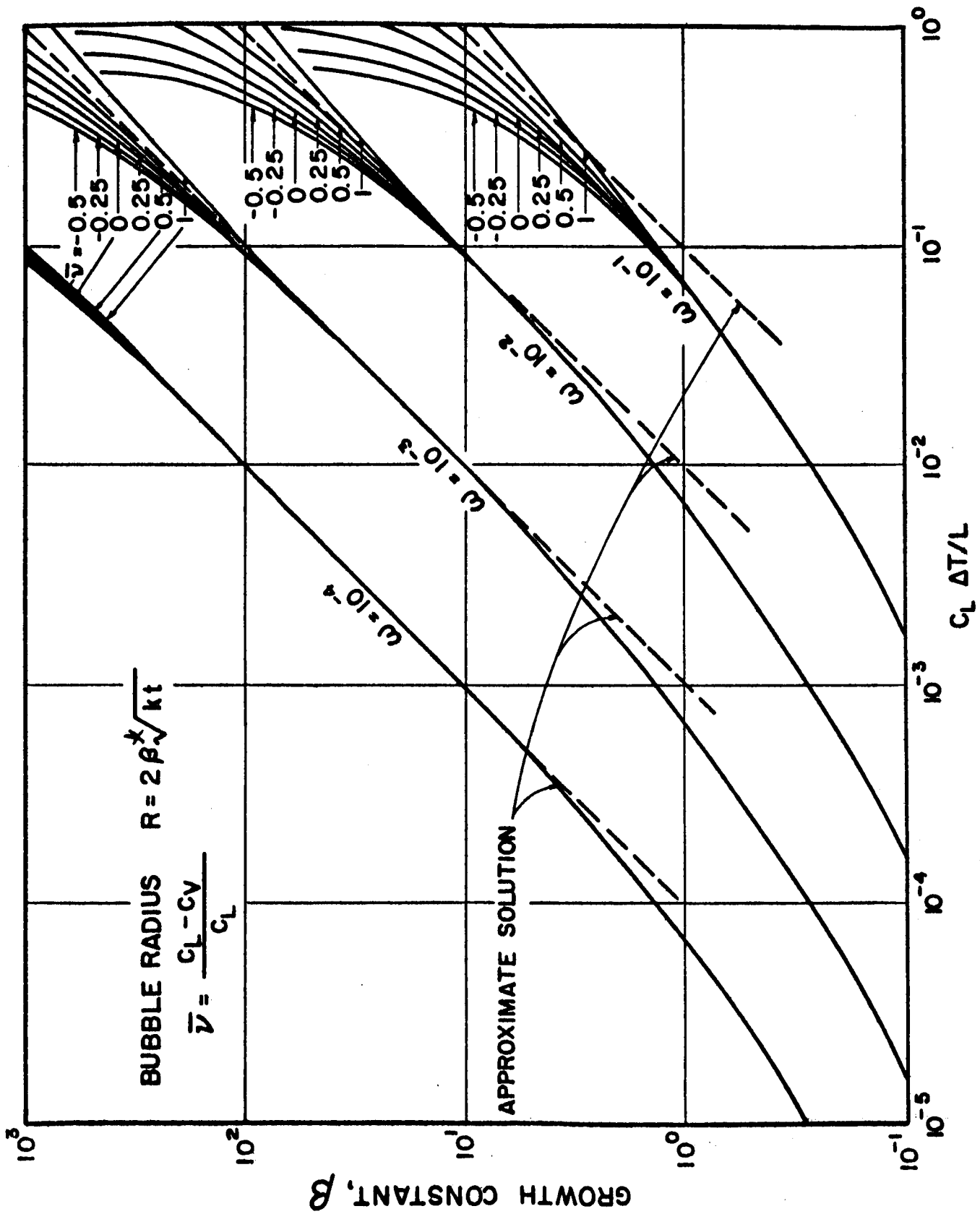
Figure 5.1 Scriven's Solution and Approximate Solutions Compared

Yang and Clark [110] solve Equation (5.3) neglecting the term $\bar{V} \cdot \bar{V}T$. The solution is almost identical to that of Forster-Zuber but a coefficient of bubble growth given by Scriven is again introduced and the final solution depends on the selection of β^*. This development is compared in a chart like Figure 5.1 to the solutions of Scriven and Plesset-Zwick. Plesset and Zwick's solution is a closer fit to the solution of Scriven than is the theory of Yang and Clark.

At a conference on bubble dynamics [111] Forster and Zwick discussed the merits of their two respective theories. The general conclusion reached was that the Plesset-Zwick theory could be as accurate as desired, depending only on the order of approximation; but that the first-order approximation in effect reduced the boundary layer to a thickness of zero and thus eliminated the convection term. The Plesset-Zwick solution requires the evaluation of twenty-two coefficients while the Forster-Zuber solution requires only two.

For all of the analytical solutions presented above, only the asymptotic growth phase has been studied experimentally because only in this phase of the bubble growth does the bubble become large enough to photograph easily. The following experimental work has been done in verifying the analytical approaches.

Degarabedian [112] observed bubble growths in superheated water, carbon tetrachloride, benzene, ethyl alcohol, and methyl alcohol, and found their growth rates close to those predicted by the Plesset-Zwick theory. The same author in reference [113] gives more details on water with the same result.

Parmentier and Schwemin [114] found that the Plesset-Zwick and

Forster-Zuber theories were adequate in predicting the bubble growth

in liquid hydrogen. The data of Ellion [115] for superheated water

is also correlated by these theories.

5.3 Bubble Collapse in a Subcooled Liquid

One reason for considering the bubble collapse separately from

growth is that for many collapse problems heat transfer effects may

be neglected and the heat Equation (5.3) need not be solved. (See

[101]. Florschuetz and Chao [116] examine the relative importance

of the effects of heat transfer and liquid inertia on collapse. In

highly subcooled liquid the liquid inertia terms dominate the collapse.

For this case the vapor pressure does not change from its initial

value.

For very small subcooling of the liquid, the collapse process

is very slow and the vapor pressure equals the external system pressure.

This results in purely heat transfer controlled collapse.

Between the two extremes the contribution of both heat transfer

and liquid inertia must be considered. For a subcooling of 78° C in

water, the heat transfer effect may be neglected with almost no error

[101].

Plesset and Zwick [101] also present a solution for the case

where heat transfer effects must be considered. The solution involves

the numerical integration of four equations given in Chapter 8. If

the experimental results from the present investigation show that the

Rayleigh solution does not apply, then the equations of [101] may be

solved for better correlation.

Bankoff and Mikesell [108] considered some experimental work of Ellion and found that the Rayleigh equation could be applied to the collapse with little error. This subcooling was 35° F.

McNieto [117] gives a power series solution of the Rayleigh equation for the collapse of a vapor bubble. This is valid for a zero vapor pressure. Numerical solutions in tabular form are presented.

Levenspiel [118] considers the Rayleigh solution in the form:

$$t = R_0 \sqrt{\frac{3 \rho_L}{2 P_\infty}} \int_{R/R_0}^{1} \left\{ \frac{(R/R_0)^3}{1 - (R/R_0)^3} \right\}^{1/2} d(R/R_0) \qquad (5.23)$$

R_0 = radius at start of collapse

He then includes the effect of residual permanent gas. However, except for this case the vapor pressure is assumed zero. The comparisons are plotted for visual observations.

Fritz [119] presents the integration of Equation (5.23) using gamma functions. The variables R/R_0 and

$$\int_{R/R_0}^{1} \frac{(R/R_0)^{3/2}}{[1 - (R/R_0)^3]^{1/2}} d(R/R_0)$$

are presented in tabular and graphical form. For each value of R, the time from the start of collapse can be determined using this table or graph and Equation (5.23) along with values of R_0, ρ_L, and P_∞.

The experimental works of Florschuetz and Chao [116] and Levenspiel [118] indicate that there is some heat transfer effect at subcooling of 30° F or less in water. It seems that more experimental work is

needed in this area. It must be pointed out that the Rayleigh equation

is not valid near the point of vanishing collapse since this equation

does not include the surface tension term.

5.4 Growth in a Non-Uniform Temperature Field

In heat transfer problems the heat is normally transferred to the

liquid from a solid boundary. This solid boundary sets up a non-uniform

temperature field in the liquid. Since all of the theoretical approaches

considered thus far have concerned only uniform temperature in the liquid,

additional boundary conditions must be applied to the previous theories.

A. Forster and Zuber

Zuber [106] extended the Fritz-Ende equation to include

the effect of a non-uniform temperature at a solid surface by adding

a term, q_b, corresponding to the heat transferred from the heating

solid to the liquid.

$$L \rho_v \frac{dR}{dT} = k \frac{T_0 - T_s}{\sqrt{\pi a t}} - q_b \tag{5.24}$$

Zuber suggests the modified equation to use in correlating data:

$$R = \frac{\Delta T \, c_{p_L} \, \rho_L}{L_v \, \rho_v} \sqrt{\pi a t} \left\{ 1 - \frac{q_b \sqrt{\pi a t}}{2 k \Delta T} \right\} \tag{5.25}$$

Forster [120] shows that another way to account for the non-uniform

temperature field results by considering an exponential temperature dis-

tribution of the form $T = T_\infty t \, (T_w - T_\infty) \, e^{-x/H}$. Here x is the distance

from the wall where the temperature is 1/e of the total change. Then

for $R \ll H$

$$R(t) \approx 2 \, \frac{\rho_L \, C_{p_L} \, \Delta T}{L_V \, \rho_V} \left(\frac{\alpha t}{\pi} \right)^{1/2}$$

and for   R >> H

$$R^2(t) = 4 \, \frac{\rho_L \, C_{p_L} \, \Delta T}{L_V \, \rho_V} \, H \left(\frac{\alpha t}{\pi} \right)^{1/2} + \text{const.} \tag{5.26}$$

This seems to indicate the correct power law for the experimental data
of Staniszewski [134] and Griffith [121].

B.   Griffith

In [121] Griffith assumes a linear variation of temperature
from the heating surface to a boundary layer depth into the liquid, b.
He gets two sets of differential equations and solves them by numerical
integration. All numerical solutions will not be presented in this
paper.

C.   Savic and Goshell

These authors in [122] consider both linear temperature
distribution from the wall and radial from the bubble. These results
are in fair agreement with the numerical results of Griffith. This
was also a numerical solution.

D.   Dougherty and Rubin

Dougherty and Rubin [123] correlate experiments according
to an asymmetry ratio, t_m/t_c, (where t_m = time to maximum bubble
radius and t_c is total bubble lifetime). For linear temperature dis-
tribution from the wall, no surface tension effects and no viscosity
effect,

$$R^2(t) \approx R_0^2(t) + \int_0^t d\tau \left\{ \frac{4 \, h_{fg}^2}{k_L \Delta v \, T_s} \left(\frac{\rho_v}{\rho_L} \right) \sqrt{\frac{a_L}{\pi} (t-\tau)} \left[R_\ell - (R - R_n) \right] - (t-\tau) R^2(\tau) \right\}$$ (5.27)

where:

    R_o = Bubble radius at start of asymptotic growth

    R_m = Maximum bubble radius

    R_n = Radius at nucleation

    R_r = Radius of isothermal bubble

The integral is made stationary using the calculus of variations and from this stationary curve

$$\frac{R}{R_m} \approx \frac{1 - (t/t_c)^{3/2} + (t_m/t_c)^{3/2} \ln (t/t_c)^{3/2}}{1 - (t_m/t_c)^{3/2} + (t_m/t_c)^{3/2} \ln (t_m/t_c)^{3/2}} .$$ (5.28)

Dougherty and Rubin checked Equation (5.28) with the data of Ellion and found close agreement. However, in most of these cases the mathematics involved is certainly complicated enough to be avoided when possible. The Zuber correlation seems to involve the least amount of complications.

Gunther [124] did some experimental work with water. This data was considered by Zuber but was not included in Zuber's article.

Ellion [115] performed experiments on subcooled boiling and this data was considered by all the papers presented on the non-uniform temperature approach. All claimed fair agreement.

The following references are for experimental work in surface boiling: [125], [126], [127], [128], [129]. Comparison to theory was not possible for many of these references.

5.5 Correlation of Boiling Heat Transfer Data

Engelberg-Forster and Grief [130] correlated boiling heat transfer data in terms of Δp (i.e., $p_v = p_\infty$) taken from Equation (5.2) and found one form of correlation that fit their experimental data. The equation is

$$\bar{q} = C_{p_l}\left(\frac{k}{25}\right)\Delta p(T_\omega - T_s)\left\{\frac{\rho_l^3 C_{p_l}^2 \pi a\, T_s^2 \Delta p^2}{N L_v^2 \rho_v^2}\right\}^{1/5}\left(\frac{N C_{p_l}}{k}\right)^{1/3}. \qquad (5.29)$$

Costello and Tuthill [131] experimented with superheated water under the effects of acceleration and found that only Equation (5.29) was satisfactory in correlating their data.

Forster and Zuber [132] show that the product of bubble radius and radial velocity is a constant and formulate a Reynolds number for flow in the superheated liquid near a heating surface. This Reynolds number becomes:

$$Re = \frac{\rho_l}{N}\left\{\frac{(T_{vs} - T_{\infty s})C_{p_l}\,\rho_l\sqrt{\pi a}}{L_v \rho_v}\right\}^2. \qquad (5.30)$$

They use this Reynolds number in correlating boiling heat transfer data and get:

$$\bar{q} = k(T_\omega - T_l)\sqrt{\frac{N Re\,\Delta p}{2\sigma\rho_l}}\cdot\sqrt[4]{\frac{\Delta p}{\rho_l}}\,Re^m \rho_r^{\,n} \qquad (5.31)$$

For n-pentane, benzene, ethanol, and water this correlation reduces to

$$Nu = 0.0015\,Re^{0.62}\rho_r^{0.33}. \qquad (5.32)$$

Equations (5.31) and (5.32) gave good experimental fits for the data of these liquids.

Zuber and Fried [133] state that in pool boiling the Forster-Zuber correlation $\left(\text{Equation (5.31)}\right)$ is valid for cryogenic fluids. It is also shown that the correlation Equation (5.29) is identical to Equation (5.32).

5.6 Summary

The fact that the analytical solutions are not consistent with each other and do not completely correlate the experimental data indicates that more work must be done in this field. However, the analytical solutions are accurate enough to be used in indicating the behavior of vapor bubbles.

The problems of non-spherical shape and non-equilibrium liquid-vapor conditions should be considered in future analytical studies.

The best pool boiling heat transfer correlation equations are based on the parameters involved in the bubble dynamics solution.

The equations governing bubble dynamics apply in the prediction of the growth and collapse of vapor bubbles in cavitating flow. The prediction of when a bubble will form is not possible from these bubble dynamics equations.

CHAPTER VI

Theoretical Investigation of Single-Phase
Conduit Models

6.1 Introduction

The purpose of this chapter is to give a detailed presentation of the theoretical investigation which has been performed concerning the dynamics of single-phase fluid conduit models. Linear and non-linear treatments are presented with attention being given to the effects of system accelerating and vibrating forces.

6.2 Exact Solution of the Linearized or First-Order Axisymmetric Navier-Stokes Equations

In Chapter II it was revealed that the Navier-Stokes equations may be linearized to give the form (see Appendix B for summary of vector notation)

$$\frac{\partial \bar{v}}{\partial t} = -\frac{1}{\rho_0} \nabla P + \nu_0 \left\{ \frac{4}{3} \nabla(\nabla \cdot \bar{v}) - \nabla \times (\nabla \times \bar{v}) \right\} \tag{6.1}$$

where $\bar{v}$ is the vector velocity given for an axisymmetric coordinate system by

$$\bar{v} = \mathbf{r}\, v_r + \mathbf{k}\, v_z \tag{6.2}$$

with $\mathbf{r}$ and $\mathbf{k}$ being the unit vectors in the r and z directions respectively. See Figure 2.1.

The first order continuity relation for a liquid may be written in vector form as

$$\frac{\partial P}{\partial t} + \rho_0 C_0^2 \, \nabla \cdot \overline{v} = 0 .$$

(6.3)

Now let's define a scalar potential φ and a vector potential $\overline{\psi}$ such that

$$\overline{v} = \nabla \varphi + \nabla \times \overline{\psi} .$$

(6.4)

If we take the divergence of (6.4) we have

$$\nabla \cdot \overline{v} = \nabla^2 \varphi$$

(6.5)

and also taking the curl of (6.4) yields

$$\nabla \times \overline{v} = \nabla \times (\nabla \times \overline{\psi}) = \nabla (\nabla \cdot \overline{\psi}) - \nabla^2 \overline{\psi} .$$

(6.6)

The vorticity vector $\overline{\zeta}$ is defined as

$$\overline{\zeta} = \nabla \times \overline{v}$$

(6.7)

so that $\overline{\zeta}$ and $\overline{\psi}$ are related by

$$\overline{\zeta} = \nabla (\nabla \cdot \overline{\psi}) - \nabla^2 \overline{\psi} .$$

(6.8)

For axisymmetric flow $\overline{\zeta}$ has only a component in the direction perpendicular to $\mathbb{r}$ and $\mathbb{k}$, thus in the $\ominus$ direction. It is necessary that $\overline{\psi}$ have only a $\ominus$ component also, as is obvious from Equation (6.8). We therefore write

$$\overline{\psi} = \ominus \psi$$

(6.9)

and now since

$$\nabla = \mathbb{r} \frac{\partial}{\partial r} + \mathbb{k} \frac{\partial}{\partial z}$$

(6.10)

104

we have from Equations (6.6), (6.8), (6.9) and (6.10) that

$$\nabla \times \bar{\mathcal{V}} = \bar{\zeta} = -\nabla^2 \bar{\psi}. \tag{6.11}$$

In summary then we see that the divergence of the velocity vector is related to φ by Equation (6.5) and the curl of the velocity vector, also referred to as the vorticity, is related to $\bar{\psi}$, for axisymmetric flow, by Equation (6.11).

If we take the divergence of Equation (6.1) we eliminate the vorticity since the divergence of a curl is zero, and thus

$$\frac{\partial \nabla \cdot \bar{\mathcal{V}}}{\partial t} = -\frac{1}{\rho_0} \nabla \cdot (\nabla p) + \frac{4}{3} \nu_0 \nabla \cdot \left[\nabla (\nabla \cdot \bar{\mathcal{V}}) \right]. \tag{6.12}$$

Substitution of (6.5) into (6.12) yields

$$\frac{\partial \nabla^2 \varphi}{\partial t} = -\frac{1}{\rho_0} \nabla^2 p + \frac{4}{3} \nu_0 \nabla^2 (\nabla^2 \varphi) \tag{6.13}$$

or

$$\frac{\partial \varphi}{\partial t} = -\frac{p}{\rho_0} + \frac{4}{3} \nu_0 \nabla^2 \varphi. \tag{6.14}$$

From Equations (6.3) and (6.5) we have also

$$\frac{\partial p}{\partial t} = -\rho_0 c_0^2 \nabla^2 \varphi. \tag{6.15}$$

Taking the partial derivative of (6.14) and substituting $\partial P / \partial t$ from (6.15) gives

$$\frac{\partial^2 \varphi}{\partial t^2} = c_0^2 \nabla^2 \varphi + \frac{4}{3} \nu_0 \frac{\partial}{\partial t} \nabla^2 \varphi. \tag{6.16}$$

If we take the curl of Equation (6.1) we have

$$\frac{\partial (\nabla \times \bar{\mathcal{V}})}{\partial t} = -\nu_0 \left\{ \nabla \times \left[\nabla \times (\nabla \times \bar{\mathcal{V}}) \right] \right\} \tag{6.17}$$

or

$$\frac{\partial \nabla^2 \overline{\psi}}{\partial t} = -\nu_0 \left\{ \nabla \times [\nabla \times (\nabla^2 \overline{\psi})] \right\} \tag{6.18}$$

or, after expanding the right side of (6.18)

$$\frac{\partial \nabla^2 \overline{\psi}}{\partial t} = \nu_0 \left\{ \nabla^2 (\nabla^2 \overline{\psi}) - \nabla[\nabla \cdot (\nabla^2 \overline{\psi})] \right\}. \tag{6.19}$$

From Equations (6.9) and (6.10) we see that $\nabla \cdot (\nabla^2 \overline{\psi}) = 0$ thus (6.19) may be reduced to

$$\frac{\partial \overline{\zeta}}{\partial t} = \nu_0 \nabla^2 \overline{\zeta} \tag{6.20}$$

or

$$\frac{\partial \psi}{\partial t} = \nu_0 \nabla^2 \psi. \tag{6.21}$$

Physically, Equation (6.16) is a viscous wave equation for plane or one-dimensional waves, thus φ is a viscous plane-wave potential function. Equation (6.20) is a vorticity diffusion equation.

Applying the Laplace transformation to (6.16) and (6.21) yields (assuming initial conditions zero)

$$s\hat{\varphi} = c_0^2 \nabla^2 \varphi + \frac{4}{3} \nu_0 s \nabla^2 \hat{\varphi} \tag{6.22}$$

and

$$s\hat{\psi} = \nu_0 \nabla^2 \hat{\psi} \tag{6.23}$$

where $\hat{\varphi}$ and $\hat{\psi}$ are the Laplace transformed quantities.

Solving Equations (6.22) and (6.23) by the method of separation of variables (see Appendix C) yields

$$\hat{\Psi} = A J_1(kr) e^{\gamma z} \tag{6.24}$$

and

$$\hat{\varphi} = B J_0(\beta r) e^{\gamma z} \tag{6.25}$$
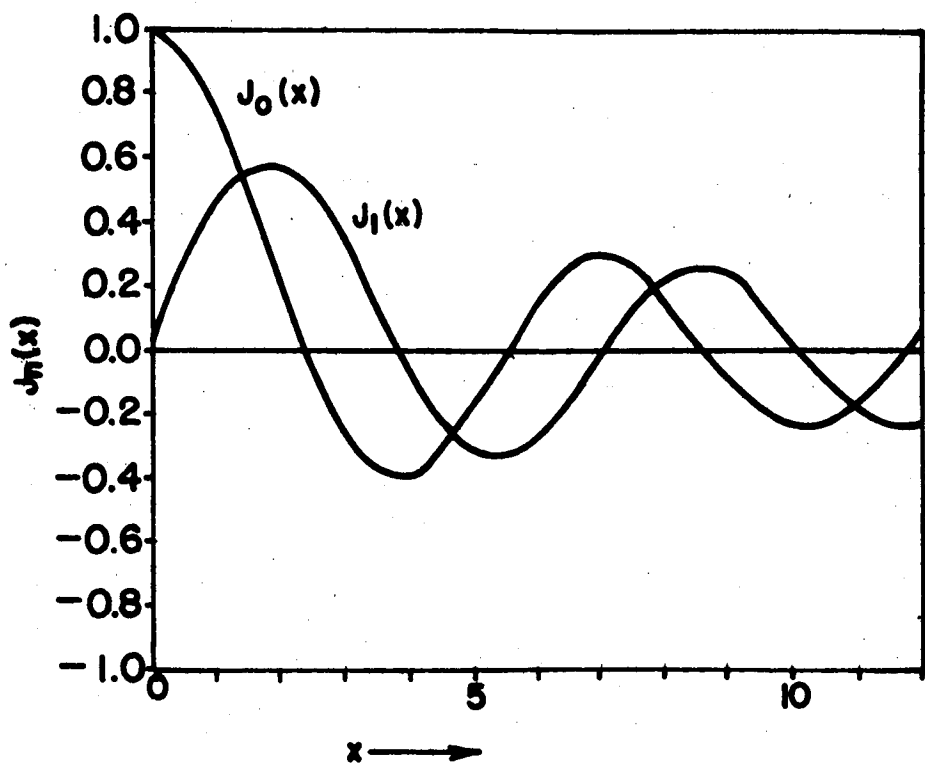
Figure 6.1 Bessel Functions

where A and B are constants of integration and γ is the separation

constant. $J_0(\beta r)$ and $J_1(Kr)$ denote the zero and first-order Bessel

functions of the first kind with arguments βr and Kr respectively

(See Figure 6.1). Also

$$K^2 = \gamma^2 - S/\nu_0 \tag{6.26}$$

and

$$\beta^2 = \gamma^2 - \frac{s^2}{c_0^2 + \frac{4}{3}\nu_0 s} \, . \tag{6.27}$$

Now that we have obtained $\hat{\varphi}$ and $\hat{\psi}$ we may obtain $\vec{V}$ from Equation (6.4)

or

$$\vec{V} = \nabla \hat{\varphi} + \nabla \times \hat{\psi} \tag{6.28}$$

where $\vec{V}$ denotes the transformed velocity vector. Since

$$\nabla \hat{\varphi} = \mathbb{r} \frac{\partial \hat{\varphi}}{\partial r} + \mathbb{k} \frac{\partial \hat{\varphi}}{\partial z} \tag{6.29}$$

and

$$\nabla \times \hat{\psi} = -\mathbb{r} \frac{\partial \hat{\psi}}{\partial z} + \mathbb{k} \frac{1}{r} \frac{\partial}{\partial r} (r \hat{\psi}) , \tag{6.30}$$

Equation (6.28) becomes

$$\vec{V} = \mathbb{r} \left\{ \frac{\partial \hat{\varphi}}{\partial r} - \frac{\partial \hat{\psi}}{\partial z} \right\} + \mathbb{k} \left\{ \frac{\partial \hat{\varphi}}{\partial z} + \frac{1}{r} \frac{\partial}{\partial r} (r \hat{\psi}) \right\} . \tag{6.31}$$

We may now write

$$V_r = \frac{\partial \hat{\varphi}}{\partial r} - \frac{\partial \hat{\psi}}{\partial z} = - \left[B\beta J_1(\beta r) + A\gamma J_1(kr) \right] e^{\gamma z} \tag{6.32}$$

and

$$V_z = \frac{\partial \hat{\varphi}}{\partial z} + \frac{\partial \hat{\psi}}{\partial r} + \frac{\hat{\psi}}{r} = \left[B\gamma J_0(\beta r) + A k J_0(kr) \right] e^{\gamma z} . \tag{6.33}$$

In Equation (6.32) and (6.33) we have implied the equality of the γ's from Equations (6.26) and (6.27), thus

$$\gamma^2 = k^2 + s/\nu_0 = \beta^2 + \frac{s^2}{c_0^2 + \frac{4}{3}\nu_0 s} \, . \tag{6.34}$$

At this point let us calculate the pressure, thus from (6.3) and (6.25) we have

108

$$\delta P = -\rho_0 c_0^2 \nabla^2 \hat{\varphi} = -\rho_0 c_0^2 B (\gamma^2 - \beta^2) J_0(\beta r) e^{\gamma z} \qquad (6.35)$$

or

$$P = -\frac{\rho_0 c_0^2}{s} B (\gamma^2 - \beta^2) J_0(\beta r) e^{\gamma z}. \qquad (6.36)$$

Equations (6.32), (6.33) and (6.36) are the simultaneous solution to the first-order axisymmetric Navier-Stokes Equation (6.1), and the continuity relation, (6.3). The constants of integration A and B and the separation constant γ are to be determined from the boundary conditions. The conditions at the pipe wall are that the fluid velocities and pipe wall velocities be equal and also that the pressure be continuous. In the sections that follow, the boundary conditions will be applied for the following cases:

    A. rigid pipe,

    B. elastic pipe with flexible walls,

    C. elastic pipe with stiff walls.

The limiting conditions which apply to this solution are:

    A. the fluid velocity at any point and time is much less than the velocity of sound in the fluid, thus justifying omission of the nonlinear terms,

    B. changes in the density ρ are small in comparison with the average density ρ_0,

    C. temperature effects are negligible,

    D. the flow field is axisymmetric.

6.3 Application of Exact Linear Solution to Case of Rigid Pipe

We will now apply boundary conditions to Equations (6.32), (6.33) and (6.36) for a fluid conduit with rigid walls. For this case we require

that both the radial and axial velocities go to zero at the pipe wall.

Applying these conditions to Equations (6.32) and (6.33) yields

$$B\beta J_1(\beta r_0) + A\gamma J_1(kr_0) = 0 \tag{6.37}$$

and

$$B\gamma J_0(\beta r_0) + Ak J_0(kr_0) = 0 . \tag{6.38}$$

Solving for A from Equation (6.38) and substituting into (6.37) gives

$$k\beta \frac{J_1(\beta r_0)}{J_0(\beta r_0)} = -\gamma^2 \frac{J_1(kr_0)}{J_0(kr_0)} . \tag{6.39}$$

The simultaneous solution of Equations (6.26), (6.27) and (6.39) will yield the allowed values for k, β, and γ. The exact solution of these relations would be rather laborous; but, fortunately, we can obtain very good approximate values. To get an idea of the range of values we are working with, consider first the case of no viscosity. Here the allowed values for $\beta_n r_0$ are

$$\beta_n r_0 = 0, \ 3.8317, \ 7.0156, \ 10.1735 \tag{6.40}$$

which shows that β is multivalued. Each value of β_n (except β_0) corresponds to a mode of radial vibration. The zeroth mode ($\beta = \beta_0$) corresponds to the primary or longitudinal mode of the conduit. The values of β_n as given by Equation (6.40) are only valid for the case of no viscosity; but, even so, an interesting observation may be made concerning the various modes of propagation. Consider the value of the propagation constant γ from (6.27) for the case of sinusoidal disturbances or

$$\gamma = \sqrt{\beta_n^2 - \omega^2/c_0^2} . \tag{6.41}$$

110

If γ is imaginary then the wave will propagate with the velocity ω/γ. If γ is real we have pure attenuation. We see then that the n'th mode of vibration will propagate only when

$$\omega > \beta_n c_0.$$

The frequency defined by $\beta_n c_0$ is a cut-off frequency below which no propagation will occur for the n'th mode.

Considering again the case with viscosity we will now get a more exact solution to Equation (6.39) for the zeroth mode than that of the inviscid case. In our first analysis we found that $\beta_0 = 0$ (zeroth mode). For this more exact analysis we will assume instead that β_0 is very small so that we may approximate $J_1(\beta_0 r_0)$ and $J_0(\beta_0 r_0)$ by their small argument values. Therefore assume

$$J_1(\beta_0 r_0) \approx \beta_0 r_0/2 \tag{6.42}$$

and

$$J_0(\beta_0 r_0) \approx 1 \;. \tag{6.43}$$

Substitution of Equations (6.42) and (6.43) into (6.39) gives

$$\beta_0^2 = 2\gamma_0^2 \left\{ \frac{J_1(k_0 r_0)}{k_0 r_0 J_0(k_0 r_0)} \right\} \tag{6.44}$$

or, by substituting Equation (6.44) into (6.34) we have

$$\gamma_0 = \left\{ \frac{\dfrac{s^2}{c_0^2 + 4/3\, \nu_0 s}}{1 - \dfrac{2 J_1(k_0 r_0)}{k_0 r_0 J_0(k_0 r_0)}} \right\} \tag{6.45}$$

where now $k_0 \approx i\sqrt{s/\nu_0}$. We have thus obtained a good approximate value for the zeroth mode propagation factor. The accuracy of the approximation

depends on the accuracy of the representations given in Equations (6.42) and (6.43).

The zeroth mode transformed axial velocity and pressure may be written from Equations (6.33), (6.36), (6.37) and (6.38) as

$$V_{z_0} = B_0 \gamma_0 J_0(\beta_0 r_0) \left\{ \frac{J_0(\beta_0 r)}{J_0(\beta_0 r_0)} - \frac{J_0(k_0 r)}{J_0(k_0 r_0)} \right\} e^{\gamma_0 z} \qquad (6.46)$$

and

$$P_0 = - B_0 \left(\frac{\rho_0 c_0^2}{S} \right) (\gamma_0^2 - \beta_0^2) J_0(\beta_0 r) e^{\gamma_0 z} . \qquad (6.47)$$

Applying the approximation of Equation (6.43) to (6.46) yields

$$V_{z_0} = B_0 \gamma_0 \left\{ 1 - \frac{J_0(k_0 r)}{J_0(k_0 r_0)} \right\} e^{\gamma_0 z} \qquad (6.48)$$

and similarly for (6.47), using (6.34) and (6.43) gives

$$P_0 = - \rho_0 S B_0 e^{\gamma_0 z} . \qquad (6.49)$$

If we consider the response of the zeroth mode velocity to a sinusoidal pressure gradient then we find that the time domain velocity may be expressed as

$$V_{z_0} = \frac{i K}{\rho_0 \omega} \left\{ 1 - \frac{J_0(r\sqrt{-i\omega/\nu_0})}{J_0(r_0\sqrt{-i\omega/\nu_0})} \right\} e^{i\omega t}$$

where the pressure gradient is

$$\frac{dP}{dz} = K e^{i\omega t} ,$$

For values of the parameter $r_0\sqrt{\omega/\nu_0} < 5$ the velocity profile is essentially parabolic while for values greater than 5 the profiles begin to look like

those shown in Figure 6.2. Notice that in the figure the fluid near the edges of the pipe responds more quickly than the fluid in the center of the pipe. This phenomena is called "Richardson's annular effect" and is discussed, for example, in Schlichting [2].
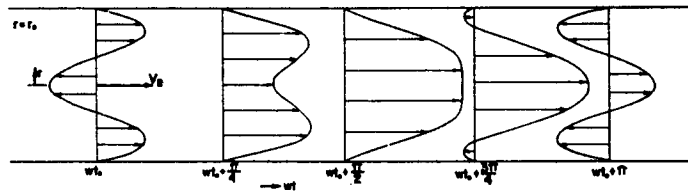
Figure 6.2   Velocity Profiles of Zeroth Mode
for Pulsating Flow in a Pipe

Thus far we have concerned ourselves with the discussion of only the zeroth mode of propagation*, or, also called the fundamental or longitudinal mode. What about the effects of the higher modes? The calculations involved in working with the higher modes is very cumbersome; but, fortunately, for most conduit dynamics applications the effects of these higher modes appear to be negligible. For this reason, all further discussions will deal with the zeroth mode unless otherwise specified.

---

*It is important to distinguish the modes of propagation being discussed here from the concept of frequency modes. Each of these modes of propagation can, in general, have an infinite number of frequency modes.

6.4 Derivation of Transfer Equations for Rigid Fluid Conduit

It is desirable to derive from Equations (6.48) and (6.49) a set of transfer equations which will describe the average conditions at some point z along the conduit in terms of the average conditions at $z = 0$.

In the previous section we found the zeroth mode axial velocity and pressure to be expressed as in Equations (6.48) and (6.49) or

$$V_{z_0} = B_0 \gamma_0 \left\{ 1 - \frac{J_0(k_0 r)}{J_0(k_0 r_0)} \right\} e^{\gamma_0 z} \tag{6.48}$$

and

$$P_0 = -\rho_0 S B_0 e^{\gamma_0 z}. \tag{6.49}$$

Since we have agreed to discuss only the zeroth mode unless otherwise specified, we will hereafter omit the "o" subscripts which refer to the zeroth mode. If we average Equation (6.48) across the conduit cross-section we have

$$\bar{V}_z = B\gamma \left\{ 1 - \frac{2 J_1(kr_0)}{kr_0 J_0(kr_0)} \right\} e^{\gamma z} \tag{6.50}$$

and

$$\bar{P} = -\rho_0 S B e^{\gamma z}. \tag{6.51}$$

Up to this point we have considered γ, for convenience, to have only positive values; but, in general, it will have both a positive and a negative value. Positive values of γ indicate waves progressing in the negative z direction and negative γ's indicate waves traveling in the positive z direction. Rewriting Equations (6.50) and (6.51) to include positive and negative values for γ yields

$$\bar{V}_z = \gamma \left\{ 1 - \frac{2 J_1(k r_0)}{k r_0 J_0(k r_0)} \right\} \cdot \left\{ B_1 e^{\gamma z} - B_2 e^{-\gamma z} \right\} \qquad (6.52)$$

and

$$\bar{P} = -\rho_0 S \left\{ B_1 e^{\gamma z} + B_2 e^{-\gamma z} \right\}. \qquad (6.53)$$

The boundary conditions which we wish to satisfy are

$$\bar{V}_z \Big|_{z=0} = \bar{V}_0$$

and

$$\bar{P} \Big|_{z=0} = \bar{P}_0 \quad .$$

Substitution of these boundary conditions into Equations (6.52) and (6.53) gives a pair of equations from which B_1 and B_2 may be found. Substituting these values back into (6.52) and (6.53) yields the transfer relations

$$\bar{V}_z = \bar{V}_0 \cosh \gamma z - \frac{\bar{P}_0}{Z_c} \sinh \gamma z \qquad (6.54)$$

and

$$\bar{P} = \bar{P}_0 \cosh \gamma z - Z_c \bar{V}_0 \sinh \gamma z \qquad (6.55)$$

where

$$Z_c = \frac{\rho_0 c_0^2 \gamma}{S} \quad . \qquad (6.56)$$

Equations (6.54) and (6.55) are then the zeroth mode transfer equations relating the average transformed conditions at some arbitrary z to the average transformed conditions at $z = 0$. We may rewrite these relations

115

in another convenient form relating the conditions at some other position

2 where 2 is oriented a +L distance from 1. This form is

$$\overline{V_2} = \overline{V_1} \cosh\Gamma - \frac{\overline{P_1}}{Z_c} \sinh\Gamma \qquad (6.57)$$

and

$$\overline{P_2} = \overline{P_1} \cosh\Gamma - Z_c \overline{V_1} \sinh\Gamma. \qquad (6.58)$$

It is convenient to omit the bar notation, which denotes the average

condition, while still keeping in mind that we are dealing with average

values.

The quantity Γ appearing in Equations (6.57) and (6.58) is re-

lated to γ by

$$\Gamma = \gamma L \qquad (6.59)$$

and is often called the propagation operator. In Chapter II it was

noted that γ, the propagation constant, consists of a real part and

an imaginary part, or

$$\gamma = \gamma_r + i\gamma_c . \qquad (2.13)$$

We may therefore write

$$\Gamma = \Gamma_r + i\Gamma_c . \qquad (6.60)$$

Figure 6.3 shows the variation of Γr with frequency number $(\omega L/c_0)$

for various values of the damping number $(\nu L/c_0 r_0^2)$. Figure 6.4 shows

a plot of the ratio c/c_0 versus frequency number with damping number

variable.

116
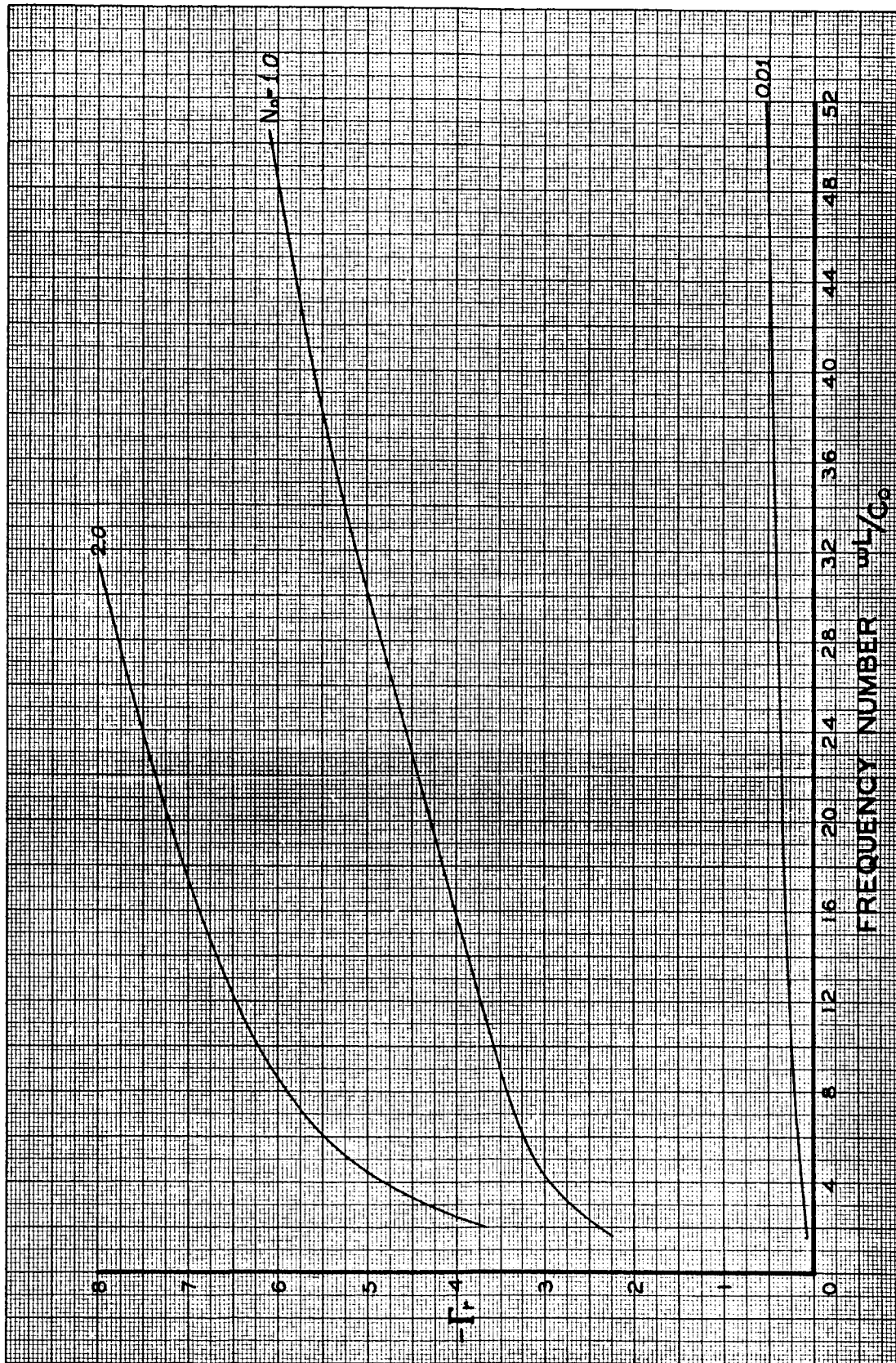
Figure 6.3 Variation of Γ_r With Frequency Number for Various Damping Numbers

117
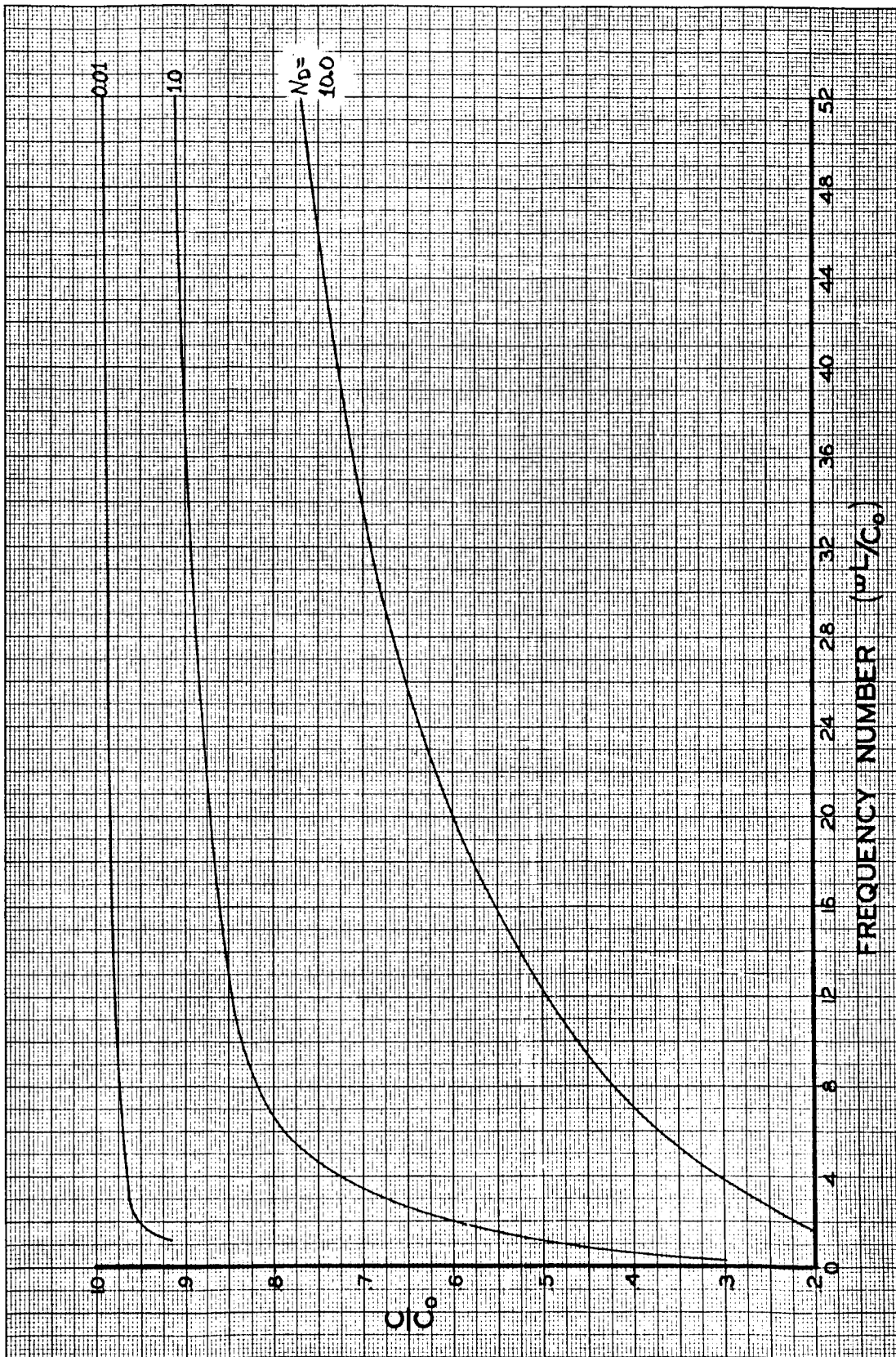
Figure 6.4 Variation of c/c_o with Frequency Number For Various Damping Numbers

118

We will now explore the application of the transfer relations in solving typical problems.

6.5 Application of Rigid Fluid Conduit Transfer Equations

Now that we have obtained a set of relations describing the average transformed conditions at two axial positions in a rigid fluid conduit, let us consider the use of these equations in solving two example problems.

Example Problem I

Consider a fluid conduit with length L and inner radius r_o terminated at end 1 by a constant pressure source such as a large reservoir; see Figure 6.5. The other end of the conduit is terminated
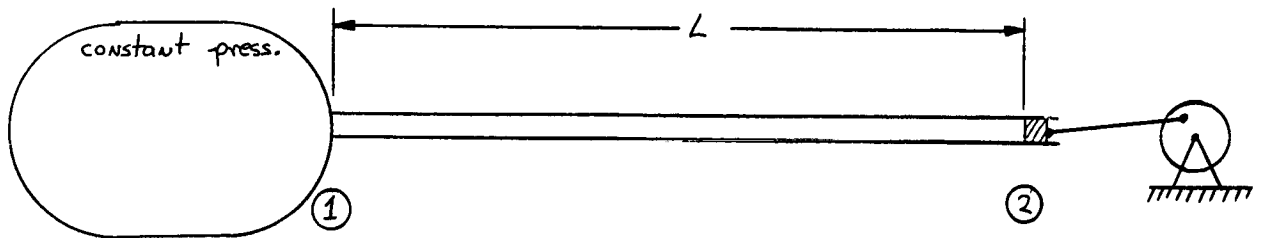
Figure 6.5 Diagram for Example Problem I

by an oscillating piston. We desire to obtain a plot of the pressure ratio $P_2/\rho c_o V_2$ versus frequency, where P_2 and v_2 are the disturbance pressure and velocity. We recognize that $P_1 = 0$ since the reservoir has a constant pressure, hence, no disturbance pressure. Applying the transfer relations (6.57) and (6.58) to this case gives
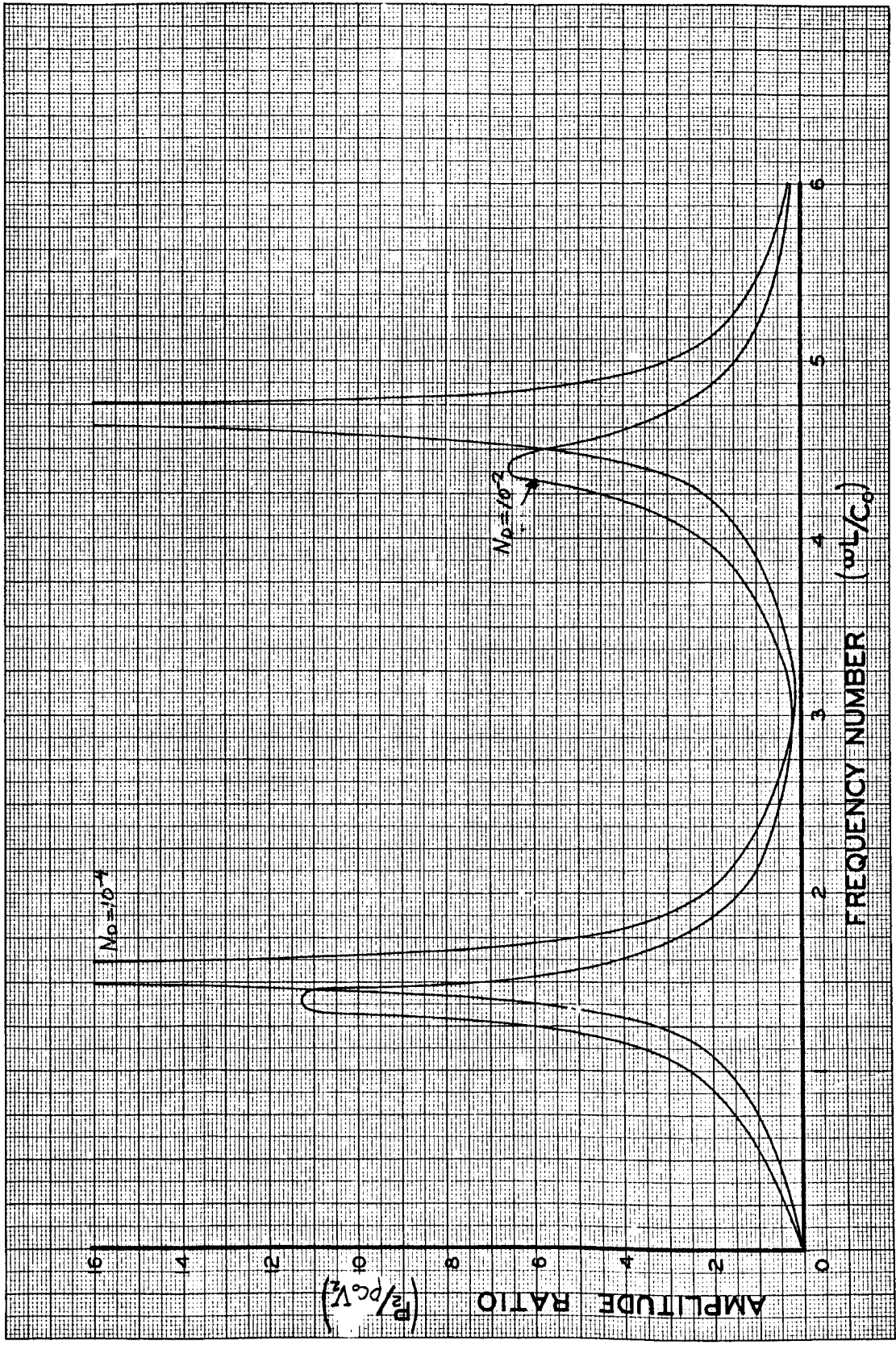
Figure 6.6 $P_2/\rho_0 c V_2$ as a Function of Frequency Number for
Two Values of Damping Numbers – Example Problem I

$$P_2 = -Z_c V_1 \sinh \Gamma$$

and

$$V_2 = V_1 \cosh \Gamma$$

thus

$$\frac{P_2}{V_2} = - Z_c \tanh \Gamma. \tag{6.61}$$

Equation (6.61) represents the Laplace transform of the ratio P_2/v_2. From linear transform theory we know that

$$\frac{P_2}{V_2} = \left| \frac{P_2}{V_2} \right|_{s=j\omega} \sin(\omega t + \varphi) \tag{6.62}$$

where φ is the phase of P_2/V_2 evaluated for $S = j\omega$. We can therefore find the information desired by calculating $\left| P_2/V_2 \right|_{S=j\omega}$. A plot of this ratio is shown in Figure 6.6.

Example Problem II

We will now investigate the response characteristics of the volume terminated fluid line shown in Figure 6.7. Here we have a conduit terminated at one end by a sinusoidal pressure generator and at the
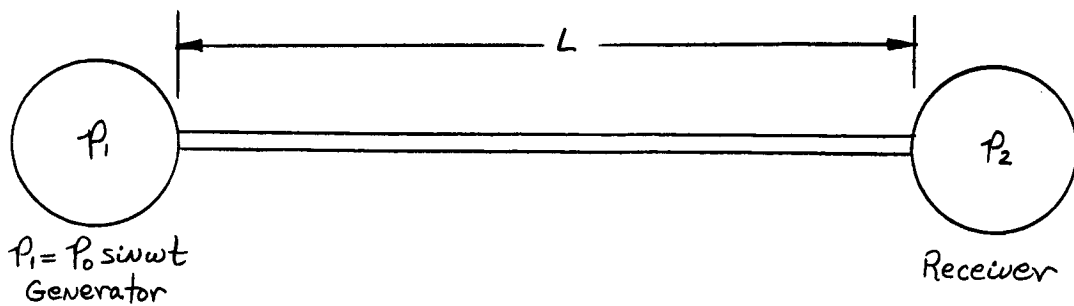
Figure 6.7 Diagram for Example Problem II

other end by a volume receiver. We will treat the volume as a pure

fluid capacitor so that from Equation (2.35a) we have

$$V_2 = C_v \, s \, P_2 \, .$$

(6.63)

For this case it is convenient to write the pressure transfer equation

in an alternate form given by

$$P_1 = P_2 \cosh \Gamma + V_2 \, Z_c \, \sinh \Gamma \, .$$

(6.64)

Substitution of (6.63) into (6.64) to eliminate V_2 yields

$$P_1 = P_2 \left\{ \cosh \Gamma + C_v \, Z_c \, \sinh \Gamma \right\}$$

or

$$\frac{P_2}{P_1} = \frac{1}{\cosh \Gamma + C_v \, Z_c \, \sinh \Gamma} \, .$$

(6.65)

Evaluating (6.65) for $S = j\omega$ and calculating the absolute value of

the resulting complex number gives $\left| P_2 / P_1 \right|$.

The example problems presented here are very simple and the cal-

culations involved are easily achieved with a digital computer. More

difficult problems involving frequency domain calculations involve

very little more effort and are also easily solved with the aid of a

computer. The utility of these equations for use in solving frequency

domain problems cannot be over emphasized. An aid which may be fruit-

fully employed in problem formulation is the matrix method discussed

in Section 2.4.

6.6 Conduit Wall Effects

The purpose of this section is to outline the analytical approach to the problem of determining the effects which nonrigid walls have on the transmission properties of a fluid conduit.

Basically, there are four types of conduit walls:

a) Rigid walls - Those walls which are assumed perfectly rigid and do not give under the influence of a pressure force. This type of wall has an infinite radial impedance, i.e., $P/v_r = \infty$.

b) Pressure release walls - Those walls which just contain the fluid but exert no force on the fluid. This type has a zero radial impedance.

c) Elastic flexible walls - Those walls which give under pressure and have some finite radial impedance but do not propagate a disturbance in the axial direction.

d) Elastic stiff walls - Those walls which have a finite radial impedance and do propagate a disturbance in the axial direction.

We have already developed the mathematical relations describing the pressure and velocity for a rigid fluid conduit. We now proceed with the description of the elastic flexible and elastic stiff cases.

Elastic Flexible Walls

If we are studying the dynamic characteristics of fluid-filled elastic tubes, such as rubber, where the major effects are those due to tube inertia and tensile stress in the wall, then the equation of motion for the tube is [45]

$$\rho_t h \frac{d^2 \delta_r}{dt^2} + \delta_r (h E_t / r_0^2) = P_t \qquad (6.66)$$

where

    h   = tube thickness

    r_o = tube radius

    Et = Young's modulus for tube material

    δ_r = wall radial deflection

    p_t = fluid pressure at tube wall

Applying the Laplace transformation to Equation (6.66) gives

$$\rho_t h s^2 \hat{\delta}_r + \hat{\delta}_r (h E_t / r_0^2) = P_t \qquad (6.67)$$

or

$$\hat{\delta}_r = \frac{P_t}{\rho_t h s^2 + h E_t / r_0^2} \qquad (6.68)$$

In terms of the radial velocity, (6.68) becomes

$$V_{rt} = \frac{s P_t}{\rho_t h s^2 + h E_t / r_0^2}$$

or

$$\frac{P_t}{V_{rt}} = \frac{\rho_t h s^2 + h E_t / r_0^2}{s} .$$

Since the radial impedance for the pipe wall must equal that of the fluid at the wall we may now write (assuming zero impedance external to the pipe wall) from Equations (6.32) and (6.36)

$$\frac{\rho_0 s}{\beta} \frac{J_0(\beta r_0)}{J_1(\beta r_0)} = \frac{\rho_t h s^2 + h E_t / r_0^2}{s} \qquad (6.69)$$

124

or

$$\frac{J_0(\beta r_0)}{\beta r_0 J_1(\beta r_0)} = \frac{\rho_t h s^2 + h E_t /r_0^2}{r_0 \rho_0 s^2} \, . \qquad (6.70)$$

Using (6.70), it is possible to solve for the allowed values of β which will depend on the parameters of the right side of the equation. Knowing β, the transfer equations could then be derived as was done in previous sections.

Elastic Stiff Walls

The approximate equations of motion for a thin-walled pipe as given by Lin and Morgan [29, 46] are (neglecting rotary inertia)

$$\rho_t h \frac{\partial^2 \bar{\delta}_z}{\partial t^2} = \frac{E_t h}{(1-\lambda)} \left\{ \frac{\partial^2 \bar{\delta}_z}{\partial z^2} + \frac{\lambda}{r_0} \frac{\partial \bar{\delta}_r}{\partial z} \right\}$$

$$\rho_t h \frac{\partial^2 \bar{\delta}_r}{\partial t^2} = K G h \frac{\partial}{\partial z} \left\{ \frac{\partial \bar{\delta}_r}{\partial z} - \xi \right\} - \frac{E_t h}{(1-\lambda^2)} \left\{ \frac{\bar{\delta}_r}{r_0^2} + \frac{\lambda}{r_0} \frac{\partial \bar{\delta}_z}{\partial z} \right\} + \rho_t [1 - h/2 r_0]$$

and

$$\frac{E_t h^3}{12(1-\lambda^2)} \frac{\partial^2 \xi}{\partial z^2} + K G h \left\{ \frac{\partial \bar{\delta}_r}{\partial z} - \xi \right\} = 0$$

where the tube axial and radial particle displacements are given by the perturbation equations

$$\delta_z(r,z,t) = \bar{\delta}_z(z,t) + (r_0-r) \xi(z,t)$$

and

$$\delta_r(r,z,t) = \bar{\delta}_r(z,t).$$

125

By transforming these equations of tube motion and assuming solutions
of the form

$$\hat{\delta_z} = \delta_{z_0} e^{\gamma_t z}$$

$$\hat{\delta_r} = \delta_{r_0} e^{\gamma_t z}$$

$$\hat{\xi} = \xi_0 e^{\gamma_t z}$$

where $\hat{\ }$ indicates transformed quantities, we have, after eliminating
δ_{z_0} and ξ_0,

$$\delta_{r_0} a_3(s, \gamma_t) = a_2 P_t / e^{\gamma_t z}$$

$$a_3(s, \gamma_t) = \left\{ \frac{s^2}{c_p^2} + \left(\frac{h^2}{12}\right) \frac{\gamma_t^4}{(1 - a_1 \gamma_t^2)} + \frac{1}{r_0^2} + \frac{\left(\frac{\lambda \gamma_t}{r_0}\right)^2}{\left(\frac{s^2}{c_p^2} - \gamma_t^2\right)} \right\}$$

$$a_1 = \frac{P_t h^2 c_p^2}{12 \, KG}$$

and

$$a_2 = \frac{1 - h/2 r_0}{P_t h \, c_p^2}$$

$$c_p^2 = \frac{Et}{P_t (1 - \lambda^2)} \, .$$

Solving for the radial tube impedance gives

$$\frac{P_t}{s \hat{\delta_r}} = \frac{P_t}{V_t} = \frac{a_3(s, \gamma_t)}{s a_2} \, .$$

From Equation (6.69) we have seen that the fluid radial impedance at
the wall is given by

$$\frac{P}{V_r} = \frac{P_0 s}{\beta} \frac{J_0(\beta r)}{J_1(\beta r)} \, .$$

In order for the radial impedance to be continuous at the wall, we
must have the tube and fluid propagation constants equal ($\gamma = \gamma_t$) and

$$\frac{P_t}{s\,\hat{s}} = \left.\frac{p}{V_r}\right|_{r=r_o}$$

or

$$\frac{\rho_o s}{\beta}\,\frac{J_o(\beta r_o)}{J_1(\beta r_o)} = \frac{a_3(s,V_t)}{s a_2}. \tag{6.72}$$

Solution of (6.72) will yield the allowed values of β.

At this point there are two ways in which we may solve for V_z. We may either neglect the pipe axial motion and assume that the fluid axial velocity is zero at r_o or we may assume that the fluid and pipe axial velocities are equal at the wall. The first approach is by far the simpler of the two and would probably not give great errors except in cases where one end of the pipe were free to move and also had a high impedance.

The major effect which flexible walls have on the transmission characteristics in a viscous fluid is to alter the propagation velocity as depicted in Figure 6.8. Also see Figure 2.16.
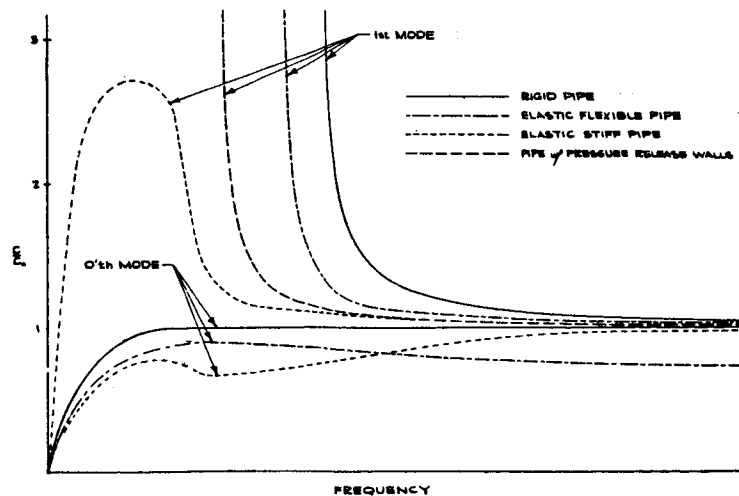
Figure 6.8 Phase Velocity Versus Frequency for
Several Types of Conduit Walls

6.7 Effect of Nonlinear Terms

In Section 2.7 we discussed, to some extent, the problems associated with analytical investigations of fluid conduits where some consideration must be made of the nonlinear terms of the equations of motion. At this time we will present a solution of the governing equations for Case 1 of Section 2.7, i.e., the case where there is a large steady flow component but the perturbation or unsteady flow components are small. We assume for the fluid velocity (axisymmetric flow)

$$\vec{v} = \hat{r}\, v_{r_1} + \hat{k}\,(v_{z_0} + v_{z_1}) = \vec{v_0} + \vec{v_1}$$

where v_{z_0} represents the steady axial velocity component, v_{r_1} represents the radial unsteady velocity component and v_{z_1} is the axial unsteady component. $\bar{v}_o$ is the steady vector velocity and $\bar{v}_1$ is the unsteady vector velocity. Making our usual assumption of a semi-compressible fluid, i.e., a fluid whose density is time but not spatially dependent, we may write for the equation of motion (calling v_{z_0} simply v_o)

$$\frac{\partial \vec{v_1}}{\partial t} + v_o\,\frac{\partial \vec{v_1}}{\partial z} = -\frac{\nabla p}{\rho_o} + \nu\left\{\frac{4}{3}\nabla(\nabla\cdot\vec{v_1}) - \nabla\times(\nabla\times\vec{v_1})\right\} \qquad (6.73)$$

and for the continuity relation (including equation of state)

$$\frac{\partial \rho}{\partial t} + \rho_o\, c_o^2\, \nabla\cdot\vec{v_1} = 0 \quad . \qquad (6.74)$$

It is convenient at this point to separate the velocity as

$$\overline{v_1} = \nabla \varphi_1 + \nabla \times \overline{\psi_1} \qquad (6.75)$$

where φ_1 represents a scalar field and $\overline{\psi}_1$ a vector field. If we now take first the divergence and then the curl of Equation (6.73) we have, respectively

$$\frac{\partial \nabla \cdot \overline{v_1}}{\partial t} + \nabla \cdot \left(v_0 \frac{\partial \overline{v_1}}{\partial z} \right) = -\frac{\nabla^2 p}{\rho_0} + \frac{4}{3} \nu \nabla^2 (\nabla \cdot \overline{v_1}) \qquad (6.76)$$

and

$$\frac{\partial \nabla \times \overline{v_1}}{\partial t} + \nabla \times \left(v_0 \frac{\partial \overline{v_1}}{\partial z} \right) = -\nu \nabla \times \left[\nabla \times (\nabla \times \overline{v_1}) \right] \qquad (6.77)$$

or, since $\nabla \cdot \overline{v}_1 = \nabla^2 \varphi_1$ and $\nabla \times \overline{v}_1 = -\nabla^2 \psi_1$, $(\overline{\psi}_1 = \theta \psi_1)$ we may rewrite Equations (6.76) and (6.77) as

$$\frac{\partial \nabla^2 \varphi_1}{\partial t} + \nabla \cdot \left(v_0 \frac{\partial \overline{v_1}}{\partial z} \right) = -\frac{\nabla^2 p}{\rho_0} + \frac{4}{3} \nu \nabla^2 (\nabla^2 \varphi_1) \qquad (6.78)$$

and

$$-\frac{\partial \nabla^2 \psi_1}{\partial t} + \nabla \times \left(v_0 \frac{\partial \overline{v_1}}{\partial z} \right) = \nu \nabla^2 (\nabla^2 \psi_1) . \qquad (6.79)$$

At this point we must make some considerations of the terms in Equations (6.78) and (6.79). Physically, φ_1 is a scalar potential for the plane wave propagation and ψ_1 is a function associated with the vorticity field. In order to be able to easily work with the terms $\nabla \cdot (v_0 \partial v_1 / \partial z)$ we need to assume that v_0 is constant even though mathematically it is some function of r.

What we are going to do is assume that v_0 is constant over the cross-section so far as Equation (6.78) is concerned. Since ψ_1 is

associated with the vorticity, this indicates that it will have a significant value only near the wall where we can assume v_o is zero. Thus, so far as Equation (6.79) is concerned $v_o = 0$. We may now reduce Equations (6.78) and (6.79) to

$$\frac{\partial \varphi_1}{\partial t} + v_o \frac{\partial \varphi_1}{\partial z} = -\frac{p}{\rho_o} + \frac{4}{3} \nu (\nabla^2 \varphi_1) \qquad (6.80)$$

and

$$\frac{\partial \psi_1}{\partial t} = -\nu \nabla^2 \psi_1 . \qquad (6.81)$$

Applying the Laplace transformation to Equations (6.74), (6.80) and (6.81) and solving, we obtain

$$\hat{\varphi}_1 = J_o(\beta r) \left\{ A_1 e^{\gamma_1 z} + A_2 e^{\gamma_2 z} \right\}$$

and

$$\hat{\psi}_1 = J_1(kr) \left\{ B_1 e^{\gamma_1 z} + B_2 e^{\gamma_2 z} \right\}$$

where $\hat{\varphi}_1$ and $\hat{\psi}_1$ are the transforms of φ_1 and ψ_1. Also γ_1 and γ_2 are solutions of

$$\gamma^2 - \frac{\gamma v_o}{\frac{c_o^2}{s} + \frac{4}{3} \nu} - \beta^2 - \frac{s}{\frac{c_o^2}{s} + \frac{4}{3} \nu} = 0 \qquad (6.82)$$

and furthermore

$$k^2 = \gamma^2 - s/\nu .$$

Now for the transformed velocities, we have

$$V_r = -\beta J_1(\beta r) \left\{ A_1 e^{\gamma_1 z} + A_2 e^{\gamma_2 z} \right\} + J_1(kr) \left\{ \gamma_1 B_1 e^{\gamma_1 z} + \gamma_2 B_2 e^{\gamma_2 z} \right\} \qquad (6.83)$$

130

and

$$V_z = J_o(\beta r) \left\{ A_1 e^{\gamma_1 z} + A_2 e^{\gamma_2 z} \right\} + K J_o(kr) \left\{ B_1 e^{\gamma_1 z} + B_2 e^{\gamma_2 z} \right\}. \qquad (6.84)$$

Zeroth Mode Transfer Equations for Rigid Pipe

We want to proceed now to develop the transfer equations for a rigid pipe which has a steady flow component v_o plus a perturbation component $v_1(t)$ which is an average for the cross-section. For the zeroth mode of propagation, we proceed with the application of boundary conditions to Equations (6.83) and (6.84) which require the velocity to be zero at the pipe wall. If this is carried out, the results are identical to those of Section 6.4 given by Equation (6.44) thus

$$\beta^2 = 2\gamma^2 \left\{ \frac{J_1(k r_0)}{k r_0 J_0(k r_0)} \right\}. \qquad (6.85)$$

Substitution of Equation (6.85) into (6.82) yields a quadratic in γ (zeroth mode only)

$$\gamma^2 \left\{ 1 - \frac{2 J_1(k r_0)}{k r_0 J_0(k r_0)} \right\} - \gamma \left\{ \frac{v_o}{c_o^2/s + 4/3 \nu} \right\} - \left\{ \frac{s}{c_o^2/s + 4/3 \nu} \right\} = 0.$$

Solving for γ from the above equation gives

$$\gamma_{1,2} = \frac{b \pm \sqrt{b^2 + 4ad}}{2a} = \gamma_a \pm \gamma_b$$

where

$$a = \left\{ 1 - \frac{2 J_1(k r_0)}{k r_0 J_0(k r_0)} \right\}$$

131

$$b = \left\{ \frac{v_0}{c_0^2/s + 4/3 v} \right\}$$

and

$$d = \left\{ \frac{s}{c_0^2/s + 4/3 v} \right\} .$$

If the relation for axial velocity is averaged over the cross-section and the averaged pressure is calculated from the continuity relation we obtain

$$V = C_1 e^{\gamma_1 z} + C_2 e^{\gamma_2 z}$$

and

$$P = - \frac{\rho_0 c_0^2}{s} \left\{ \gamma_1 C_1 e^{\gamma_1 z} + \gamma_2 C_2 e^{\gamma_2 z} \right\} .$$

Applying the conditions $V_1(s)$ and $P_1(s)$ at $z=0$ leads to the transfer equations given by

$$V_2(s) = e^{\gamma_a L} \left\{ V_1(s) \cosh \gamma_b L - \frac{P_1(s)}{\gamma_b Z_c'} \sinh \gamma_b L - \frac{\gamma_a}{\gamma_b} \sinh \gamma_b L \right\} \qquad (6.86)$$

and

$$P_2(s) = e^{\gamma_a L} \left\{ P_1(s) \left[\frac{\gamma_a}{\gamma_b} \sinh \gamma_b L + \cosh \gamma_b L \right] - \right.$$

$$\qquad (6.87)$$

$$\left. - Z_c' V_1(s) \left[\gamma_a \cosh \gamma_b L + \gamma_b \sinh \gamma_b L \right] + Z_c' \left[\frac{\gamma_a^2}{\gamma_b^2} \sinh \gamma_b L + \gamma_a \cosh \gamma_b L \right] \right.$$

where

$$Z_c' = \frac{\rho_0 c_0^2}{s} .$$

Equations (6.86) and (6.87) are now the desired transfer equations relating the variables of a four-terminal fluid conduit such as shown in Figure 2.5. It is important to note that if we let $v_o=0$ then these relations reduce identically to the standard form as given by Equations (2.23) and (2.24).

Figure 6.9 displays a plot of the frequency response Log $\left[V_1(o)/V_1(L)\right]$ for a pipe with constant pressure at $z=0$ and a "disturbance generator" at $z=L$. $V_1(o)$ is the transformed velocity at $z=0$ and $V_1(L)$ is the transformed velocity as $z=L$. Note that the greater U_o (mean steady velocity) the smaller the disturbance effect.

6.8 Effect of System Body and Vibration Forces

Consider a typical fluid system, such as the fuel system of a rocket, which under normal operating conditions has imposed accelerating and vibrating forces. We will adopt, for convenience, a frame of reference which moves with the motion of the rocket. Listed below are some of the accelerating and vibrating forces which may be present:

1) A body force on the entire system due to the acceleration of the rocket.

2) Vibrations of parts of the fluid system relative to the motion of the entire rocket.

The analytical procedure for fluid conduits in the above cases is outlined below.
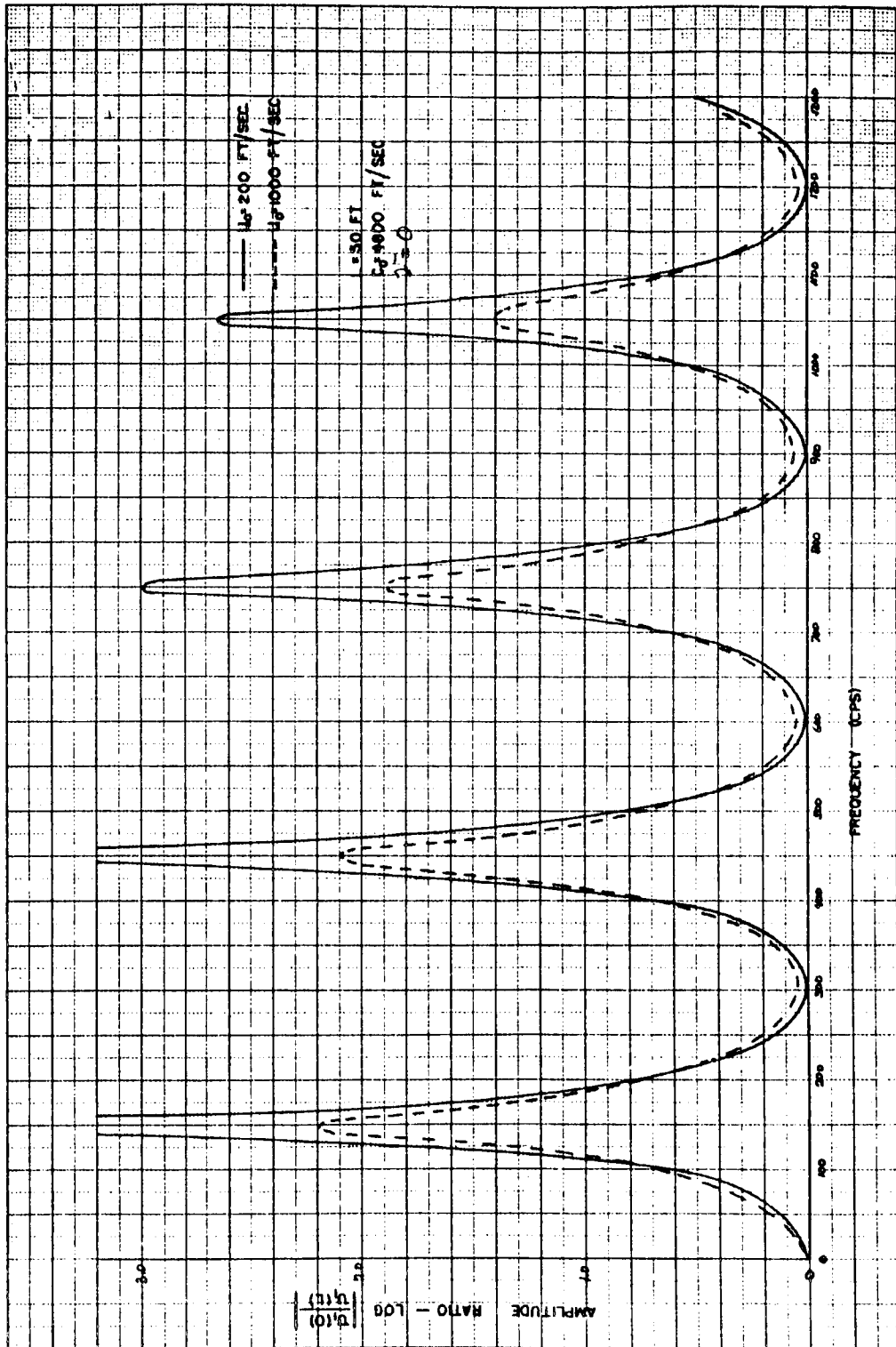
Figure 6.2   Amplitude Ratio vs. Frequency
for Nonlinear Model.

Body Force on Entire System

Now consider the effects which system body forces have upon the fluid contained within the system. Writing the first-order equation of motion for a viscous fluid, including a body force term, we have in vector form

$$\frac{\partial \bar{v}}{\partial t} = \frac{\bar{F}}{\rho_0} - \frac{\nabla p}{\rho_0} + \nu \left\{ \frac{4}{3} \nabla(\nabla \cdot \bar{v}) - \nabla \times (\nabla \times \bar{v}) \right\} \tag{6.88}$$

where $\bar{F}$ represents the vector body force acting on the fluid and may be a function of both space and time. Assume that $\bar{v}$ is representable as

$$\bar{v} = \nabla \varphi + \nabla \times \bar{\psi} \tag{6.89}$$

also

$$\nabla \cdot \bar{v} = \nabla^2 \varphi \tag{6.90}$$

and

$$\nabla \times \bar{v} = \nabla(\nabla \cdot \bar{\psi}) - \nabla^2 \bar{\psi}. \tag{6.91}$$

Taking the divergence of Equation (6.88) gives

$$\frac{\partial \nabla \cdot \bar{v}}{\partial t} = \frac{1}{\rho_0} \left\{ \nabla \cdot \bar{F} - \nabla \cdot (\nabla p) \right\} + \frac{4}{3} \nu \nabla \cdot \left\{ \nabla(\nabla \cdot \bar{v}) \right\}$$

or, introducing Equation (6.90) yields

$$\frac{\partial \nabla^2 \varphi}{\partial t} = \frac{1}{\rho_0} \left\{ \nabla \cdot \bar{F} - \nabla^2 p \right\} + \frac{4}{3} \nu \nabla^2 (\nabla^2 \varphi) \tag{6.92}$$

135

Similarly, taking the curl of Equation (6.88) and substituting Equation (6.91), we have (assuming axisymmetric flow)

$$\frac{\partial \nabla^2 \bar{\psi}}{\partial t} = \nu \nabla^2 (\nabla^2 \bar{\psi}) + \frac{\nabla \times \bar{F}}{\rho_0} . \tag{6.93}$$

Only if we can now represent $\bar{F}$ as

$$\bar{F} = \nabla \varphi_f + \nabla \times \bar{\psi}_f \tag{6.94}$$

are we able to obtain a solution to Equations (6.92) and (6.93) in this manner. If $\bar{F}$ is not representable as in Equation (6.94) then we must use some other method. We are mainly interested in the case where $\bar{F}$ represents some time varying body force. If $\bar{F}$ is only time variant then it may not be expressed as in Equation (6.95).

For the case where $\bar{F}$ is only time variant we may easily obtain a solution for the zeroth mode of propagation. The resulting transfer equations are given by

$$P_2(s) = P_1(s) \cosh \Gamma - Z_c [V_1(s) - A(s)/s] \sinh \Gamma$$

and

$$V_2(s) = [V_1(s) - A(s)/s] \cosh \Gamma - \frac{P_1(s)}{Z_c} \sinh \Gamma + \frac{A(s)}{s}$$

where $A(s)$ is the Laplace transform of the system axial acceleration resulting from the time variant body force $\bar{F}$.

Relative Vibration of Parts of Fluid System

The most convenient method of solution in this case is to account for the vibration effect by introducing it as a boundary condition on

136

the fluid and omit the body force term.

Consider a fluid conduit in which the walls are undergoing some axial motion as shown in Figure 6.10. $v_c(t)$ is the velocity which
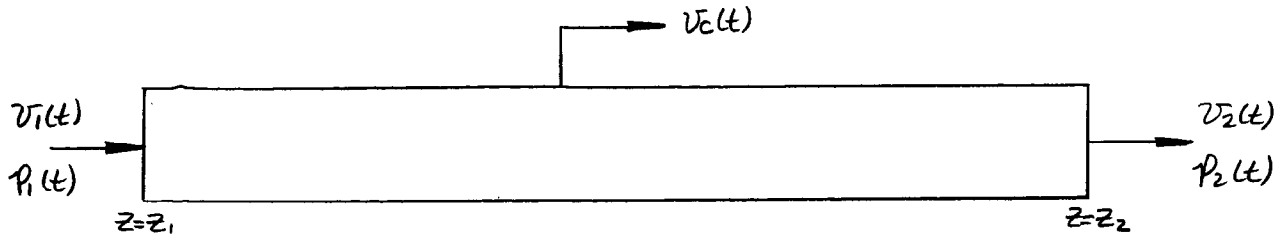
Figure 6.10 Fluid Conduit With Axial Vibration

the conduit wall attains as a result of the time variant body force. In order to obtain a solution, we will apply boundary conditions to a general solution without body forces in such a manner that the fluid has the velocity $v_c(t)$ at the wall. Thus, we are not considering there to be a body force but rather a boundary motion.

In order to avoid some mathematical difficulties, we will only discuss the zeroth mode for a rigid pipe at this time; thus we may reduce Equation (6.88) for this case to

$$\frac{\partial v}{\partial t} = -\frac{1}{\rho_0}\frac{\partial p}{\partial z} + \nu\left\{\frac{\partial^2 v}{\partial r^2} + \frac{1}{r}\frac{\partial v}{\partial r}\right\} \tag{6.95}$$

We will assume that for this mode the pressure is only a function of axial position so that in Equation (6.95) it represents a forcing function. A general solution in the Laplace domain is

$$V(r,z,s) = h(z,s)\, J_0\!\left(ir\sqrt{\tfrac{s}{\nu}}\right) - \frac{1}{\rho_0 s}\frac{\partial p}{\partial z}. \tag{6.96}$$

137

Applying the boundary condition $V(r_o,s) = V_c(s)$ gives

$$h(z,s) = \frac{V_c(s) + (1/\rho_o s) \, \partial P/\partial z}{J_0(i r_0 \sqrt{\frac{s}{\nu}})} \, . \tag{6.97}$$

Substituting (6.97) into (6.96) yields

$$V(r,z,s) = V_c(s) \frac{J_0(\xi r)}{J_0(\xi r_0)} + \frac{1}{\rho_o s} \frac{\partial P}{\partial z} \left\{ \frac{J_0(\xi r)}{J_0(\xi r_0)} - 1 \right\} . \tag{6.98}$$

We may now derive our standard transfer equations. If we average Equation (6.98) and combine the result with the continuity equation averaged over the cross-section, we obtain a second-order ordinary differential equation whose solution gives the propagation constant as

$$\gamma = \frac{(s/c_0)}{\left\{ 1 - \frac{2 J_1(\xi r_0)}{\xi r_0 \, J_0(\xi r_0)} \right\}^{1/2}}, \quad \xi = i \gamma \sqrt{\frac{s}{\nu}}$$

which is almost identical to the form given by Equation (6.45) for the zeroth mode. The corresponding transfer equations are

$$V_2(s) = V_1(s) \cosh \gamma L - \frac{P_1(s)}{Z_c} \sinh \gamma L + V_c(s) f(s) \left[1 - \cosh \gamma L \right] \tag{6.99}$$

and

$$P_2(s) = P_1(s) \cosh \gamma L - Z_c V_1(s) \sinh \gamma L + Z_c V_c(s) f(s) \sinh \gamma L \tag{6.100}$$

where

$$f(s) = \frac{2 J_1(\xi r_0)}{\xi r_0 \, J_0(\xi r_0)}$$

and Z_c is defined by Equation (2.26). Notice from Equations (6.51) and (6.52) that the effect of the system adds to each of the standard form transfer equations a term which is porportional to $V_c(s)$. If we put $V_c(s)=0$, then the equations reduce to the standard form for a conduit with no vibration

Example Problem III

Let us now apply the above transfer relations to the case of a rigid conduit which is closed at one end and has a constant pressure source at the other end. We also specify that the conduit experiences an axial sinusoidal vibration such that its transformed velocity is $V_c(s)$, Figure (6.11)
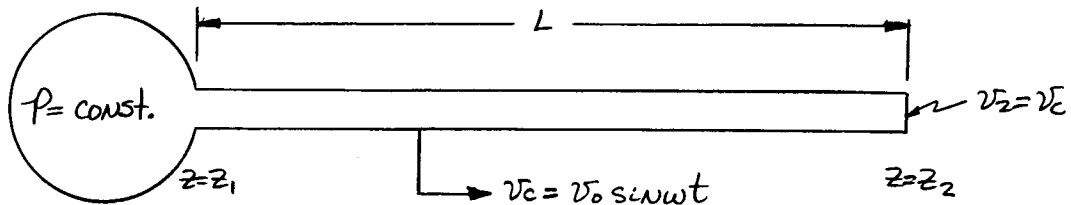
Figure 6.11 Diagram for Example Problem III

Applying Equation (6.99) and (6.100) in this case, we may obtain

$$\frac{P_2(s)}{V_c(s)} = -Z_c \left(1-f(s)\right) \tanh \Gamma .$$

(6.101)

Equation (6.101) is now the transfer relation for the ratio of transformed pressure at the closed end to the vibration velocity. This example is similar to the problem of a vibrating piston in one end of a stationary pipe with a constant pressure at the other end.

Example Problem IV

Consider the fluid conduit shown in Figure 6.12. For this problem we have a conduit which is vibrating in the axial direction with a velocity v_c. An orifice is situated in one end of the conduit. There is a constant pressure reservoir at each end with p_1 being greater than p_3 and of such a magnitude to produce a steady flow velocity v_o when there is no line vibration. We wish to determine the pressure perturbation at point 2 due to the vibration of the line.

Writing the matrix representation for the transformed pressure and velocity perturbation terms for the conduit we have $(p_1 = 0)$

$$\begin{bmatrix} P_2 \\ V_2 \end{bmatrix} = \begin{bmatrix} -Z_c \sinh \Gamma & Z_c f(s) \sinh \Gamma \\ \cosh \Gamma & f(s)(1 - \cosh \Gamma) \end{bmatrix}$$
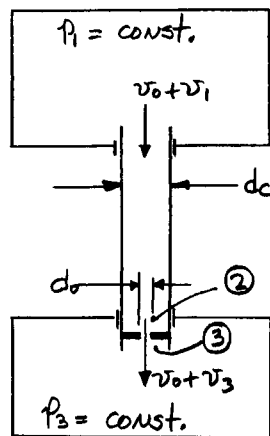
Figure 6.12   Diagram for Example Problem IV

Assuming the orifice to have only a resistance to the perturbation terms we may write

$$P_2 = R(V_2 - V_c)$$

140

where $R = 2Kv_o$. V_c is the transformed vibration velocity. Combining these equations leads to the relation

$$\frac{P_2}{\rho_o c_o V_c} = -\left\{ \frac{1 - f(s)}{\frac{\rho_o c_o}{R} + \frac{\rho_o c_o}{Z_c} \coth \Gamma} \right\}.$$

If R is derived from the steady flow orifice equation, then

$$R = \frac{1}{C_d}\left[\left(\frac{d_c}{d_o}\right)^4 - 1\right]\sqrt{2\rho_o \Delta P_o}$$

where ΔP_o is the pressure drop due to the steady flow velocity v_o. Table 6.1 shows some typical values of R for water. Also

C_d	ΔP_o (psi)	d_c/d_o	$R(\frac{\text{psi-sec}}{\text{ft}})$
.6	100	4	3.64
.6	100	2	.882
.6	100	1.5	.457
.6	500	1.5	1.02

Table 6.1 Typical Values of R for Water

Figure 6.13 shows a plot of $|P_2/\rho_o c_o V_c|$ versus N_f (frequency number) for various values of N_D (damping number) and R where

$$N_f = \frac{\omega L}{c_o}$$

and

$$N_D = \frac{\nu L}{c_o r_o^2}$$
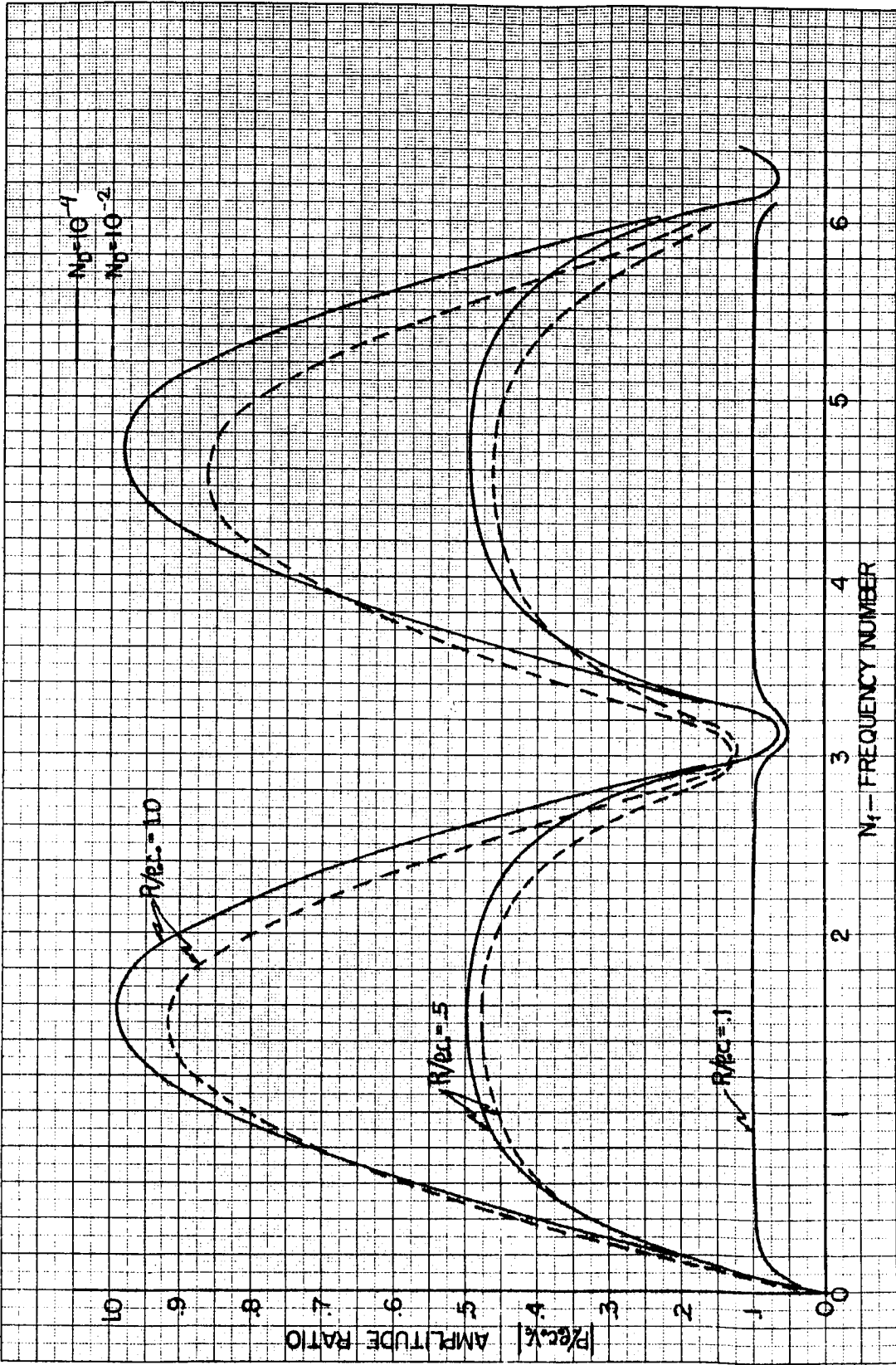
Figure 6.13 The Dependence of Pressure Amplitude Ratio on Frequency Number for Various Values of Damping Number and Resistance

6.9 Lumped Parameter Models

In Section 2.5 we discussed the applicability of lumped parameter models in solving conduit problems. It was stated that these models are valid if the frequencies involved are less than about one-eighth of the first critical frequency of the lumped element. This restriction suggests a very convenient method of obtaining such a model if the corresponding distributed parameter model is known.

Similarity Between Lumped and Distributed Models

Consider now the transfer relations (2.23) and (2.24) for the case of low frequency, i.e., frequency low enough for a lumped model to be valid. This means that $\gamma_0 < \pi/16$ so that we may approximate $\cosh \gamma_0 L$ and $\sinh \gamma_0 L$ by the first terms of their series expansions, thus

$$P_2(s) = P_1(s)\left(1 + \frac{\Gamma^2}{2}\right) - Z_c \Gamma V_1(s) \tag{6.102}$$

and

$$V_2(s) = V_1(s)\left(1 + \frac{\Gamma^2}{2}\right) - \frac{\Gamma}{Z_c} P_1(s). \tag{6.103}$$

By a critical comparison of Equations (6.102) and (6.103) with the relations for the fundamental lumped model, Equations (2.41) and (2.42), we see that by neglecting some of the small order terms the equations will be equivalent if

$$s I_v + R(v) = Z_c \Gamma \tag{6.104}$$

and

$$SC_v = \frac{\Gamma}{Z_c}.$$

(6.105)

We have seen, Equation (2.26), that $Z_c = \rho_0 c_0^2 \gamma_0/s$, thus from Equation (6.105) we must have

$$SC_v \frac{\Gamma}{\rho_0 c_0^2 \gamma/s} = \frac{SL}{\rho_0 c_0^2} = \frac{SL}{\chi}$$

which is correct, see Equation (2.35a). Considering now Equation (6.104) we see that we must have

$$SI_v + R(v) = \frac{\rho_0 c_0^2 \gamma^2 L}{s}.$$

(6.106)

Using the value of γ_0 for the two-dimensional viscous model, Equation (6.45), we may rewrite Equation (6.106) as

$$SI_v + R(v) = \frac{\rho_0 SL}{\left\{ 1 - \frac{2 J_1(\xi r_0)}{\xi r_0 J_0(\xi r_0)} \right\}}.$$

(6.107)

If we expand the right side of Equation (6.107) in a power series we have

$$SI_v + R(v) = \rho_0 SL \left\{ 1 + f + f^2 \cdots \right\}.$$

(6.108)

$$f = \frac{2 J_1(\xi r_0)}{\xi r_0 J_0(\xi r_0)}$$

144

From Equation (6.108) it is evident that we must have

$$R(v) = \rho_0 SL \left\{ f + f^2 + f^3 + \cdots \right\} . \qquad (6.109)$$

We have now shown that the transfer equations for the fundamental lumped model and a low-frequency form of the distributed parameter model are approximately equivalent if $R(v)$ is given by Equation (6.109). This result suggests that we may obtain lumped parameter models from all of our existing distributed parameter models by simply writing them in approximate low-frequency form. This will yield forms which are mathematically much more tractable and which should be more easily inverted back to the time domain.

CHAPTER VII

Theoretical Investigation of the Onset of Cavitation

7.1 Introduction

When the stream pressure of a flowing liquid is reduced below
the vapor pressure, it becomes possible for a bubble to grow from
a small nucleus within the liquid or at the liquid-solid boundary.
The experimental evidence available (Harvey, McElroy, and Whiteley
[60]) indicates that permanent gas nuclei are necessary for the
onset of cavitation. These may, or may not, have come out of
solution on solid nuclei. A third possibility exists when the
liquid contains solid particles that are not wetted by the liquid;
in this case, it is feasible that gas-free cavities may develop
on what are essentially solid nuclei. Whatever their mode of
origin, the bubbles will certainly gain vapor from the surrounding
liquid as they grow.

The experimental cavitation studies by Hammitt [91], Ruggeri
and Gelder [87], and others have proved that the formation and/or
collapse of bubbles, which were produced by decreasing the stream
pressure, can be detected by audible means before they become
visible. The tunnel operating conditions had to be changed once
an audible sound was detected before the bubbles could be observed
with the eye. This indicates that bubbles, formed by decreasing
the stream pressure, are very small during the early stages of

growth. Therefore, we believe that a closer look should be taken at the equation which describes the growth of small bubbles.

The rate of growth of a bubble, once formed, is controlled by the surface tension, the liquid inertia, the liquid viscosity, and the difference between the pressure within the bubble and the external pressure (pressure within the liquid). In the initial stages of bubble expansion, the growth is slow but it is accelerated with increase in bubble size because of a reduction in the surface tension force and the decrease in stream pressure (for liquids flowing in conduits). When the rate of growth becomes appreciable, however, the temperature and hence the pressure within the bubble drop and the rate of growth is decreased.

7.2 Hydrodynamics of the Growth of Small Bubbles

During the following discussion we will consider a spherical bubble growing in a viscous, incompressible liquid. The growing bubble will generate a velocity field within the liquid which, in turn, will generate a stress field tending to retard the bubble's growth. The assumption of a spherical bubble is valid for small bubbles since the force exerted by surface tension is large. In order to further simplify the problem a model with constant fluid velocity and no turbulence will be assumed. This model is similar to the mathematical model being used in our studies with the Bubble Chamber. However, in order to study some of the causes of cavitation we must focus our attention on bubbles which are invisible to the eye.

The spherical symmetry of the situation makes it convenient to choose a spherical coordinate system with its origin at the center

of the bubble. The velocity field generated in the liquid by the expanding bubble will have only a radial component $V_r(r,t)$ with respect to the center of the bubble, where t is the time measured from the instant of bubble formation. The pressure p at any point in the liquid is also a function of r and t. Therefore, the Continuity and Momentum equations may be reduced to

$$\frac{\partial V_r}{\partial r} + \frac{2}{r} V_r = 0 \tag{7.1}$$

and

$$\rho_L \left\{ \frac{\partial V_r}{\partial t} + V_r \frac{\partial V_r}{\partial r} \right\} = -\frac{\partial p}{\partial r} + \mu_L \left\{ \frac{1}{r} \frac{\partial^2 (r V_r)}{\partial r^2} - \frac{2}{r^2} V_r \right\} \tag{7.2}$$

In Equation (7.2), ρ_L is the density and μ_L the viscosity of the liquid. Both are assumed uniform and constant.

At the bubble wall, the liquid velocity must equal $\dot{R}(t)$ where a superimposed dot denotes ordinary differentiation with respect to time. Thus, integration of Equation (7.1) yields

$$V_r(r,t) = \frac{1}{r^2} \left[R(t) \right]^2 \cdot \dot{R}(t) . \tag{7.3}$$

If we substitute Equations (7.1) and (7.3) into Equation (7.3) and integrate from the bubble radius to infinity, we obtain

$$\ddot{R} R + \frac{3}{2} [\dot{R}]^2 = \frac{p(R+0,t) - p}{\rho_L} \tag{7.4}$$

148

The stress components for the velocity field given by Equation (7.3) are [135], (for the liquid outside the bubble)

$$\sigma_{rr} = -p(r,t) - \frac{4\mu_L}{r^3} \dot{R} R^2,$$

$$\sigma_{\theta\theta} = \sigma_{\phi\phi} = -p(r,t) + \frac{2\mu_L}{r^3} \dot{R} R^2, \qquad (7.5)$$

$$\sigma_{\theta\phi} = \sigma_{\phi r} = \sigma_{r\theta} = 0.$$

Within the bubble,

$$\sigma_{rr} = \sigma_{\theta\theta} = \sigma_{\phi\phi} = -(p_v - p_g),$$

$$\qquad (7.6)$$

$$\sigma_{\theta\phi} = \sigma_{\phi r} = \sigma_{r\theta} = 0,$$

where p_v is the partial pressure of the vapor and p_g is the partial pressure of an inert gas.

The stress component σ_{rr} must experience a jump of magnitude $\frac{2\sigma}{R}$ at the bubble wall. Comparing the first of Equations (7.5) with the first of Equations (7.6), we find that the pressure just outside the bubble wall is given by

$$p(R+0,t) = p_v + p_g - \frac{2\sigma + 4\mu_L \dot{R}}{R}. \qquad (7.7)$$

If we substitute Equation (7.7) into Equation (7.4) we obtain an ordinary differential equation for the bubble radius as a function of the pressures inside and outside the bubble. This equation is:

$$R\ddot{R} + \frac{3}{2}\dot{R}^2 + \frac{2\sigma}{R\rho_L} + \frac{4\mu_L \dot{R}}{R} = \frac{p_v + p_g - p(t)}{\rho_L} \qquad (7.8)$$

149

7.3 Discussion of Equation (7.8)

Equation (7.8) is similar to the well-known Rayleigh [98] equation. Several solutions to Equation (7.8) exists under a variety of assumptions. However, most of the existing solutions are applicable only to bubbles of fairly large size. We are interested in bubbles from the time they are formed until they become visible. Therefore, we must examine each term in Equation (7.8) to determine its influence on the bubble growth within this time interval. Listed below is a discussion of each term in Equation (7.8).

(a) The inertia and surface tension terms are significant during the initial expansion of the original bubble nucleus [109].

(b) The viscous term is significant during the early stages of growth in a highly viscous liquid.

(c) The vapor pressure term usually decreases as the bubble radius increases. Since the growth is fairly fast, this term might be assumed to remain constant and equal to its value at time, t, equal to zero.

(d) The inert gas term may be neglected if the liquid is nearly free of dissolved gases.

(e) The liquid pressure term will decrease with time and will depend upon the test section shape and stream conditions at the inlet to the test section.

Each term in Equation (7.8) appears to be important during the early stages of growth. Thus, we are unable to linearize Equation (7.8).

7.4 Previous Solutions for Equation (7.8)

The influence of time-dependent factors on bubble growth has been investigated by Noltingk and Neppiras [62], [63], Parkin [72], and others. Noltingk and Neppiras solved Equation (7.8) on a differential analyzer for the growth of an air bubble in a fluctuating pressure, p(t), field. They neglected the viscosity term in Equation (7.8) and assumed the inert gas within the bubble to undergo an isothermal expansion. The pressure outside the bubble was repre-sented as one cycle of a negative sign function. Noltingk and Neppiras found by trial that wide variations in boundary values of radial velocity, $\dot{R}$, (at $R = R_0$) produced insignificant changes in the contour of the R-t curves.

In another investigation of the effect of time, based on Equation (7.8), Parkin [72] defined the onset of cavitation to be the bubble growth to a particular radius of 0.10 cm. Parkin neglected the viscosity term in Equation (7.8) and assumed the inert gas within the bubble to undergo an isothermal expansion. He also assumed the surface tension to vary linearly from zero to its value of σ. This change in surface tension was assumed to take place during the early stages of bubble growth. The pressure, p, within the liquid was represented by a parabolic pressure function.

There has been no attempt to correlate solutions of Equation (7.8) to liquids flowing through conduits. Thus, we believe that Equation (7.8) could yield some useful results in predicting the effect of pressure distribution on the onset of cavitation.

151

7.5 Solution to Equation (7.8)

Before a solution to Equation (7.8) can be obtained it will be necessary to determine the boundary conditions. This will have to be done by trial because no exact method exists for determining the initial bubble radius.

The initial radial velocity, $\dot{R}_O$, will be zero at some particular value of the external pressure. This value of the external pressure may be determined by

$$p(o) = p_{V_O} + p_{g_O} - \frac{2\sigma}{R_O} . \tag{7.9}$$

Thus, the initial bubble radius, R_O, is the only unknown since p_{g_O} can be estimated by Henry's Law, $p_{g_O} = \bar{H}\bar{C}$, and p_{V_O} is approximately equal to the liquid vapor pressure.

The major problem is that of determining the correct value for R_O. Parkin [72] assumed a value of 10^{-3} cm for R_O. The correct value or values for R_O may be determined by trial by selecting R_O so that R and $\dot{R}$ can be satisfied once the bubble becomes visible.

7.6 Pressure Inside Bubble

The pressure within a small bubble will undergo an expansion as the bubble grows from an invisible size to a visible size. This expansion will be neither isentropic nor isothermal. However, if we solve Equation (7.8) first by assuming the gaseous mixture to undergo an isentropic expansion and second by assuming the expansion to be isothermal, then the actual expansion should yield results

which are between these two assumed processes. The actual expansion

will probably follow a polytropic process. However, the polytropic

exponent is unknown and must be determined by experimental methods.

CHAPTER VIII

Theoretical and Experimental Investigations
of Bubble Dynamics

8.1 Introduction

The purpose of this chapter is to present a complete review of

what has been done in the bubble dynamics investigation and to acquaint

the reader with the final objectives of this investigation.

First the analytical work already done is considered. Then experi-

mental methods for verifying the theoretical work are given. Finally,

the possibilities of future investigations are reviewed.

8.2 Analytical Solutions of Bubble Dynamics Problems

A. Bubble growth in a superheated liquid has been considered in

references [99], [100], [101], [102], [103], [104], [105], [106], [107],

[108], [109], [110], and [111]. For the case of initially uniform super-

heat in the liquid and with the assumptions of Section 5.2, the analytical

solutions for the asymptotic growth rate of a vapor bubble has the form:

$$R = A t^{1/2}. \tag{8.1}$$

The coefficient, A, is a function of the physical properties of the

system and also contains a numerical constant depending upon the refer-

ence under consideration.

The analytical approaches of Forster-Zuber, Plesset-Zwick, and

Scriven are compared in Figure 8.1. This data was taken for a vapor
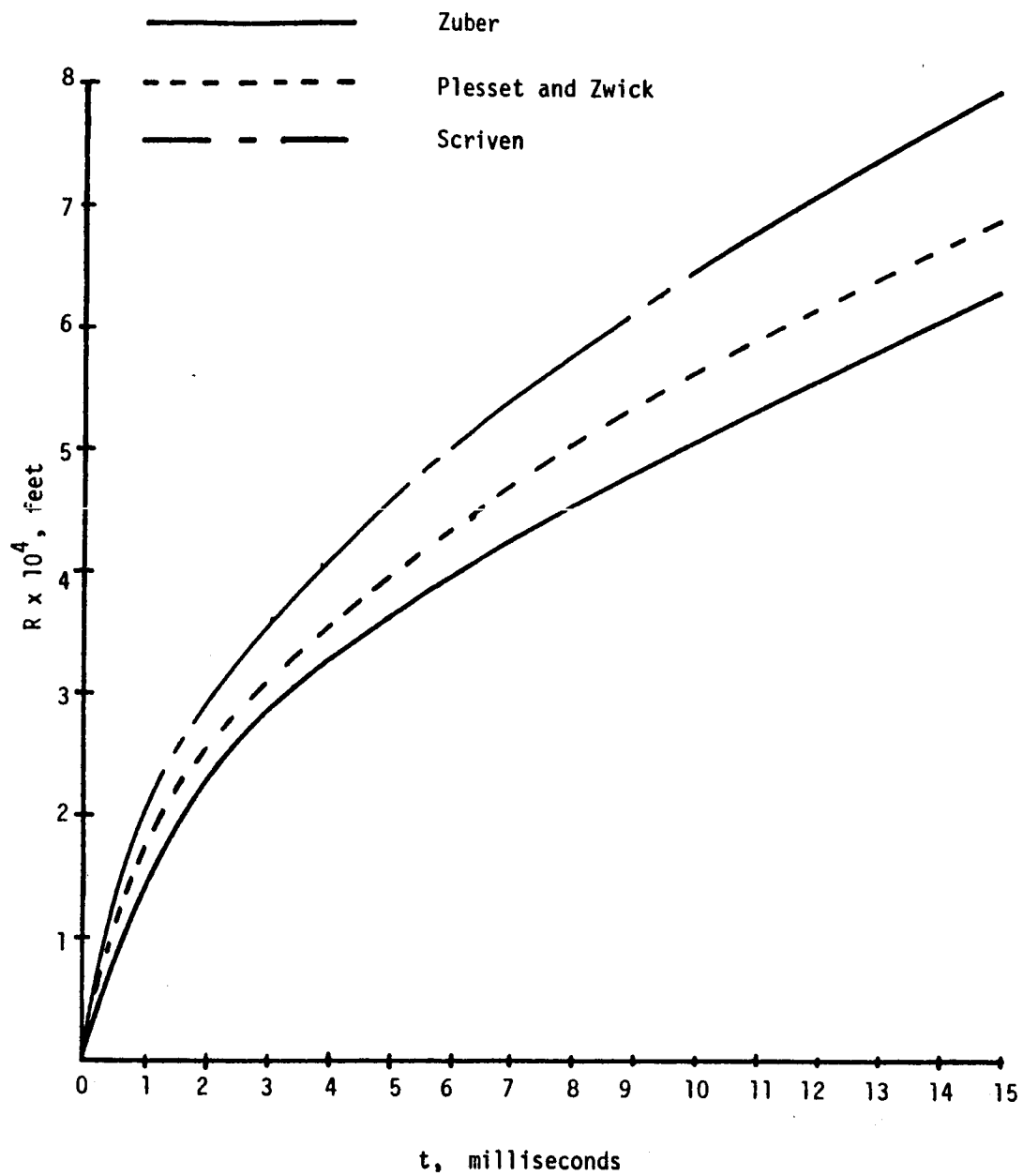
Figure 8.1 Analytical Solutions Compared

bubble in liquid nitrogen superheated by $3^{\circ}F$ at atmospheric pressure.
For these three solutions the equations are:

Forster-Zuber

$$R = \frac{\Delta T \, C_{PL} \, \rho_L}{L_v \, \rho_v} \sqrt{\pi a t} \tag{8.2}$$

Plesset-Zwick

$$R = \sqrt{\frac{12}{\pi}} \, \frac{\Delta T \, C_{PL} \, \rho_L}{L_v \, \rho_v} \sqrt{a t} \tag{8.3}$$

Scriven

$$R = 2\beta \sqrt{\pi a t} \tag{8.4}$$

where β was solved by numerical integration from the equation:

$$\frac{\Delta T}{\frac{\rho_v L_v}{\rho_L C_{PL}} + \frac{\rho_v \Delta T (C_{PL} - C_{pv})}{\rho_L C_{PL}}} = \left\{ 2\beta^2 \exp\left(\beta^2 + 2\epsilon\beta^2\right) \right\} \int_{\beta}^{\infty} x^{-2} \exp\left(-x^2 - \frac{2\epsilon\beta^3}{x}\right) dx$$

and $\epsilon = 1 - \rho_v/\rho_L$. For the properties listed below β was found
to be 3.4.

Properties		Source
T_L	$= 142.255^{\circ}$ R	Ref. 136
T_V	$= 139.255^{\circ}$ R	Ref. 136
P_L	$= 14.7$ psia	Ref. 136
C_{PL}	$= .496$ Btu/lb$^{\circ}$ R	Ref. 137
C_{VL}	$= .258$ Btu/lb$^{\circ}$ R	Ref. 138
P_L	$= 50.506$ lb/ft^3	Ref. 136

Properties   Sources

$$\rho_V = .2875 \text{ lb/ft}^3$$ Ref. 136

$$K_{C_L} = 2.2025 \times 10^{-5} \text{ Btu/ft-sec}^\circ \text{R}$$ Ref. 137

The analytical approach for this investigation will be Equation

(8.1) and the value of A will be one of the primary results to be

obtained by experiment.

For the present problem the analytical solution to the bubble

growth is not considered in the range where the bubble can not be

studied adequately from photographs. Absolute verification of the

analytical results in the early growth range is non-existent at pre-

sent. The practicability of study in this range has not been con-

sidered here.

 B. Bubble collapse in a subcooled liquid was considered in

references: [101], [116], [108], [117], [118], [119]. Bubble collapse

will be considered in two parts:

 1. When the subcooling of the liquid is more than 35° F the

  collapse will be considered to be controlled entirely by

  inertia forces and heat transfer effects will be neglected.

  The Rayleigh equation, (5.23), becomes valid.

$$t = R_0 \sqrt{\frac{3\rho_L}{2\rho_\infty}} \int_{R/R_0}^{1} \left\{ \frac{(R/R_0)^3}{1-(R/R_0)^3} \right\}^{1/2} d\left(R/R_0\right).$$

(8.5)

  The arbitrary 35° F subcooling must be verified and this is

  one aim of the experimental work.

 2. For subcooling less than 35° F two methods of predicting

  collapse are available. Since work in cryogenics is con-

  cerned primarily with the case where a liquid is usually

157

only subcooled by a few degrees, it seems that a review of these two analytical approaches is necessary.

Plesset and Zwick [101] obtained the system of equations shown below for the situation in bubble collapse where both heat transfer and inertia must be considered.

$$\frac{1}{6} \frac{d}{dp} \left[p^{7/8} \dot{p}^2 \right] + p^{-1/3} + \Phi(\theta) = 0 \tag{8.6}$$

$$\Upsilon(\theta) p - 1 = \frac{2}{\pi c} \int_0^u \dot{\theta}(u-v)^{1/2} \, dv \tag{8.7}$$

Boundary conditions:

$$p(0) = 1 \quad , \quad \dot{p}(0) = 0 \, , \quad \theta(0) = 0 \tag{8.8}$$

where

$$p = \left(R/R_0 \right)^3 \, , \qquad\qquad R_0 = \text{Radius at start of collapse}$$

$$C = \frac{L_v \, \rho_{ov} \, R_0}{3k} \left(\frac{a D}{\pi} \right)^{1/2}, \quad u = \left(\frac{a}{R_0^4} \right) \int_0^t R^4(y) \, dy$$

$$\Upsilon = \frac{\rho_v(T)}{\rho_{ov}} \, , \quad \Phi = \frac{R_0 (\rho_\infty - \rho_v)}{2\sigma} \, , \text{ and } \theta = -C \int_0^u \frac{\frac{d(\Upsilon p)}{dv}}{(u-v)^{1/2}} \, dv.$$

The system of Equations (8.6), (8.7), and (8.8) was solved by a numerical integration technique in Appendix II of this reference [101].

Florschuetz and Chao [116] obtained the same equations but put them in an altered form. Their equations may also be solved by numerical integration methods.

These are the systems of equations necessary to treat the ana-
lytical approach to collapse in slightly subcooled collapse.

C. Bubble growth in a nonuniform temperature field was con-
sidered in references [106], [120], [122], [123], [121].

Zuber [106] offers the simplest correlation of data with the
equation:

$$R = \frac{(T_\infty - T_{sat}) \, C_{PL} \, \rho_L}{L_v \, \rho_v} \, \sqrt{\pi a t} \left\{ 1 - \frac{q_b \sqrt{\pi a t}}{2 K_L (T_\infty - T_{sat})} \right\} \qquad (8.9)$$

q_b is the heat transferred from the surface to the liquid. This
equation is convenient because of its simplicity. Physically q_b
is a measure of how nonuniform the temperature field may be.

If it is possible to get a good correlation of data with Equation
(8.9), it may be necessary to assume a linear temperature variation
from the heating surface of the form:

$$T = (T_{wall} - T_\infty)\left(1 - \frac{r}{b} \cos \phi\right) + T_\infty \qquad (8.10)$$

where r and ϕ are spherical coordinates and b is the distance
from the surface where $T_L = T_\infty$. (See Griffith [121]). Then use
this along with the equations:

$$\nabla^2 T = \frac{\rho_L \, C_{PL}}{K_1} \left[\frac{\partial T}{\partial t} + \vec{V} \cdot \nabla T \right] \qquad (8.11)$$

and

$$\vec{V} = -\frac{R^2}{r^2} \left(\frac{K_L}{\rho_v L_v} \right) \int_0^{\pi/2} \left(\frac{\partial T}{\partial r} \right)_{r=R} \sin \phi \, d\phi . \qquad (8.12)$$

These equations can also be solved by a numerical integration technique.

8.3 Experimental Approach to Bubble Dynamics

The observation of bubble growth and collapse in non-cryogenic fluids has indicated that the preceeding analytical approaches can give adequate predictions of bubble dynamics. However, experimental verification with cryogenic fluids has not yet been carried out. To furnish information on cryogenic fluids, the bubble chamber of Figure 8.2 was designed for use with liquid nitrogen.

It has been found that plexiglas is very sensitive to clamping stresses at liquid nitrogen temperatures and consequently no adequate seal has been obtained with this material. The windows on the inner chamber are made of pyrex glass 7/16 inch thick and sealed to an invar metal holder with Armstrong epoxy cement. The CryoVac Company of Columbus, Ohio indicated that this arrangement gave satisfactory sealing properties.

The vacuum jacket around the inner chamber serves two purposes. It maintains a low level of heat transfer to the inner chamber and prevents frost from forming on the windows.

There are three ways in which bubbles can be generated in the viewing area: 1. vapor can be forced in through Tube A of Figure 8.2; 2. current can be passed through the heater; and 3. Chamber A can be evacuated and the valve between it and the inner chamber can be opened rapidly and cavitation would result. The first two methods will be used for a source of bubbles to verify the analytical results of Section 8.2.
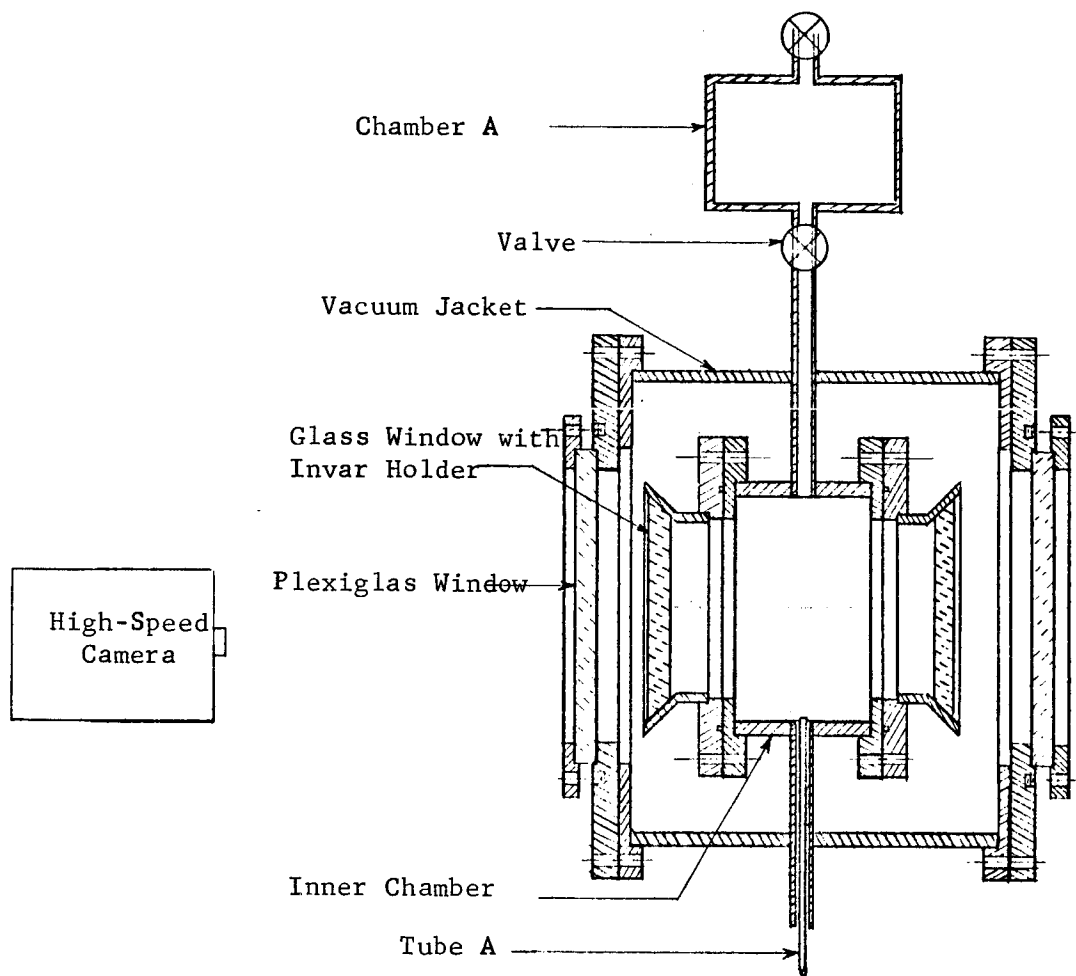
Figure 8.2 Bubble Observation Chamber

The subcooled liquid will be obtained by rapidly increasing the pressure in the inner chamber; the superheated liquid will be obtained by rapidly decreasing the pressure in the inner chamber; and a nonuniform temperature field will result when the heater is activated.

A photographic record of the bubble dynamics will be made in all combinations of temperature fields. A high-speed camera that takes 2,000 to 10,000 pictures per second will be used. The other data to be taken includes pressure above the liquid, temperature of the liquid away from the bubble formation, and the temperature of the heater.

8.4 Experimental Instrumentation and Calibration

A. Pressure Measurement - Static pressure in the inner chamber will be determined by measuring the pressure in Chamber A of Figure 8.1. The inner chamber is connected to Chamber A by a small stainless steel tube. Chamber A will be filled with nitrogen vapor which has essentially zero velocity. A static pressure tap in Chamber A is attached to a mercury manometer. Static pressures measured in Chamber A will be approximately 1/2 inch of liquid nitrogen less than the static pressure at the liquid-vapor interface in the bubble chamber. The manometer at room temperature in coordination with a barometer can be used as a standard for static pressure measurement.

B. Temperature Measurement - The temperature away from the point of bubble formation and the temperature of the heater are to be

measured by use of copper-constantan thermocouples. Two thermocouples will be made by cutting one long thermocouple wire and welding both at the cut. The composition of the thermocouples should be the same at this point. These two thermocouples will be placed in the liquid nitrogen in the same horizontal plane from the floor to measure the temperature at a distance from the bubble. One additional thermocouple will be located in the heater.

All thermocouples will use a reference temperature at the ice point. Reference [139], page 159, states that the ice point is reproducible enough to be used as a standard. Reference [139], page 206, gives a plot of some calibration work for this arrangement. Figure (8.3) is a reproduction of the calibration work done.

Thermocouple tables for copper-constantan in the temperature range of interest are given in reference [139], page 211, reference [140], and reference [141].

The thermocouple output will be measured with a Rubicon type B bridge. The temperature should reach steady state after cool-down and remain fairly stable. One microvolt accuracies are expected.

It can be seen that the thermocouple output for the range of -183° C to -200° C for any single thermocouple can be calibrated with a high degree of accuracy by knowing two temperatures in this range (see Figure 8.3). The thermodynamic properties of nitrogen [136] can be used along with the corrected static pressure in the bubble chamber and boiling nitrogen to determine these temperatures. By adjusting the pressure in the bubble chamber and letting the nitrogen boil, it is possible to find the temperature of the liquid.
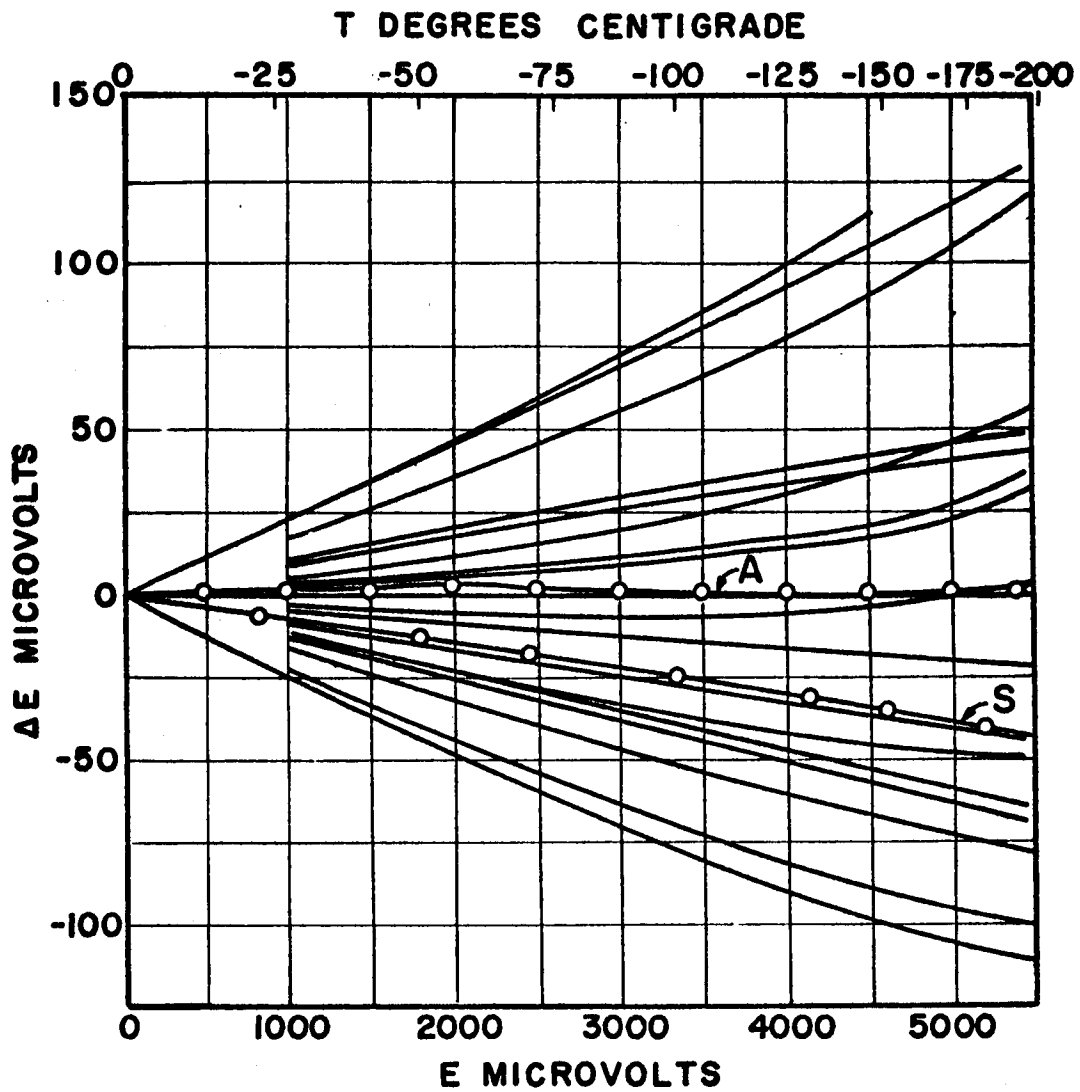
Figure 8.3 Differences Between the emfs of Some
Copper-Constantan Thermocouples and
True Values.

The corresponding voltage output of all three thermocouples will be read for various temperatures and a correction curve for each thermocouple will be drawn in this pressure range.

Before each test run, the thermocouples will be calibrated at atmospheric pressure to insure reproducibility. The expected accuracy of temperature measurement will be determined from this reproducibility. The technique of Scott [137], page 125, will be used to insure that the voltage measurement is reliable.

C. Length Measurement - The bubble radius must be measured from a photograph. The lighting will be such that liquid will photograph black and bubbles will be white. There is a vertical plane in which the bubbles are to be studied and the camera will be focused for that object plane. A polished spherical glass bead will be placed in the bubble chamber near the point of bubble formation and in the object plane. With the nitrogen in the chamber, a filar measuring microscope will be used to determine this size. Each frame taken by the camera will have this known length on it.

D. Time Measurement - The high speed camera to be used has a timing mark generator which marks the film one thousand times a second. This device is simply an oscillator in the camera timing light circuit. The timing marks will then be one millisecond apart.

Calibration for the internal oscillator can be accomplished by comparing the 1,000 cylces per second signal from the National Bureau of Standards Radio Station WWV to the oscillator on an oscilloscope. The internal oscillator will be adjusted until a one-to-one Lissajous pattern is obtained.

165

8.5 Additional Experimental Studies

With the addition of a transient pressure transducer experimental

data can be taken in three other areas.

A. The equation governing bubble growth and collapse,

$$R\ddot{R} + \frac{3}{2}\dot{R}^2 = \frac{P_v(T_v) - P_{L\infty}}{\rho_L} - \frac{2\sigma}{R\rho_L} \qquad (8.13)$$

can be solved for very fast transient pressures by assuming that $P_v(T_v)$

is almost a constant. The external pressure, $P_{L\infty}$, (measured with the

transient pressure transducer) will be put into a computer in tabular

form and the equation can be solved by numerical integration. This

will be another check on the validity of Equation (8.13).

For slowly varying transient pressures, heat transfer must be

considered and $P_v(T_v)$ can no longer be assumed constant.

B. Pressure transients in the liquid can be generated using a

piston-cylinder arrangement in the place of Chamber A (Figure 8.2).

By selecting the proper driving linkage for the piston, a rapid

decrease in pressure followed by a dwell at the minimum pressure

and then a gradual increase in pressure can be produced. This is

the type of pressure transient experienced by a liquid flowing through

a venturi. The bubble observation chamber with a piston-cylinder could

be used to compare cavitation produced in the bubble chamber to cavitation

produced in a flowing stream. This arrangement could be used to determine

the effect of fluid velocity and fluid acceleration on cavitation.

The elimination of fluid flow removes the effect of fluid viscosity

from consideration. There is still one viscosity effect if it is not

neglected in Equation (8.13).

$$RR\ddot{} + \frac{3}{2}\dot{R}^2 + \frac{4\mu_L \dot{R}}{\rho_L R} = \frac{P_v(T_v) - P_{L\infty}}{\rho_L} - \frac{2\sigma}{R \rho_L}.$$

(8.14)

In cavitation studies for a flowing liquid Equation (8.14) is used.

It appears that the difference in pressure drop required for cavitation between the flow and non-flow liquids is a function of the fluid velocity in the flowing system. If this is true, the prediction of when cavitation will occur can be made for any system by generating the transient pressure of that system in a static bubble chamber and applying the velocity function. This is the ultimate goal of the present study. It is hoped that the hydro-dynamic tunnel and the bubble observation chamber can be used concurrently in this endeavor.

C. This experimental apparatus including a transient pressure transducer could be placed on a vibrating platform and the effect of vibration upon cavitation could be studied with a high-speed camera.

8.6 Summary

The experimental arrangement described in this chapter will be used to verify the analytical solutions to the problems of growth in a superheated liquid, collapse in a subcooled liquid, and growth in a nonuniform temperature field.

It will also be used to study the effect of transient pressure on bubble dynamics. There is a possibility of comparing the transient pressure required for cavitation in a non-flow system to that in a flowing system.

The study of the effect of vibration upon cavitation can also be accomplished with the bubble observation chamber.

CHAPTER IX

Experimental Studies on Single-Phase Conduit Models

9.1 Introduction

In the following material a description is given of the experimental work which has been conducted in association with the single phase part of the study. The material includes a discussion of experimental apparatus which has been constructed.

9.2 Description of Apparatus

For the purpose of implementation of the experimental studies, the following equipment has been constructed.

Oscillating Piston and Drive Unit

The oscillating piston and drive unit (Figure 9.1 and 9.2) was constructed to drive the two basic sets of experimental apparatus detailed below. The piston is driven by a hydraulic motor capable of speeds from nearly zero to 4000 rpm. The power supply (Figure 9.3) consists of a gear pump directly coupled to an electric motor and employs a flow divider valve for control of oscillator speed.

Simple Hydraulic Line Pulsation Unit

The first experimental setup (Figure 9.4) utilizes the drive unit to impose a true sinusoidal pressure transient on the fluid contained in an eighty foot, one inch o.d., stainless steel line which terminated in the constant pressure reservoir (Figure 9.5).

TUBE
CONNECTING ROD
HYDRAULIC MOTOR
OSCILLATING HEAD
PISTON
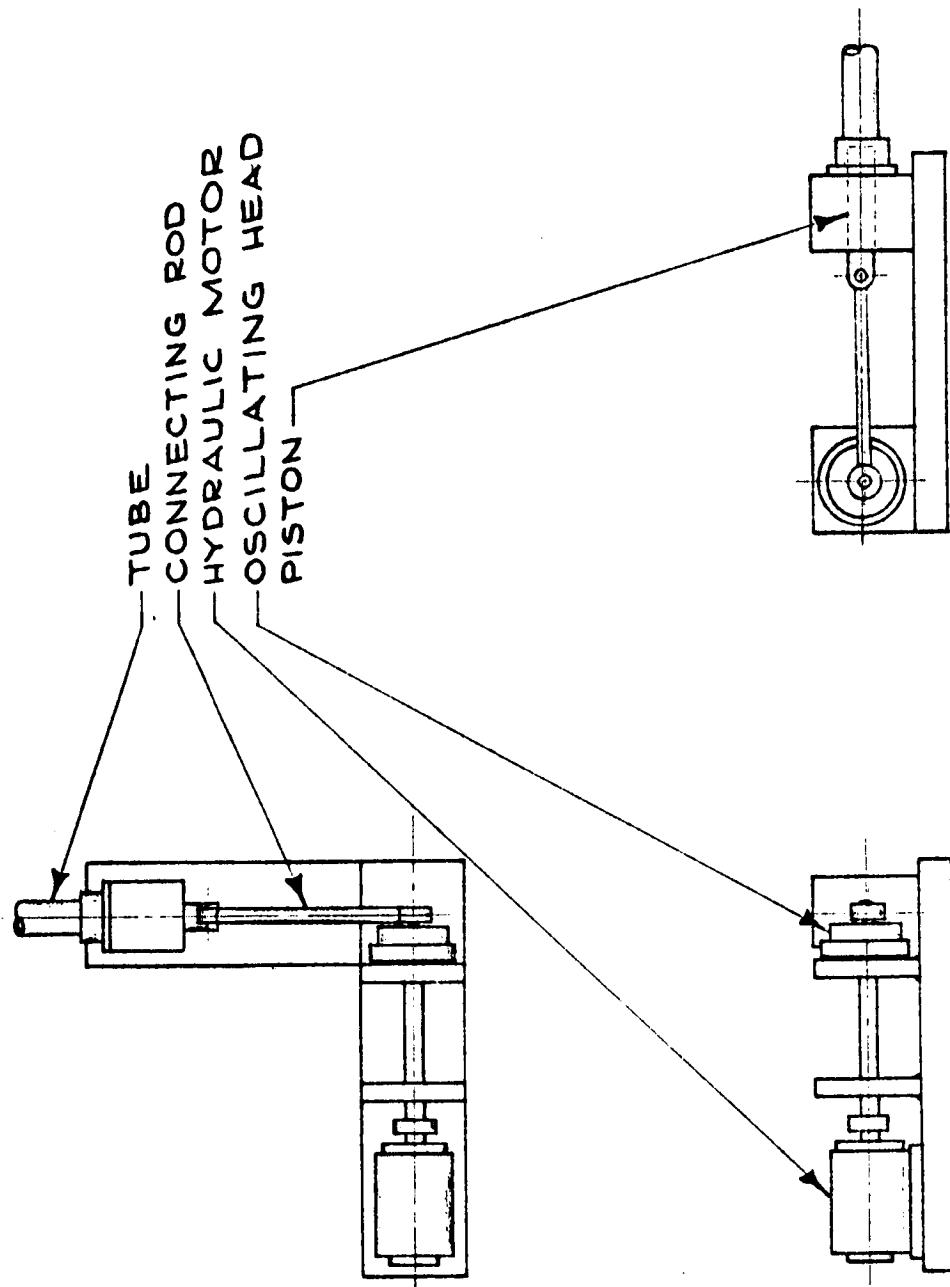
Figure 9.1 Oscillating Piston and Drive Unit
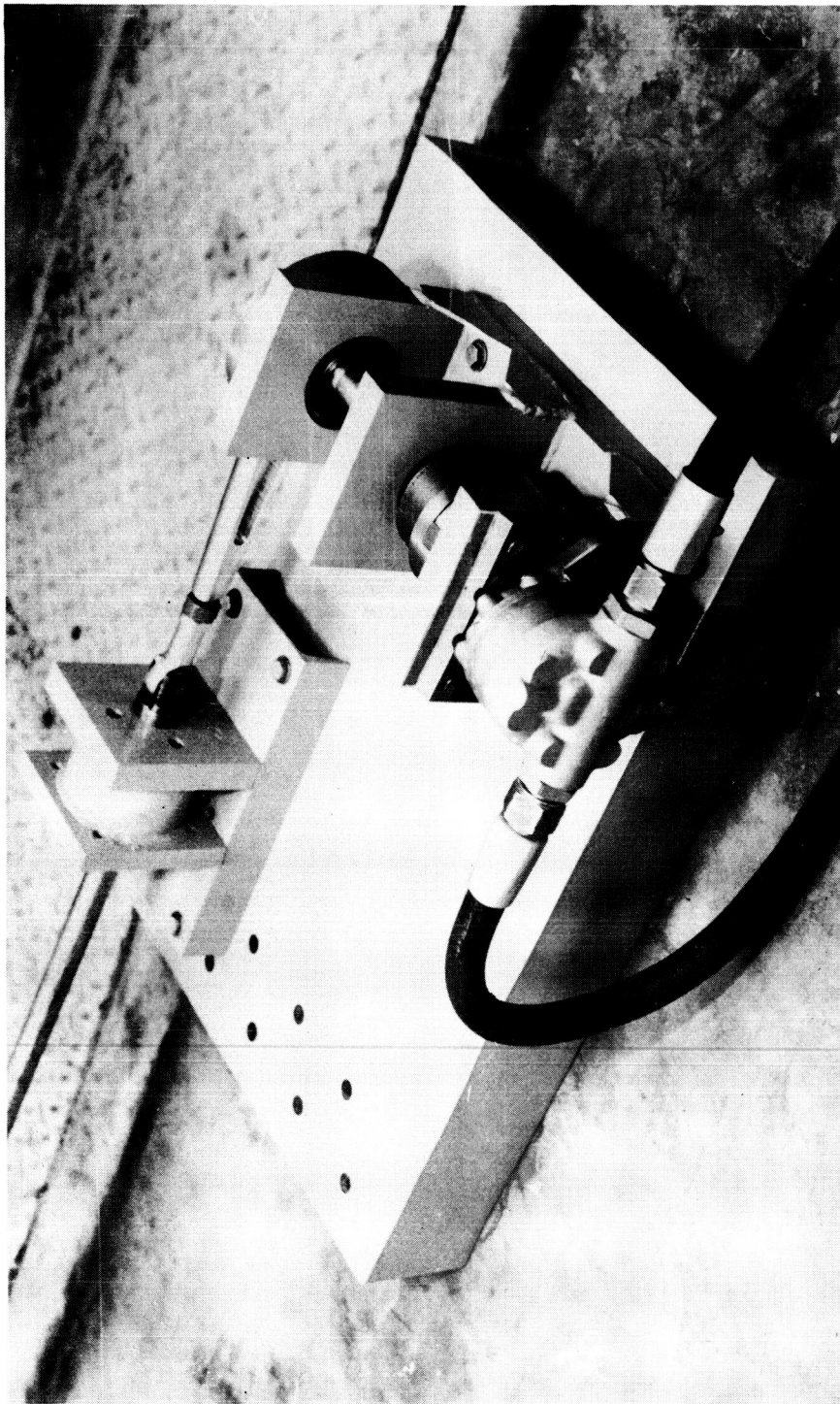
Figure 9.2 Oscillator Unit
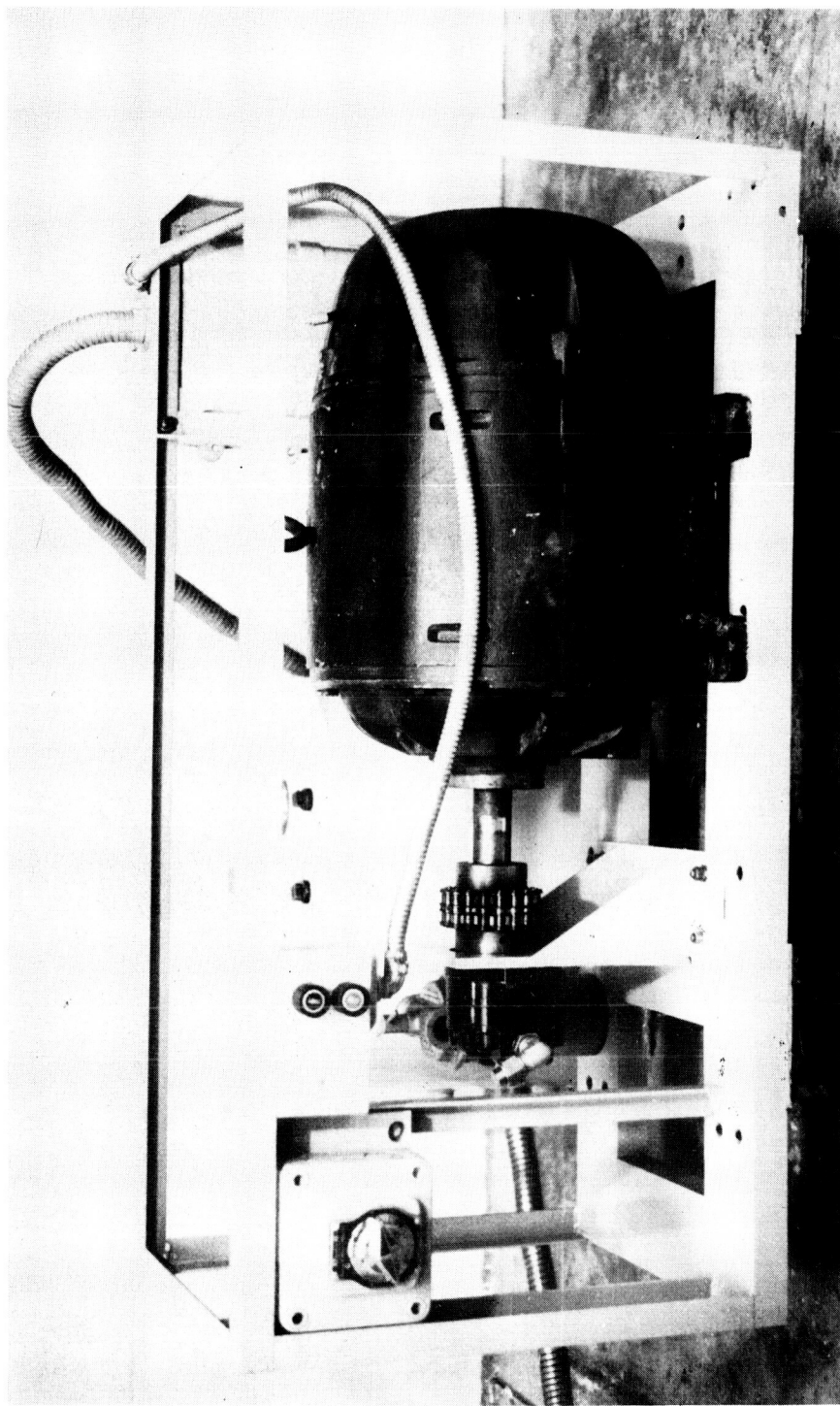
Figure 9.3 Hydraulic Power Supply
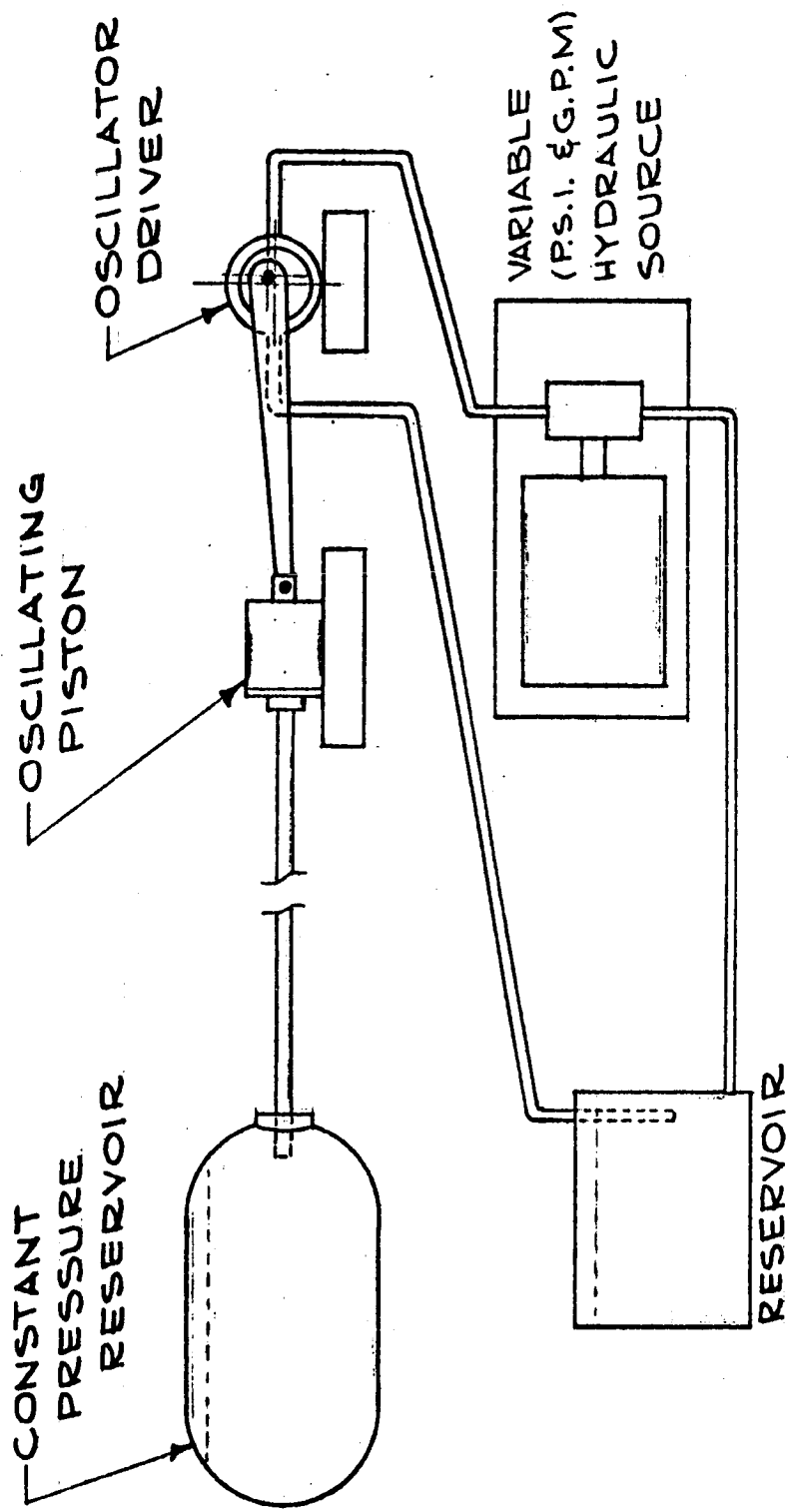
Figure 9.4 Conduit with Oscillator at One End and Constant Pressure Reservoir at Other End

Figure 9.5 Constant Pressure Reservoirs

A 1000 pound cement pad was used to provide a firm base for the driver unit. Instrumentation was provided to read out driver frequency, pressure at the pistonface, and reservoir pressure.

The Liquid Filled Vibrating Tube Unit I

The basic oscillating driver unit has been constructed so that it may be mounted in a vertical as well as a horizontal position. The vibrating tube unit I employed the driver, mounted in a vertical position with the base of a plexiglas tube attached as shown in Figure 9.6. This unit is intended for use in determining system vibration effects both for single-phase and two-phase fluid studies. Instrumentation is available to measure driver frequency and system fluid pressure at various points along the tube.

Orifice Study Experimental Apparatus

In order to investigate experimentally the transmission properties of orifices in fluid conduit systems and to compare acoustic data in the literature with hydraulic data, the test equipment shown in Figure 9.7 was constructed.

9.3 Experimental Results

The following is a description of the tests which have been performed using the test equipment detailed above.

Verification of Two-Dimensional Conduit Model

The first series of tests was conducted (using the hydraulic line pulsation unit, Figure 9.4) in order to verify the two-dimensional viscous model represented by the transfer relations (Equations 2.23 and 2.24) and using the propagation factor given

175
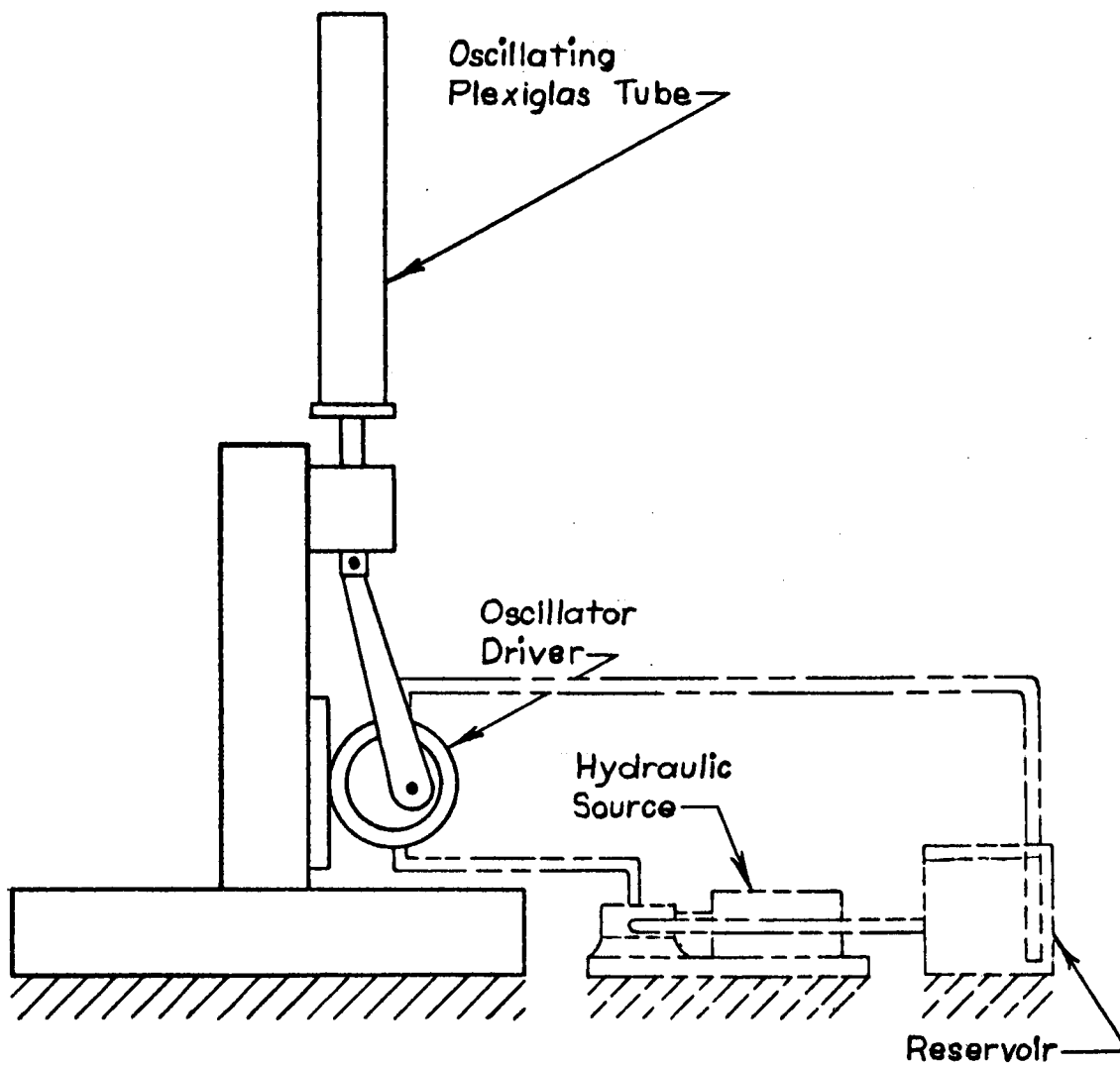
Figure 9.6 Vibrating Tube Unit I
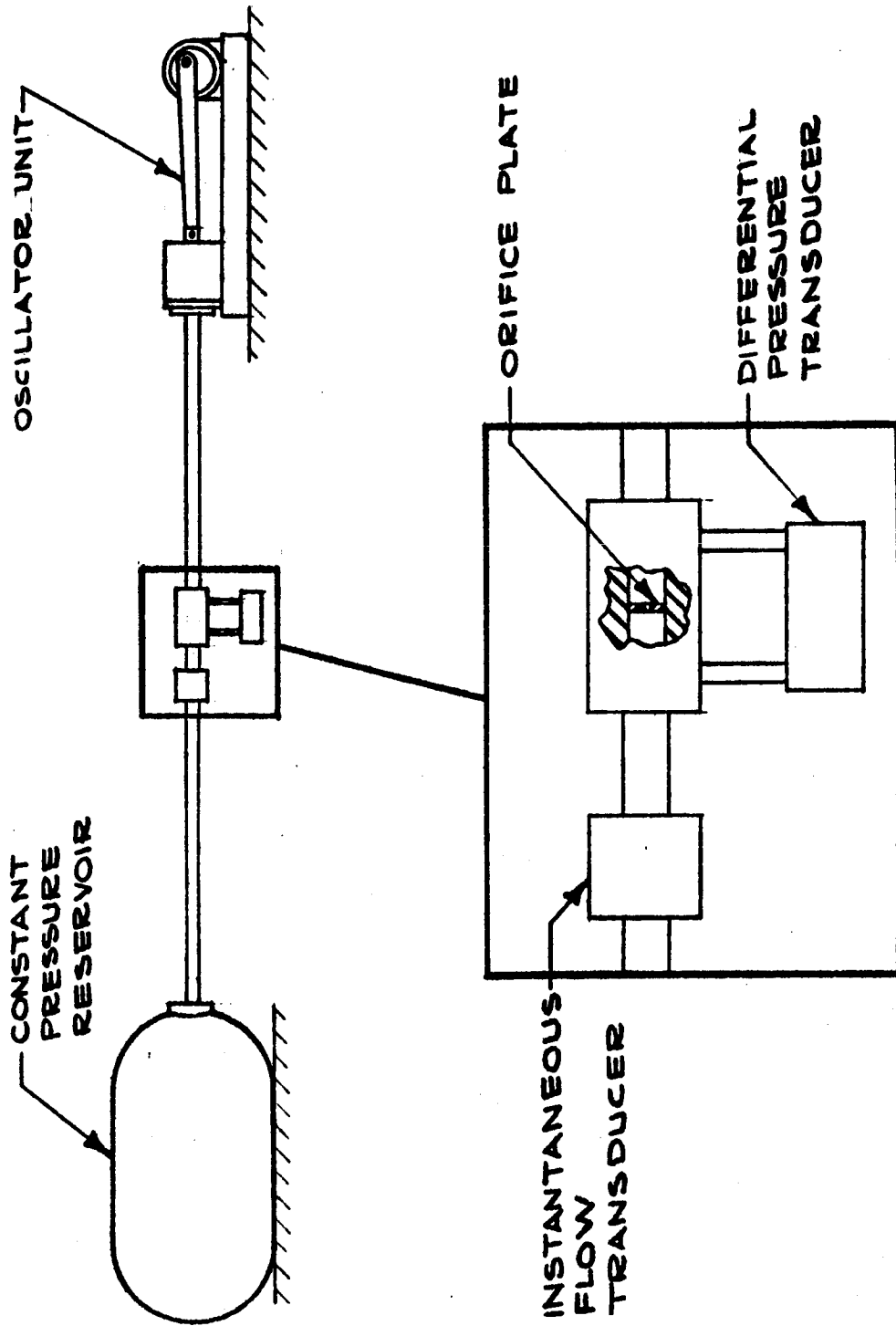
Figure 9.7   Schematic of Test Equipment
for Orifice Study

177

in Equation (6.45). Tests were conducted first with water as the operating fluid. The frequency of the driver unit was varied from 400 rpm to 3000 rpm and the pressure disturbance at the driver end was recorded. The pressure recording equipment consisted of a pressure transducer with both single pin recorded and scope output. The recorder was used in the low rpm ranges to record the traces and a camera fitted to the scope recorded the traces in the higher rpm ranges. The system static pressure was maintained at 500 psi, thus allowing up to 1000 psi peak-to-peak pressure variations. Figure 9.8 shows an experimental and theoretical plot for an experimental run made with a driver amplitude of .025 inches. The experimental data follows the theoretical predictions well in the region of the first resonant point, but there appears to be some discrepancy on the second resonant point. This difference stems from the fact that there is about a 2 per cent difference in the resonant frequencies between the experimental and theoretical data. This is a rather small experimental error and could easily be accounted for in the calculation of the effective speed of sound of the fluid. Since the tube walls are not perfectly rigid, Equation (2.43) was used in calculating the effective speed of sound. The values of K, c_o, and E_t used in the calculations were obtained from a handbook and there is no assurance of their accuracy.

It is interesting to note that a common practice among writers reporting upon conduit studies is to correct their analytical value of the speed of sound to match their experimental data. This is mainly due to the lack of knowledge concerning accurate values of
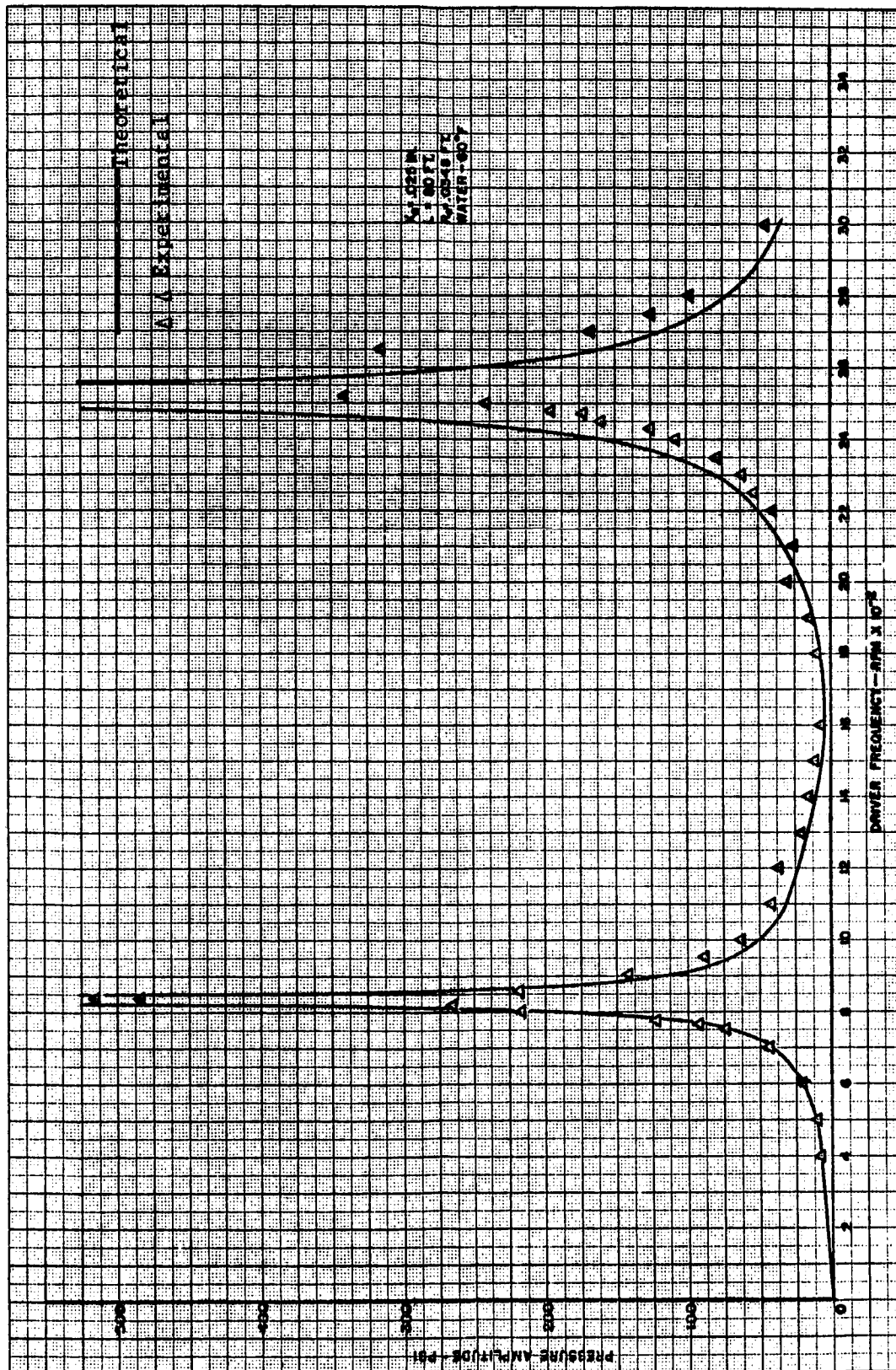
Figure 9.8 Theoretical and Experimental Pressure Amplitude
vs. Driver Frequency for Setup in Figure 9.4
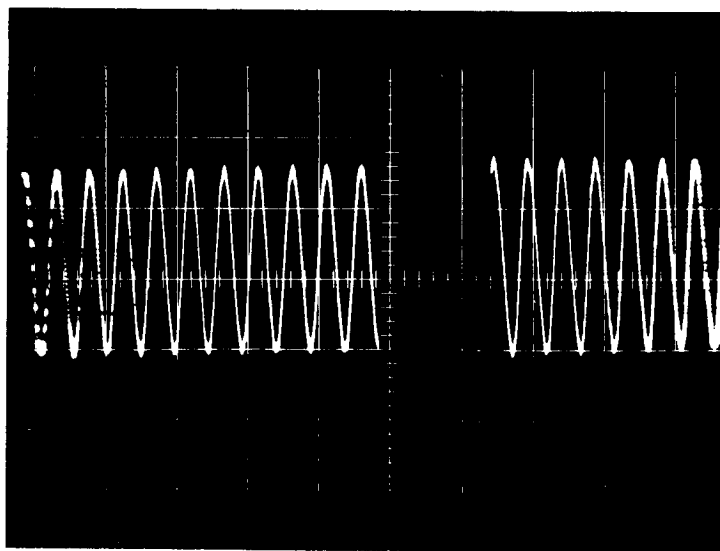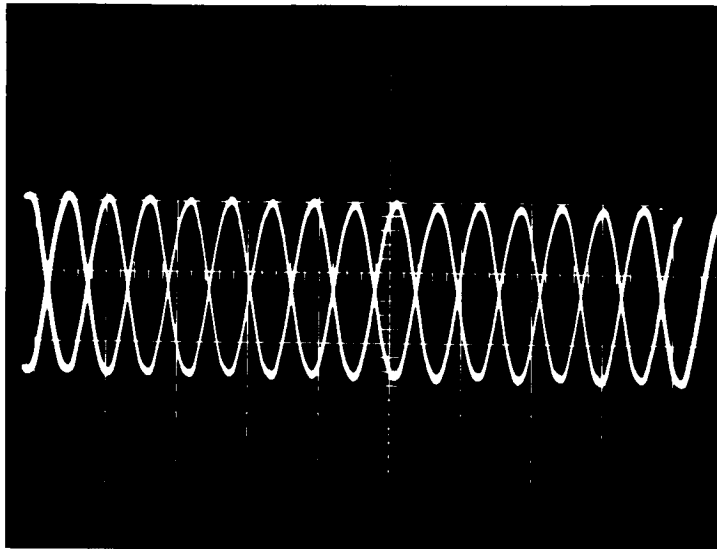
Figure 8.8   Typical Pressure Traces
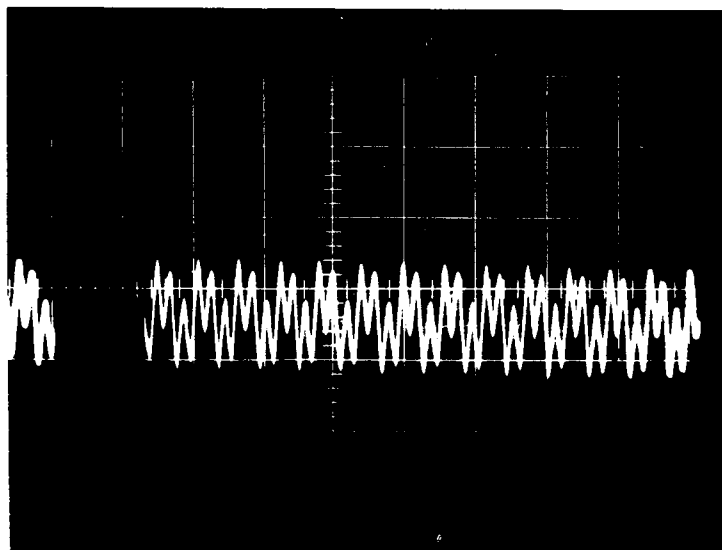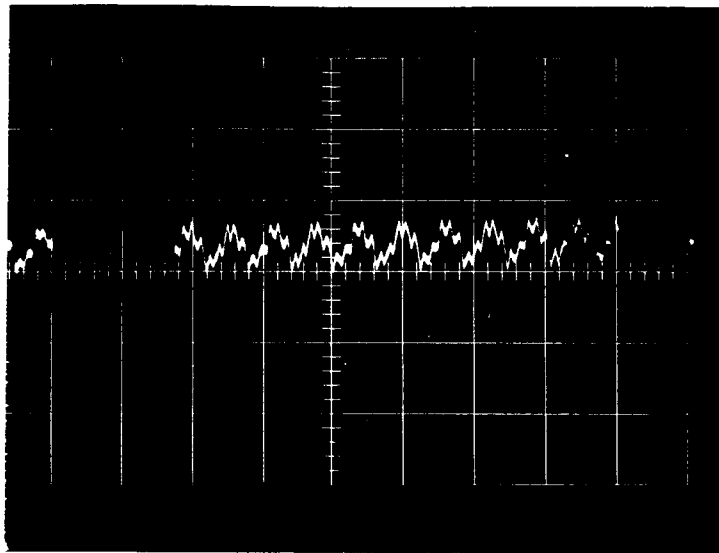
Figure 9.10 Typical Pressure Traces
With Superimposed Sine Wave

K and c$_o$ for many fluids. These constants are difficult to determine and may vary drastically depending on the type of fluid, its additives, and other fluid parameters.

Two phenomena which occurred during the tests are worthy of note at this point. The first was that frequency oscillations occurred in the hydraulic drive system when the system is operated very close to a resonant peak. This is apparently due to the great change in power per change of frequency near these points. Because of this, the resonant points must be approached very slowly in order to not induce this oscillation. It was found to be impossible to get the system to operate exactly at resonance. The other phenomena was the occurrence of a superimposed sine wave upon the main disturbance at certain frequencies. The exact cause of this superimposed disturbance has not yet been determined, but it is suspected that it may be the natural frequencies of the driver. Figure 9.9 shows typical pressure traces when this superimposed disturbance is not noticeably present. Figure 9.10, on the other hand, shows the main sine wave plus the superimposed wave. It was rather hard to determine the amplitude of the main disturbance from these traces so the peak-to-peak values were used. This gives values which are too high as may be seen from the points at 1200 and 2000 in Figure 9.8. Very similar results were obtained using the same experimental configuration but with a driver amplitude at .050 inches.

Again, using the first experimental setup with MIL-5606 hydraulic fluid as the media, a test was made with the .025 inch driver amplitude. All other conditions were similar to the previous tests. Figure 9.11
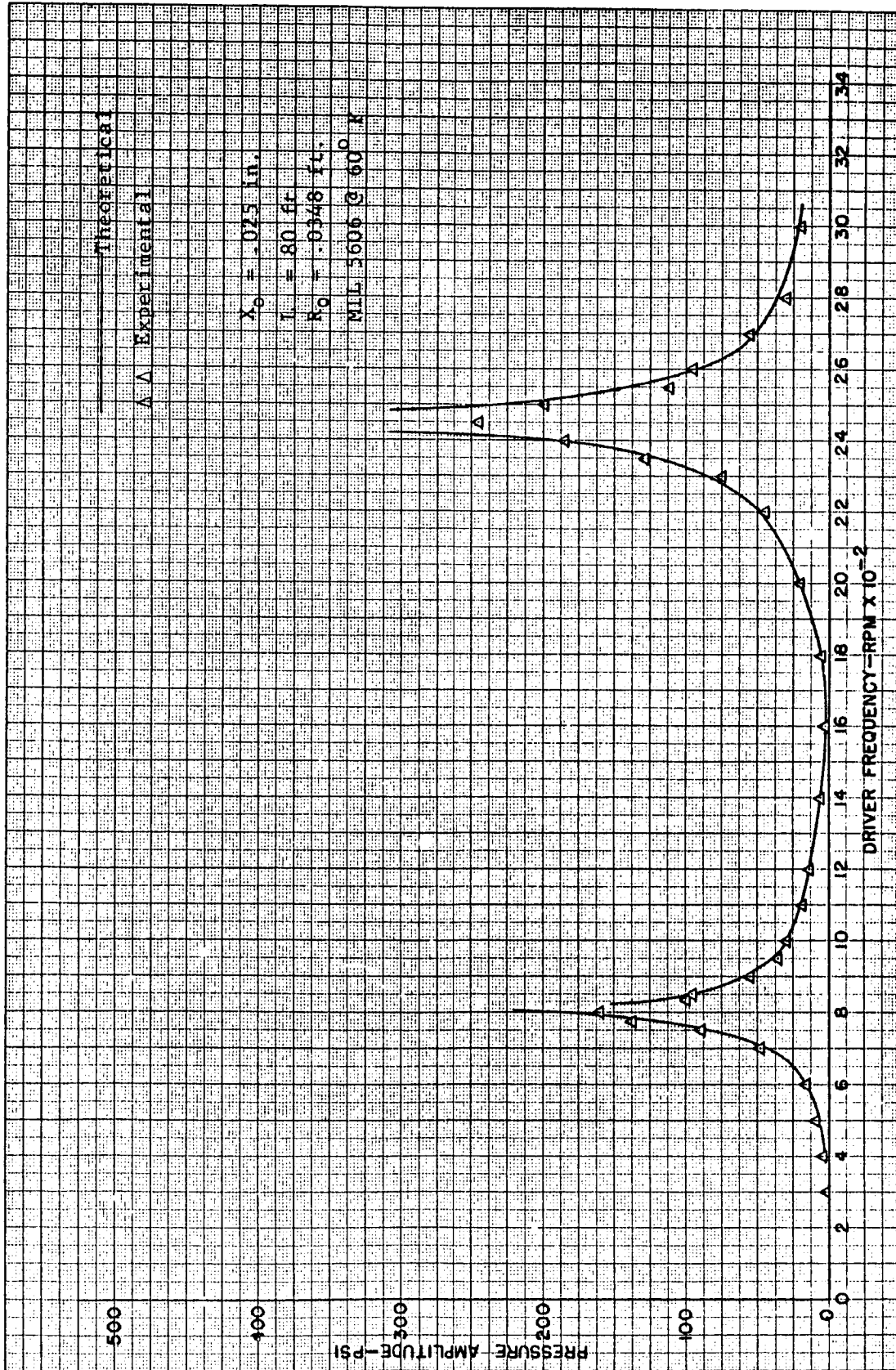
Figure 9.10 Theoretical and Experimental Pressure Amplitude vs.
Driver Frequency for Setup in Figure 9.4

183

shows the pressure amplitude vs. driver frequency plot for the test.
The plot of theoretical values shows good agreement with the experi-
mental data.

Orifice Study

A series of six tests were performed to determine the resistance
of various orifices situated in a fluid line as shown in Figure 9.7.
For the tests, the reservoir was pressurized to prevent cavitation
and the driver unit was utilized to impose a true sinusoidal pressure
transient on the fluid. Water at room temperature was used in the tests
and was assumed to be incompressible over the twenty-inch length between
the piston face and the orifice manifold.

Instrumentation (Figure 9.12) was provided to measure rpm of the
driver, differential pressure across the orifice, and instantaneous
flow volume.
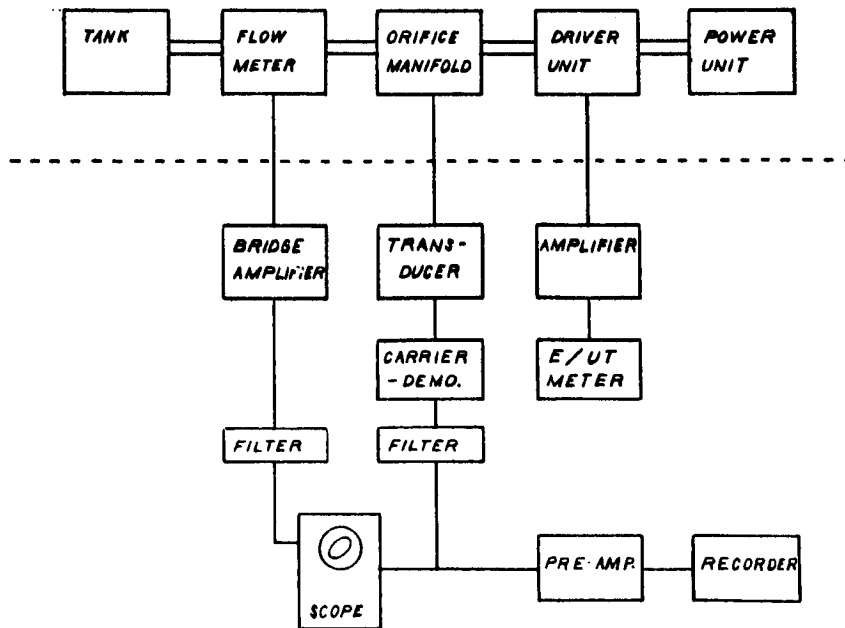
Figure 9.12 Instrumentation for Orifice Study

184

In addition to the data taken under pulsating conditions, steady flow differential pressure data was also taken so that a comparison could be made between the steady flow resistance and nonsteady resistance. The resistance values for each case were calculated by dividing the differential pressure amplitude by the fluid velocity amplitude.

Plots of velocity resistance versus velocity are presented in Figures (9.13), (9.14), and (9.15) for the 0.100 inch flat, 0.2015 inch flat, and 0.2015 inch sharp edged orifices, respectively. Due to equipment limitations, the linear region of resistance is not well defined for this data; however, there is a marked discontinuity at the beginning of the nonlinear region. Figure (9.16) shows a resistance versus velocity plot of the data reported by Thurston and Martin [34].

We observe that the nonlinear region begins in the range of $v = 60$ to 100 in/sec for the 0.1 inch orifice, 15-17 in/sec for the .2015 inch flat orifice and 18-20 in/sec for the .2015 inch sharp edged orifice. Thurston's data becomes nonlinear at a value of 0.9, 1, and 13 in/sec for the three orifices which he tested. The above information leads us to the conclusion that there exists a characteristic velocity at which the nonlinear region begins which is most critically dependent on orifice size. In this respect, the velocity impedance is the most convenient impedance dimension to study.

A comparison of steady flow impedance (that is resistance) with that for purely pulsating flow is also made in Figure (9.13), (9.14) and (9.15). In Figure (9.13) where the nonlinear region falls in the velocity range of 10 to 100 in/sec, it can be seen that the transient

185
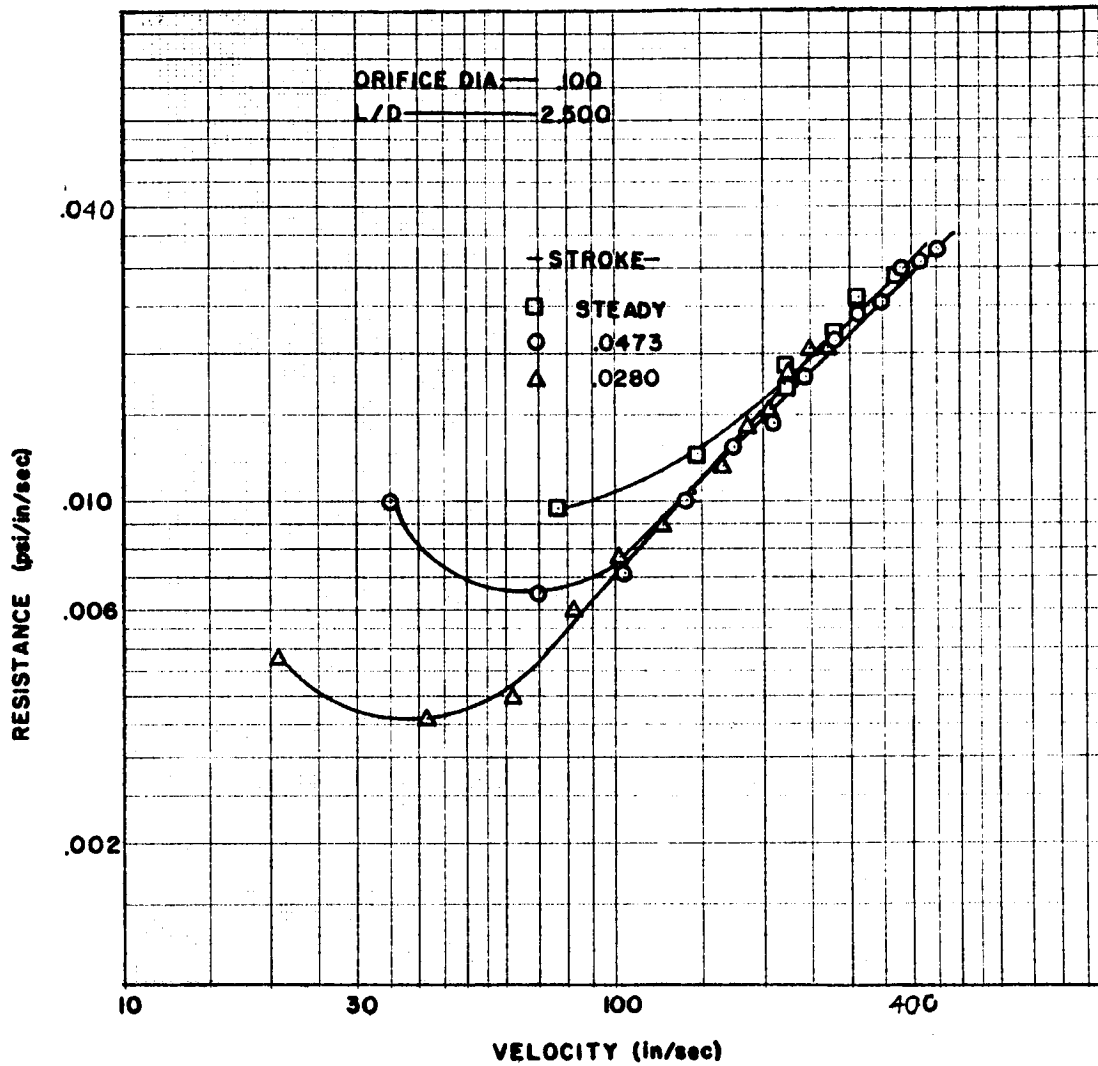
Figure 9.13 Resistance Versus Velocity
for .100 Inch Orifice
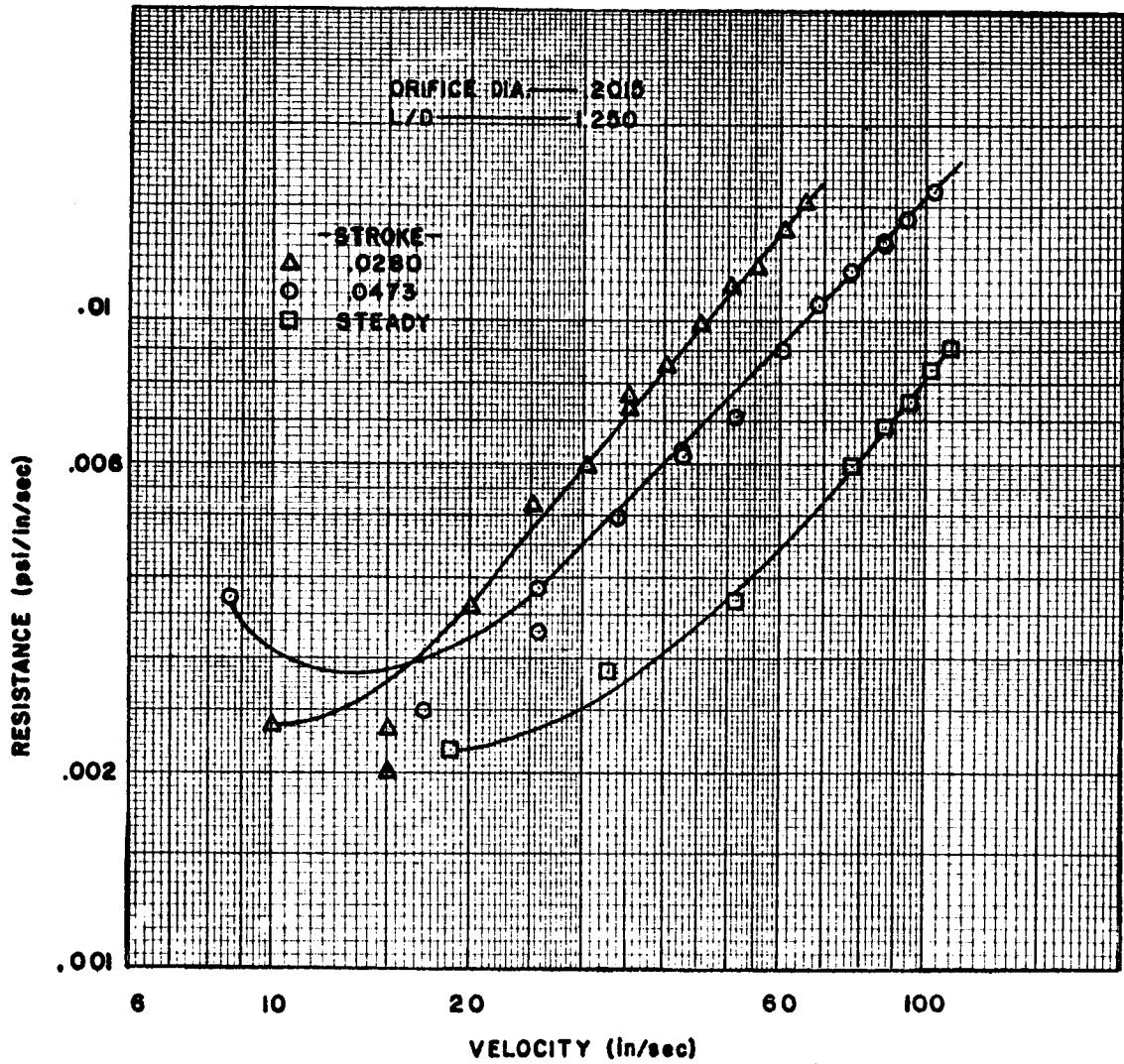
Figure 9.14   Resistance Versus Velocity
for .2015 Inch Orifice
L/D = .250 inches

187
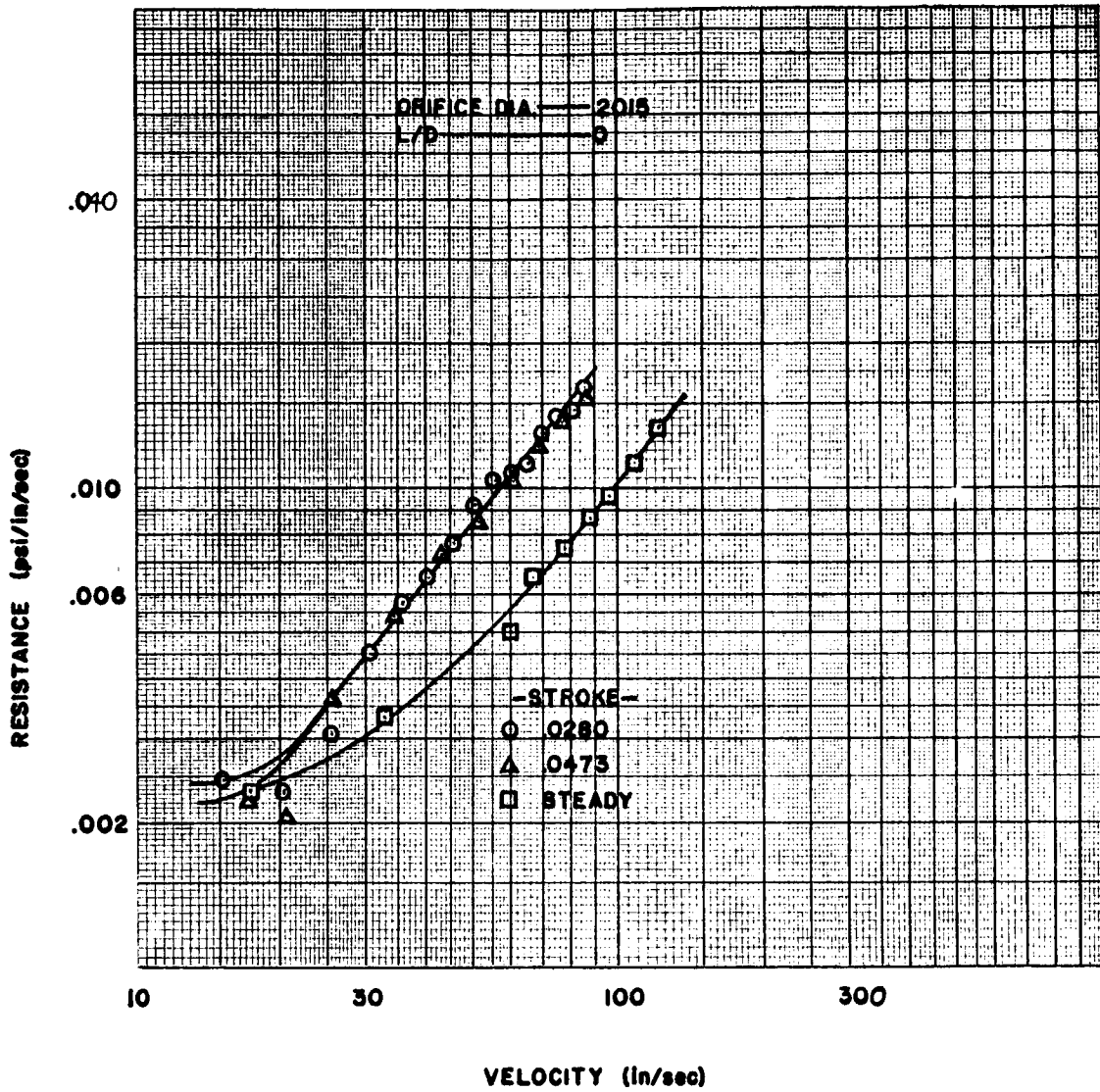
Figure 9.15 Resistance Versus Velocity
for .2015 Inch Sharp-Edged Orifice
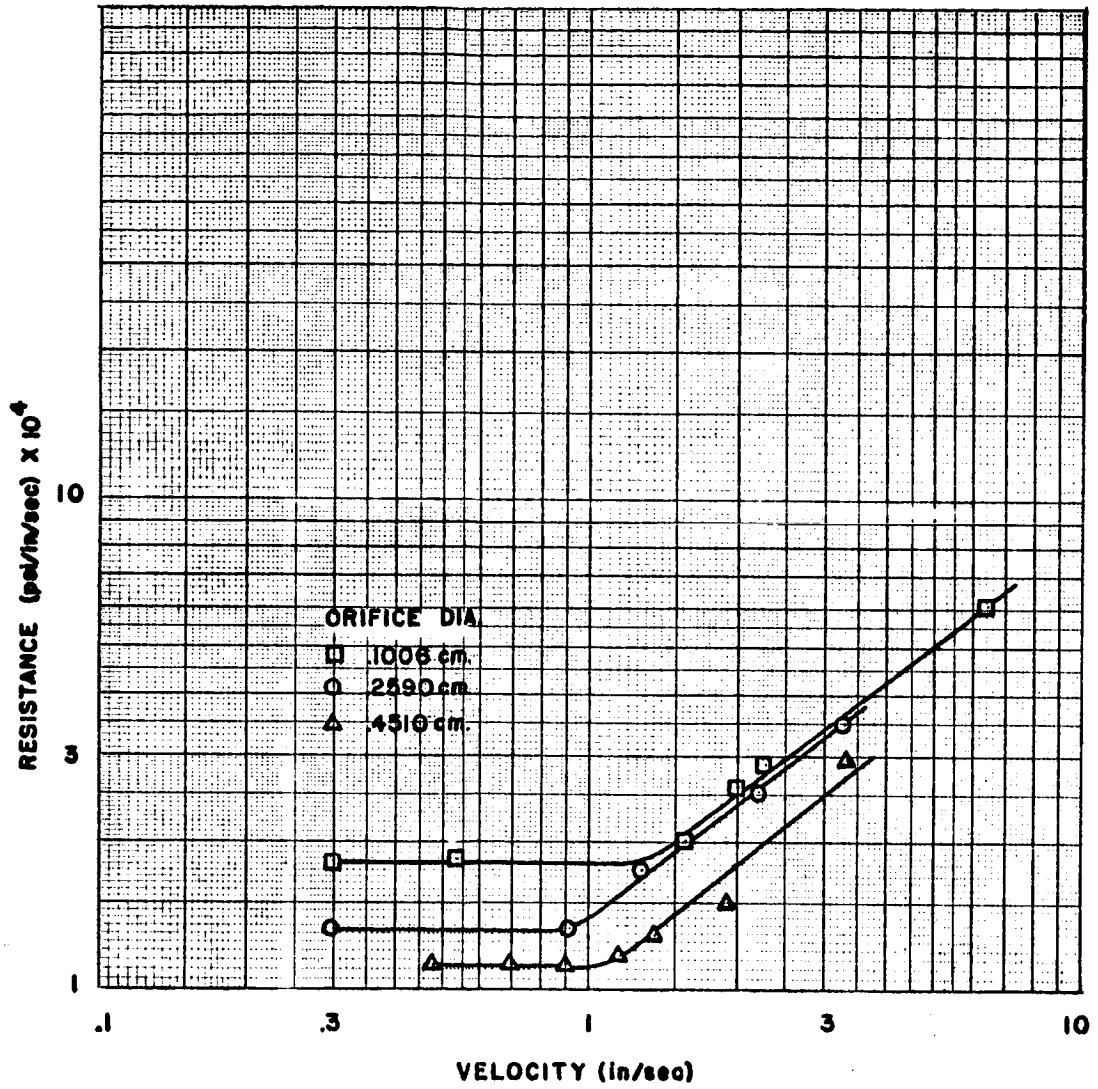
Figure 9.16   Resistance Versus Velocity
From Reference [34]

flow resistance is very closely approximated by steady flow resistance. In Figures (9.14) and (9.15), however, there is a correction factor needed to make the same assumption since the velocity range of the nonlinear region falls between 1 and 10 in/sec. The pulsating flow resistance is plotted against peak velocity.

From an analysis of the experiment results we have found that there are four distinct cases which may occur.

Case I - No steady flow component - small perturbations

For Case I we have no net steady flow component and we assume that the pressure and velocity perturbations are small. The experimental studies have shown that for this case the unsteady pressure drop, ΔP, and the unsteady velocity are related by the relation

$$\Delta P = R v + I \frac{dv}{dt}$$

where R is a linear resistance and I a linear inertance. Generally, in the linear region, the inertance is very much smaller than the resistance for practical frequency ranges.

Case II - No steady flow component - large perturbations

For this case we assume that the pressure and velocity fluctuations are large enough so that we are in the nonlinear region of the resistance and inertance. It has been shown that in this region the relationship between the velocity and pressure drop is given approximately by the steady flow orifice equation (neglecting the inertance) or

$$\Delta P = K v^2 \qquad (9.1)$$

where K is adjusted to agree with experimental data.

Case III - Steady flow component - small perturbations

   If the velocity and pressure fluctuations are small

then we may use the linearized relation given by (2.53).

Case IV - Steady flow component - large perturbations

   For this case Equation (9.1) must also be used.

CHAPTER X

Experimental Study of the Formation of Two-Phase Flow
As Caused by Pressure Drop

10.1 Introduction

Considerable progress has been made in the development of a mathematical model which will describe the flow of a single-phase fluid through conduits (see Chapter VI). The development of a mathematical model which will describe single- and two-phase flow has been limited because of insufficient information about the cavitation properties of various liquids while flowing through different pressure distributions (see Chapter IV). A small hydrodynamic tunnel is being constructed so that we can determine the conditions under which profuse and limited cavitation starts and the conditions which will cause these cavities to collapse.

This chapter will be limited to a discussion of the experimental investigations to be performed with the hydrodynamic tunnel and the tunnel design. This is necessary because the hydrodynamic tunnel is not in operation.

10.2 Experimental Investigations

The hydrodynamic tunnel will serve as a useful apparatus in the study of the formation of two-phase single-component flow. This tunnel is designed so that additional investigations can be performed without any major change in the present design.

192

The experimental investigations to be performed with the hydro-dynamic tunnel are:

1. Determine the effect of acceleration or pressure distribution on cavitation relaxation time for limited- and profuse-cavitation occurring in venturi and elbow test sections.

2. Determine the conditions under which these cavities will collapse.

3. Determine the effect of flow patterns on items 1 and 2.

4. Determine the validity of the experimental work performed by Lehman and Young [57] (see Figure 4.17).

5. Determine the boundary conditions for the theoretical investigation.

These investigations will be performed using several different liquids. This will be necessary in order to determine the effect of fluid properties such as viscosity, surface tension, etc.

The items listed in the preceeding paragraph constitute the first phase of an experimental program designed to study the effects of vibration on the cavitation properties of cryogenic fluids flowing through various geometries. The ultimate goal of this test program is to provide information for use by the designer of cryogenic equipment. This may be accomplished by undertaking a systematic experimental program with dynamic (flow) and static (nonflow) systems.

10.3 Discussion of Tunnel Design

The facility to be used in the study of bubble formation and collapse, for flowing fluids, is a closed-return hydrodynamic tunnel designed to handle cryogenic as well as ordinary liquids. The facility

is shown schematically in Figure 10.1. The tunnel is designed to accommodate 18-inch long venturi test sections and elbow test sections with various $\bar{R}/r_o$ ratios. It will be fabricated of 304 stainless steel except for the heat exchanger and test sections and has a total liquid capacity of about 5 U. S. gallons. The venturi test sections will be operated in a vertical position to help simulate actual flow patterns within a missile. A variable-speed pump-drive unit, which is capable of providing operational flow velocities from 15 to 100 feet per second in the test sections, will be used. The Centrifugal pump is a commercially available unit designed to handle liquid nitrogen. In order to reduce tunnel losses, only one test section will be installed at any time. Corner-turning vanes and flow straighteners will be used when uniform, steady, irrotational flow is desired at the test section.

The tunnel facility is designed to operate over a pressure range from 0 to 250 psia and a temperature range from 130 to -320 F. High pressure nitrogen gas will be used as the tunnel pressurizing medium. Tunnel pressures less than atmospheric will be obtained by means of a vacuum system connected to the pressurizing line.

The heat exchanger consists of a double-pipe arrangement. The inner pipe will be fabricated of copper to provide a good heat transfer between the tunnel and the cooling or heating liquids. Provision has been made so that fins can be installed on the copper pipe if they are needed. The outer tube of the heat exchanger will be made of 304 stainless steel. An O-Ring seal will be used at the upper end of the heat exchanger to eliminate the formation of thermal stresses.

A float type liquid level control valve will be used to control the coolant (liquid nitrogen) level when nitrogen is being studied in the tunnel.

The tunnel will be insulated with cork or some commercially available material which has a thermal conductivity of about 0.01 Btu/hr ft. F. This will insure almost isothermal flow except through the pump and heat exchanger.

The free gas present in the tunnel will be controlled with a resorber. There is some question, however, of the optimum design of a resorber; if they are too "efficient," the amount of free gas, or nuclei, may be insufficient for purposes of modeling inception. Therefore, the tunnel will be operated without a resorber during initial testing.
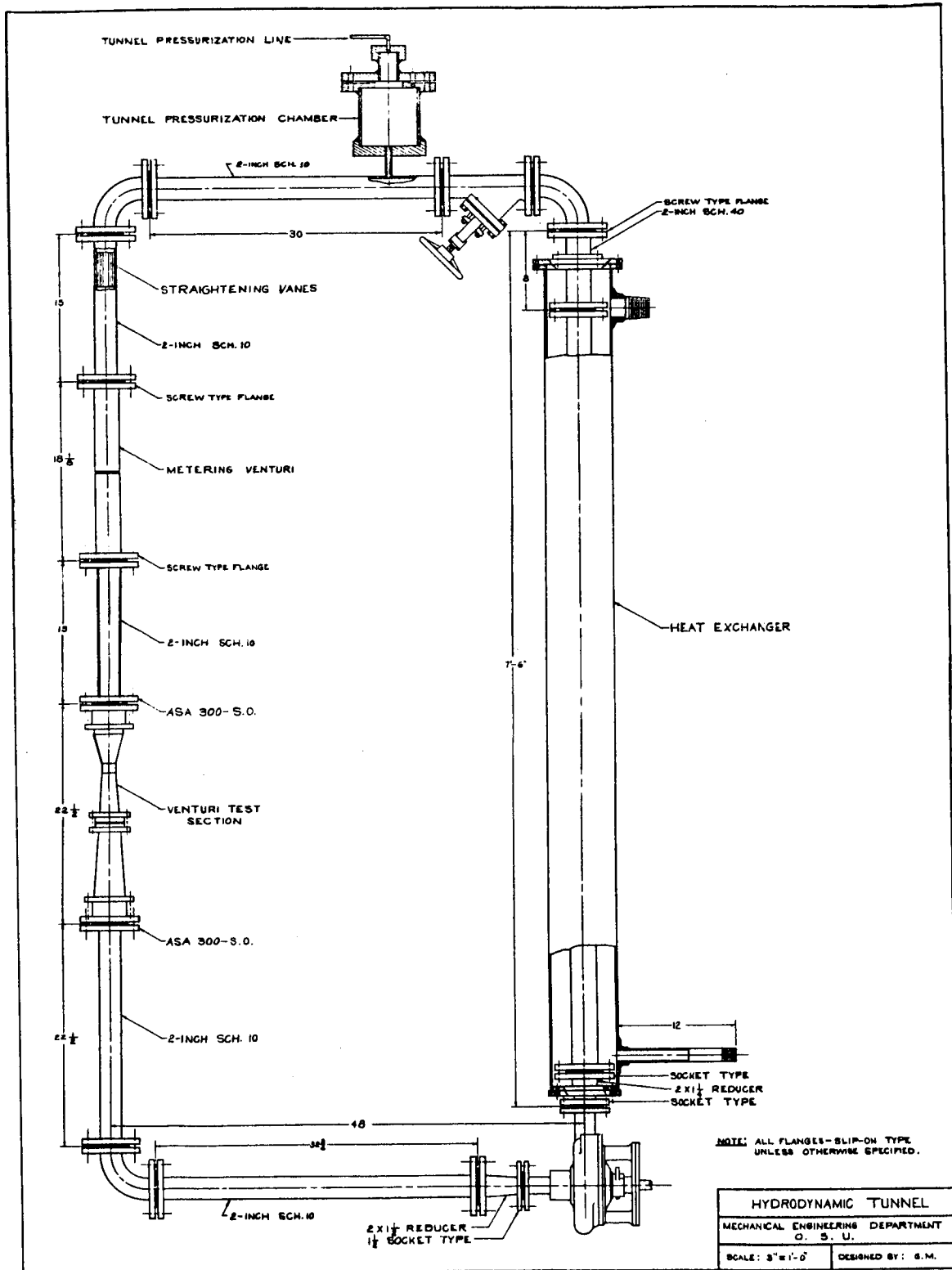
Figure 10.1 Hydrodynamic Tunnel

APPENDICES

APPENDIX A

BIBLIOGRAPHY

References for Chapter II

1.   Lass, H., Vector and Tensor Analysis, McGraw-Hill Book
            Co., Inc., 1950.

2.   Schlichting, H., Boundary Layer Theory, McGraw-Hill Book
            Co., Inc., 1960.

3.   Bird, R. B., W. E. Steward, and E. N. Lightfoot, Transport
            Phenomena, John Wiley and Sons, Inc., New York, 1960.

4.   Joukowsky, N., "Water Hammer," Proceedings American Water
            Works Association, 1904, p. 341.

5.   Allievi, Lorenzo, "Theory of Water Hammer," translated by
            E. E. Halmos, 1925. See "Symposium on Water Hammer,"
            ASME publication, 1933, Second Printing, 1949.

6.   Rich, G. R., Hydraulic Transients, McGraw-Hill Book Co.,
            Inc., New York, 1955.

7.   Paynter, H. M., "Section 20, Fluid Transients in Engineering
            Systems," from Handbook of Fluid Dynamics, by V. L.
            Streeter, Ed., McGraw-Hill Book Co., Inc., New York, 1961.

8.   Walker, M. L., Jr., E. T. Kirkpatrick and W. T. Rouleau,
            "Viscous Dispersion in Water Hammer," Trans. ASME, Vol.
            82, 1960, pp. 759-764.

9.   Schuder, C. B. and R. C. Binder, "The Response of Pneumatic
            Transmission Lines to Step Inputs," Trans. ASME, Series
            D, Vol. 81, 1959, pp. 578-584.

10.   Oldenburger, R. and R. E. Goodson, "Simplification of
            Hydraulic Line Dynamics by Use of Infinite Products,"
            Trans. ASME, Series D, Vol. 86, 1964, pp. 1-10.

11.   Schiesser, Boonshaft and Fuchs, Inc., "The Frequency
            Response of an Actuator Supplied by Two Long Hydraulic
            Lines," Trans. AIChE, 1964 Joint Automatic Control
            Conference, Stanford University.

Chapter II

12.   Rouleau, W. T., "Pressure Surges in Pipelines Carrying
         Viscous Liquids," Trans. ASME, Vol. 82, 1960, pp.
         912-920.

13.   Sarlat, I. M. and T. L. Wilson, "Surge Pressures in
         Liquid Transfer Lines," Trans. ASME, Vol. 84, 1962,
         pp. 363-368.

14.   Waller, E. J., "Response of Pipe Line Systems to Transient
         Flow Using the Generalized Impedance Method," Oklahoma
         Engineering Experiment Station Publication, Oklahoma
         State University, January, 1960.

15.   Nichols, N. B., "The Linear Properties of Pneumatic
         Transmission Lines," ISA Trans., Vol. 1, January,
         1962, pp. 5-14.

16.   Iberall, A. S., "Attenuation of Oscillatory Pressures
         in Instrument Lines," Journal of Research, National
         Bureau of Standards, Vol. 45, July, 1950, pp. 85-108.

17.   Brown, F. T., "The Transient Response of Fluid Lines,"
         Trans. ASME, Series D, Vol. 84, 1962, pp. 547-553.

18.   D'Souze, A. F. and R. Oldenburger, "Dynamic Response of
         Fluid Lines," Trans. ASME, September, 1964, pp. 589-598.

19.   Watson, G. N., A Treatise on the Theory of Bessel Functions,
         Cambridge University Press, Cambridge, 1958, pp. 77-83,
         Appendix, p. 78, p. 498.

20.   Blackburn, J. F., Gerhard Reethof and J. L. Shearer, Fluid
         Power Control, The M.I.T. Press, Cambridge, Mass., 1960.

21.   Aseltine, J. A., Transform Method in Linear System Analysis,
         McGraw-Hill Book Co., Inc., New York, 1958.

22.   Waller, E. J., L. E. Hove and W. D. Bernhart, "Liquidborne
         Noise Reduction," Volumes I, II and III, Engineering
         Report, Oklahoma State University, 1963.

23.   Pipes, L. A., "The Matrix Theory of Four-Terminal Networks,"
         Philosophical Magazine, Vol. 30, 1940, pp. 370-395.

24.   Bergeron, Waterhammer in Hydraulics and Wave Surges in
         Electricity, ASME Publication, 1961.

25.   Technical Documentary Report No. APL TDR 64-109, "Research Investigation of Hydraulic Pulsation Concepts," October, 1964.

26.   Paynter, H. M., U. S. Patent No. 3044703; Filed on June 24, 1954, Issued on July 17, 1962.

27.   Lamb, H., "On the Velocity of Sound in a Tube, as Affected by the Elasticity of the Walls," Manchester Memoirs, Vol. XLII (1898) No. 9, pp. 1-16.

28.   Jacobi, W. J., "Porpagation of Sound Waves Along Liquid Cylinders," Journal of the Acoustical Society of America, Vol. 21, 1949, pp. 120-127.

29.   Morgan, G. W. and J. P. Kiely, "Wave Propagation in Viscous Liquid Contained in a Flexible Tube," Journal of the Acoustical Society of America, Vol. 26, May, 1954, pp. 323-328.

30.   Lin, T. C. and G. W. Morgan, "Wave Propagation Through Fluid Contained in a Cylindrical, Elastic Shell," Journal of the Acoustical Society of America, Vol. 28, November, 1956, pp. 1165-1176.

31.   Skalak, R., "An Extension of the Theory of Water Hammer," Trans. ASME, Vol. 78, 1956, pp. 105-116.

32.   Regetz, J. D., Jr., "An Experimental Determination of the Dynamic Response of a Long Hydraulic Line," NASA Technical Report D-576, December, 1960, pp. 1-38.

33.   Shapiro, A. H., Compressible Fluid Flow, The Ronald Press Company, New York, 1953.

34.   Goodson, R. E., Viscous and Boundary Effects in Fluid Lines, University Microfilms, Inc., Ann Arbor, Michigan, Ph.D. Thesis, January, 1963.

35.   Thurston, G. B. and C. E. Martin, Jr., "Periodic Fluid Flow Through Circular Orifices," Journal of the Acoustical Society of America, Vol. 25, January, 1953, pp. 26-31.

36.   Rayleigh, J., The Theory of Sound, Dover, Vol. II, pp. 180-181, 1960.

Chapter II

37.   Thurston, G., L. Hargrove, and B. Cook, "Nonlinear Properties of Circular Orifices," _Journal of the Acoustical Society of America_, Vol. 29, pp. 992-1001.

38.   Wood, J., "The Acoustic Resistance of a Pipe Orifice to Steady Flow," _Journal of the Acoustical Society of America_, Vol. 26, pp. 492-494.

39.   Sivian, L., "Acoustic Impedance of Small Orifices," _Journal of the Acoustical Society of America_, Vol. 7, pp. 94-101.

40.   Thurston, G. and J. Wood, "End Corrections for a Circular Orifice in a Circular Tube," _Journal of the Acoustical Society of America_, Vol. 25, pp. 861-863.

41.   Ingard, U. and S. Labate, "Circulation Effects and Impedance of Orifices," _Journal of the Acoustical Society of America_, Vol. 22, pp. 211-218.

42.   Karal, F., "The Analogous Acoustical Impedance for Discontinuities and Constriction of Circular Cross Section," _Journal of the Acoustical Society of America_, Vol. 25, pp. 327-334.

43.   Bolt, R., S. Labate, and U. Ingard, "The Acoustic Reactance of Small Circular Orifices," _Journal of the Acoustical Society of America_, Vol. 21, pp. 94-97.

44.   Crandall, I., _Theory of Vibrating Systems and Sound_, Van Nostrand, New York, pp. 151 and 237, 1927.

45.   Morse, P. M., and Feshbach, H., _Methods of Theoretical Physics_, McGraw-Hill Book Company, p. 1459.

46.   Lin, T. C. and G. W. Morgan, "A Study of Axisymmetric Vibrations and Cylindrical Sheels as Affected by Rotatory Inertia and Transverse Shear," _Transactions ASME_, Vol. 78, 1956, pp. 255-261.

References for Chapter III

47.   Gouse, S. W., Jr., "An Introduction to Two-Phase Gas-Liquid Flow," AD-No. 603659, June, 1964.

48.   Kepple, R. R. and T. V. Tung, "Two-Phase (Gas-Liquid) System: Heat Transfer and Hydraulics; An Annotated Bibliography," ANL-6734, July, 1963.

Chapter III

49.   Gouse, S. W. Jr., "An Index to the Two-Phase Gas-Liquid
        Flow Literature - Part I," AD-No. 411512, May, 1963.

50.   Maurer, G. W., "Bibliography on Two-Phase Heat Transfer,"
        WAPD-TM-249, 1960.

51.   Maung-Myint, M., "A Literature Survey of Two-Phase Flow
        of Gas and Liquid," S. B. Thesis, M.I.T., 1959.

52.   Gouse, S. W., Jr. and G. A. Brown, "A Survey of the Velocity
        of Sound in Two-Phase Mixtures," ASME Paper No. 64-WA/FE-
        35, December, 1964.

53.   Martinelli, R. C. and D. B. Nelson, "Prediction of Pressure
        Drop During Forced-Circulation Boiling of Water," Trans.
        ASME, Vol. 70, 1948, pp. 695-702.

54.   Gouse, S. W., Jr., "Two-Phase Gas-Liquid Flow Oscillations:
        Preliminary Survey," AD-No. 603652, July, 1964.

References for Chapter IV

55.   Strasberg, M., "Undissolved Air Cavities as Nuclei,"
        Cavitation in Hydrodynamics (Proc. Nat. Phys. Lab.
        Symposium), Paper 6, Her Majesty's Stationery Office,
        London, 1956.

56.   Holl, J. W., "An Effect of Air Content on the Occurrence
        of Cavitation," Trans. ASME, Series D, Journal of Basic
        Engineering, Vol. 82, pp. 941-946., 1960.

57.   Lehman, A. F. and J. O. Young, "Experimental Investigations
        of Incipient and Desinent Cavitation," Trans. ASME, Series
        D, Journal of Basic Engineering, Vol. 86, 1964, pp. 275-
        284.

58.   Kermeen, R. W., "Some Observations of Cavitation on Hemi-
        spherical Head Models," Report E-35.1, Hydrodynamics
        Laboratory, California Institute of Technology.

59.   Eisenberg, P., "On the Mechanism and Prevention of Cavitation,"
        The David W. Taylor Model Basin Report 712, July, 1950.

60.   Harvey, E. N., Wm. D. McElroy, and A. H. Whiteley, "On
        Cavity Formation in Water," Journal of Applied Physics,
        Vol. 18, February, 1947, pp. 162-172.

Chapter IV

61. Johnson, V. E., Jr., "Mechanics of Cavitation," *Journal of the Hydraulics Division*, ASCE, Vol. 89, No. HY 3, Proc. Paper 3530, May, 1963, pp. 251-275.

62. Noltingk, B. E., and E. A. Neppiras, "Cavitation Produced by Ultrasonics," *Proceedings Physical Soc. (B).*, London, Vol. 63, 1950, pp. 674-685.

63. Neppiras, E. A. and B. E. Noltingk, "Cavitation Produced by Ultrasonics: Theoretical Conditions for the Onset of Cavitation," *Proceedings Physical Society (B).*, London, Vol. 64, 1951, pp. 1032-1038.

64. Schweitzer, P. H. and V. G. Szebehely, "Gas Evolution in Liquids and Cavitation," *Journal of Applied Physics*, Vol. 21, December, 1950, pp. 1218-1224.

65. Knapp, R. T., "Cavitation and Nuclei," *Transactions of the ASME*, Vol. 80, 1958, pp. 1315-1324.

66. Kermeen, R. W., J. T. McGraw, and B. R. Parkin, "Mechanism of Cavitation Inception and the Related Scale-Effects Problem," *Trans. ASME*, Vol. 77, 1955, pp. 533-541.

67. Robertson, J. M., "Cavitation in Hydraulic Structures: Scale Effects Involved in Cavitation Experiments," *Journal of the Hydraulics Division*, ASCE, Vol. 89, No. HY 3, Proc. Paper 3520, May, 1963, pp. 167-180.

68. Holl, J. W. and G. F. Wislicenus, "Scale Effects on Cavitation," Trans. ASME, Series D, *Journal of Basic Engineering*, Vol. 83, 1961, pp. 385-398.

69. Schlichting, H., *Boundary Layer Theory*, McGraw-Hill Book Company, Inc., 1960.

70. Knapp, R. T. and A. Hollander, "Laboratory Investigations of the Mechanism of Cavitation," *Trans. ASME*, Vol. 70, 1948, pp. 419-435.

71. Daily, J. W. and V. E. Johnson, Jr., "Turbulence and Boundary-Layer Effects on Cavitation Inception from Gas Nuclei," *Trans. ASME*, Vol. 78, 1956, pp. 1695-1706.

72. Parkin, B. R., "Scale Effects in Cavitation Flow," Ph.D. Dissertation, California Institute of Technology, 1952.

73.   Holl, J. W., "The Effect of Surface Irregularities on
        Incipient Cavitation," Ph.D. Dissertation or TM 5.3410-03,
        Ordnance Research Laboratory, The Pennsylvania State
        University, 1958.

74.   Calehuff, G. L. and Wislicenus, G. F., "ORL Investigations
        of Scale Effects on Hydrofoil Cavitation," TM 19.4212-03,
        Ordnance Research Laboratory, The Pennsylvania State
        University, February, 1956.

75.   Abbott, I. H., A. E. von Doenhoff, and L. S. Stivers, Jr.,
        "Summary of Airfoil Data," NACA Report 824, 1945.

76.   Parkin, B. R. and J. W. Holl, "Incipient-Cavitation Scaling
        Experiments for Hemispherical and 1.5 Caliber Ogive-Nosed
        Bodies," Report NOrd 7958-264, Ordnance Research Lab-
        oratory, The Pennsylvania State University, May, 1954.

77.   Oshima, R., "Theory of Scale Effects on Cavitation Inception
        on Axially Symmetric Bodies," Trans. ASME, Series D,
        Journal of Basic Engineering, Vol. 83, 1961, pp. 379-
        384.

78.   Knapp, R. T., "Cavitation Mechanics and Its Relation to
        the Design of Hydraulic Equipment," Engineering, Vol.
        173, 1952, pp. 566.

79.   Holl, J. W., "The Inception of Cavitation on Isolated
        Surface Irregularities," Trans. ASME, Series D, Journal
        of Basic Engineering, Vol. 82, 1960, pp. 169-183.

80.   McCormick, B. W. Jr., "On Cavitation Produced by a Vortex
        Trailing From a Lifting Surface," Trans. ASME, Series D,
        Journal of Basic Engineering, Vol. 84, 1962, pp. 369-
        379.

81.   Kermeen, R. W. and B. R. Parkin, "Incipient Cavitation
        and Wake Flow Behind Sharp-Edged Disks," Report 85-4,
        Hydrodynamics Laboratory, California Institute of
        Technology, August, 1957.

82.   Robertson, J. M., J. H. McGinley, and J. W. Holl, "On
        Several Laws of Cavitation Scaling," La Housille Blanche,
        September, 1957, p. 540.

83.   Numachi, F. and T. Kurokawa, "Über den Einfluss des
        Luftgehaltes auf die Kavitationsentstehung," [On the
        Effect of Air Content on the Appearance of Cavitation],
        Werft-Reederei-Hafen, Vol. 20, 1939.

Chapter IV

84.   Crump, S. F., "Determination of Critical Pressures For
        The Inception of Cavitation in Fresh and Sea Water as
        Influenced by Air Content of the Water," The David W.
        Taylor Model Basin, Report 575, October, 1949.

85.   Crump, S. F., "Critical Pressures for the Inception of
        Cavitation in a Large-Scale Numachi Nozzle as Influenced
        by the Air Content of the Water," The David W. Taylor
        Model Basin, Report 770, July, 1951.

86.   Williams, E. E. and P. McNulty, "Some Factors Affecting
        the Inception of Cavitation," Cavitation in Hydrodynamics
        (Proc. Nat. Phys. Lab. Symposium) Paper 2, Her Majesty's
        Stationery Office, London, 1956.

87.   Ruggeri, R. S. and T. F. Gelder, "Effects of Air Content
        and Water Purity on Liquid Tension at Incipient Cavitation
        in Venturi Flow," National Aeronautics and Space Admin-
        istration, TN D-1459, March, 1963.

88.   Ruggeri, R. S. and T. F. Gelder, "Cavitation and Effective
        Liquid Tension of Nitrogen in a Tunnel Venturi," National
        Aeronautics and Space Administration, TN D-2088, February,
        1964.

89.   Gelder, T. F., R. D. Moore, and R. S. Ruggeri, "Incipient
        Cavitation of Freon-114 in a Tunnel Venturi," National
        Aeronautics and Space Administration, TN-D-2722, March,
        1965.

90.   Ruggeri, R. S., R. D. Moore, and T. F. Gelder, "Incipient
        Cavitation of Ethylene Glycol in a Tunnel Venturi,"
        National Aeronautics and Space Administration, TN-D-2722,
        March, 1965.

91.   Hammitt, F. G., "Observation of Cavitation Scale and Thermo-
        dynamic Effects in Stationary and Rotating Components,"
        Trans. ASME, Series D, Journal of Basic Engineering, Vol.
        85, 1963, pp. 1-16.

92.   Jacobs, R. B. and K. B. Martin, "Cavitation Problems in
        Cryogenics," Trans. ASME, Series D, Journal of Basic
        Engineering, Vol. 82, 1960, pp. 756-757.

93.   Numachi, F., M. Yamabe, and R. Ōba, "Cavitation Effect on
        the Discharge Coefficient of the Sharp-Edged Orifice
        Plate," Trans. ASME, Series D, Journal of Basic Engineering,
        Vol. 82, 1960, pp. 1-11.

Chapter IV

94.   Ball, J. W. and W. P. Simmons, "Progress Report on Hydraulic Characteristics of Pipeline Orifices and Sudden Enlargements Used for Energy Dissipation," Bureau of Reclamation, Hydraulics Branch, Report No. Hyd.-519, December, 1963.

95.   Mikol, E. P. and J. C. Dudley, "A Visual and Photographic Study of the Inception of Vaporization in Adiabatic Flow," Trans. ASME, Series D, _Journal of Basic Engineering_, Vol. 86, 1964, pp. 257-264.

96.   Fauske, H. K. and T. C. Min, "A Study of the Flow of Saturated Freon - 11 Through Apertures and Short Tubes," ANL-6667, January, 1963.

97.   Eisenberg, P., "A Brief Survey of Progress on the Mechanics of Cavitation," The David W. Taylor Model Basin Report 842, June, 1953.

References for Chapter V

98.   Rayleigh, Lord, "On the Pressure Developed in a Liquid During Collapse of a Cavity," _Philosophical Magazine_, Vol. 34, 1917, pp. 94-98.

99.   Zwick, S. A., "The Growth and Collapse of Vapor Bubbles," AD-54059, December, 1954.

100.   Plesset, M. S. and S. A. Zwick, "A Nonsteady Head Diffusion Problem with Spherical Symmetry," _Journal of Applied Physics_, Vol. 23, 1952, p. 95.

101.   Plesset, M. S. and S. A. Zwick, "On the Dynamical of Small Vapor Bubbles in Liquids," _Journal of Mathematics and Physics_, Vol. 33, 1955, p. 308.

102.   Plesset, M. S. and S. A. Zwick, "The Growth of Vapor Bubbles in Superheated Liquids," _Journal of Applied Physics_, Vol. 25, 1954, p. 493.

103.   Plesset, M. S., "Bubble Dynamics," AD-298566, February, 1963.

104.   Forster, H. K., "Diffusion in a Moving Medium with Time-Dependent Boundaries," _A.I.Ch.E. Journal_, Vol. 4, 1957, p. 535.

105.   Forster, H. K. and Zuber, N., "Growth of a Vapor Bubble in a Superheated Liquid," _Journal of Applied Physics_, Vol. 25, 1954, p. 474.

Chapter V

106.   Zuber, N., "The Dynamics of Vapor Bubbles in Nonuniform
          Temperature Fields," International Journal of Heat and
          Mass Transfer, Vol. 2, 1961, p. 83.

107.   Birkhoff, G., R. S. Margulies, and W. A. Horning, "Spherical
          Bubble Growth," The Physics of Fluids, Vol. 1, 1958, p.
          201.

108.   Bankoff, S. G. and R. D. Mikesell, "Bubble Growth Rates
          in Highly Sbucooled Nucleate Boiling," Chemical Engineering
          Progress Symposium Series, No. 29, Vol. 55, 1959, p.95.

109.   Scriven, L. E., "On the Dynamics of Phase Growth," Chemical
          Engineering Science, Vol. 10, 1959, p. 1.

110.   Yang, W. and J. A. Clark, "On the application of the Source
          Theory to the Solution of Problems Involving Phase Change.
          Part I - Growth and Collapse of Bubbles," Trans. ASME,
          Journal of Heat Transfer, 1964, p. 207.

111.   "Summary of Conference on Bubble Dynamics and Boiling Heat
          Transfer Held at the Jet Propulstion Laboratory June 14
          and 15, 1965," AD-118586.

112.   Dergarabedian, P., "Observations on Bubble Growth in
          Various Superheated Liquids," J. Fluid Mechanics, Vol.
          9, Pt. 1, 1960, p. 39.

113.   Dergarabedian, P., "The Rate of Growth of Vapor Bubbles
          in Superheated Water," Journal of Applied Mechanics,
          1953, p. 537.

114.   Parmentier, D., Jr., and A. J. Schwemin, "Liquid Hydro-
          gen Bubble Chambers," The Review of Scientific Instru-
          ments, Vol. 26, 1955, p. 954.

115.   Ellion, M. E., "A study of the Mechanism of Boiling Heat
          Transfer," Jet Propulsion Lab. Report Memo. 20-88, Calif.
          Inst. Tech., 1954.

116.   Florschuetz, L. W. and B. T. Chao, "On the Mechanics of
          Vapor Bubble Collapse," Trans. ASME, Paper Number 64-
          HT-23.

117.   McNieto, J., "An Exact Solution of the Rayleigh-Besant
          Equation," Internal Report No. 18, Office of Research
          Administration, Dept. of Nuckar Engineering, University
          of Michigan, 1962.

118. Levenspiel, O., "Collapse of Steam Bubbles in Water," _Industrial and Engineering Chemistry_, Vol. 51, 1959, p. 787.

119. Fritz, C. G., "Study of Gas Bubble Dynamics (Part I)," George C. Marshall Space Flight Center Internal Note - P & VE-P-64-5, 1964.

120. Forster, K. E., "Growth of a Vapor-Filled Cavity Near a Heating Surface and Some Related Questions," _The Physics of Fluids_, Vol. 4, 1961, p. 448.

121. Griffith, P., "Bubble Growth Rates in Boiling," ASME, Vol. 85, April, 1958, p. 721.

122. Savic, P., and Gosnell, J. W., "The Dynamics of the Expanding Vapor Bubble in a Boiling Liquid," _The Canadian J. of Chem. Engr._, Dec., 1962, p. 238.

123. Dougherty, D. E., and H. H. Rubin, "The Growth and Collapse of Vapor Bubbles on a Heating Surgace," _Heat Transfer and Fluid Mechanics Institute_, Univ. of Washington, Seattle, Washington, 1962.

124. Gunther, F. C., "Photographic Study of Surface Boiling Heat Transfer to Water with Forced Convection," _Trans. ASME_, 1951, p. 115.

125. Fareuff, C. E., E. A. McLean, and V. E. Scheffer, "Some Aspects of Surface Boiling," _J. Appl. Phy._, Vol. 29, 1958, p. 80.

126. Semeria, R. L., "An Experimental Study of the Characteristics of Vapor Bubbles," _Proc. Instr. Mech. Engrs._, Symp. Two-Phase Flow, 1962, p. 57.

127. Sharp, R. R., "The Nature of Liquid Film Evaporation During Nucleate Boiling," NASA TN D-1997.

128. Graham, R. W., "Experimental Observations of Transient Boiling of Subcooled Water and Alcohol on a Horizontal Surface," NASA TN D-2507.

129. Hsu, Y., "Gradual Transition of Nucleate Boiling from Discrete-Bubble Regime to Multibubble Regime," NASA TN D-2564.

130. Engelberg-Forster, K. and R. Greif, "Heat Transfer to a Boiling Liquid-Mechanism and Correlation," _Trans. ASME, Journal of Heat Transfer_, 1959, p. 43.

Chapter V

131.   Costello, C. P. and W. E. Tuthill, "Effects of Acceleration on Nucleate Pool Boiling," Chemical Engineering Progress Symposium Series, No. 32, Vol. 57, p. 189.

132.   Forster, H. K. and N. Zuber, "Dynamics of Vapor Bubbles and Boiling Heat Transfer," A.I. Ch.E. Journal, Vol. I 1955, p. 531.

133.   Zuber, N. and E. Fried, "Two-Phase Flow and Boiling Heat Transfer to Cryogenic Liquids," American Rockets Society Journal, September, 1962, p. 1332.

134.   Staniszewski, B. M., "Nucleate Boiling Bubble Growth and Departure," AD-227262, August, 1959.

References for Chapter VII

135.   Landau, L. D. and E. M. Lifshitz, Fluid Mechanics, Pergamon Press, Oxford, 1959, p. 52.

References for Chapter VIII

136.   Strobridge, T. R., "The Thermodynamic Properties of Nitrogen From 114 to 540° R Between 1.0 and 3000 psia," Supplement A., U. S. Department of Commerce, NBS Technical Note 129 A.

137.   Scott, R. B., Cryogenic Engineering, D. Van Nostrand Company, Inc., 1959.

138.   Eckert, E. R. G. and R. M. Drake, Heat and Mass Transfer, McGraw-Hill Book Company, Inc., 1959.

139.   Temperature: Its Measurement and Control in Science and Industry, Vol. I, Amer. Insti. of Physics, N. B. S. National Reserach Council.

140.   Temperature: Its Measurement and Control in Science and Industry, Vol. III, Amer. Insti. of Physics, N. B. S. National Research Council, pp. 65-77.

141.   Powell, R. L., M. D. Bunch, and R. J. Corruccini, "Low Temperature Thermocouples - 1. Gold-Cobalt or Constantan Versus Copper or 'Normal' Silver," Cryogenics, March, 1961, pp. 139-150.

ADDITIONAL REFERENCES

Chapter II

142.   Abbott, M. R., "Axially Symmetric Steady Motion of a
         Viscous Incompressible Fluid: Some Numerical Experi-
         ments," February, 1963. (AD 407-510)

143.   Abbott, M. R., "Solution of Non-Linear Wave Equation,"
         May, 1962. (AD 283-590)

144.   Aerospace Information Division Library of Congress,
         "Use of Variational Methods in Problems of Vibration
         of Liquid and Liquid-filled Bodies," December, 1962.
         (AID Report 62-203) (AD 292-340)

145.   Babenko, G. S., and A. M. Smirnov, "Effect of the Viscosity
         of Liquids in Hydraulic Piping on its Dynamic Properties,"
         Automation and Remote Control, Vol. 24, Part 1, January,
         1963, pp. 106-109.

146.   Barn, M. L., A. T. Matthews, and H. H. Bleich, "Forced
         Vibrations of an Elastic Circular Cylindrical Body of
         Finite Length Submerged in an Acoustic Fluid," June,
         1962. (AD 286-905)

147.   Beatty, R. E., Jr., "Boundary Layer Attenuation of Higher
         Order Modes in Rectangular and Circular Tubes," Journal
         of the Acoustical Society of America, Vol. 22, November,
         1950, pp. 850-854.

148.   Bennett, M. D., "Pressure Response in a Long Tube Which
         is Closed at One End," Aero-Thermodynamics, SC-4646(RR),
         November, 1951, pp. 1 and 3-22.

149.   Biot, M. A., "Propagation of Elastic Waves in a Cylindrical
         Bore Containing a Fluid," Journal of Applied Physics,
         Vol. 23, September, 1952, pp. 997-1005.

150.   Blackstock, David T., "Approximate Equations Governing Finite-
         Amplitude Sound in Thermoviscous Fluids," May, 1963,
         General Dynamics Corporation. (AD 415-442)

151. Blackstock, D. T., "Propagation of Plane Sound Waves of Finite Amplitude in Nondissipative Fluids," _Journal of the Acoustical Society of America_, Vol. 34, January, 1962, pp. 9-30.

152. Blokhintzev, D., "The Propagation of Sound in an Inhomogeneous and Moving Medium I," _Journal of the Acoustical Society of America_, Vol. 18, October, 1946, pp. 322-328.

153. Bochner, S., "Almost Periodic Solutions of the Inhomogeneous Wave Equation," _Proc. National Academy Science_, Vol. 46, Part 2, 1960, pp. 1233-1236.

154. Browder, J. E., "On Non-Linear Wave Equations," _Mathematics Zeitschr_, Vol. 80, 1962, pp. 249-264.

155. Brown, F. T., S. E. Nelson, "Step Responses of Liquid Lines With Frequency-Dependent Effects of Viscosity," _Trans. ASME_, Paper No. 64-WA/FE-6, pp. 1-7.

156. Chang, S. S. L., "Transient Effects of Supply and Connecting Conduits in Hydraulic Control Systems," _Franklin Institute Journal_, Vol. 262, 1956, pp. 437-452.

157. Cohen, Hirsh and Yih-O-Tu, "Viscosity and Boundary Effects in the Dynamic Behavior of Hydraulic Systems," _Trans. ASME_, Series D, Vol. 84, 1962, pp. 593-601.

158. Contractor, D. N., "The Reflection of Waterhammer Pressure Waves from Minor Losses," _Trans. ASME_, Paper No. 64-WA/FE-16, pp. 1-7.

159. Eckart, C., "Vortices and Streams Caused by Sound Waves," _Physical Review_, Vol. 73, 1948, pp. 68-76.

160. Elrod, H. G., Jr., "The Theory of Pulsating Flow in Conical Nozzles," _Trans. ASME_, Vol. 85, Part E, March, 1963, pp. 1-6.

161. Ezekiel, F. D., "The Effect of Conduit Dynamics of Control-Valve Stability," _Trans. ASME_, Vol. 80, 1958, pp. 904-908.

162. Fay, R. D., "Waves in Liquid-Filled Cylinders," _Journal of the Acoustical Society of America_, Vol. 24, No. 5, September, 1952, pp. 459-462.

163.   Grace, S. F., "Oscillatory Motion of a Viscous Liquid in a
        Long Straight Tube," _Philosophical Magazine_, Vol. V.,
        Ser. 17, 1928, pp. 933-939.

164.   Hunt, F. V., "Notes on the Exact Equations Governing the
        Propagation of Sound in Fluids," _Journal of the Acoustical
        Society of America_, Vol. 27, No. 6, November, 1955, pp.
        1019-1039.

165.   Khokhlov, R. V., and S. I. Soluyan, "Propagation of Acoustic
        Waves of Moderate Amplitude Through Dissipative and Relaxing
        Media," _Acustica_, Vol. 14, 1964, No. 5, pp. 241-247.

166.   Kittredge, C. P., "Hydraulic Transients in Centrifugal Pump
        Systems," _Trans. ASME_, August, 1956, pp. 1307-1322.

167.   Knapp, R. T., "Complete Characteristics of Centrifugal Pumps
        and Their Use in the Prediction of Transient Behavior,"
        Trans. ASME, Vol. 59, 1937, pp. 683-689.

168.   Lambert, J. W., "On the Nonlinearities of Fluid Flow in
        Nonrigid Tubes," _Journal of The Franklin Institute_, Vol.
        266, August, 1958, pp. 83-103.

169.   Long, R. H., Jr., "Experimental and Theoretical Study of
        Transverse Vibration of a Tube Containing Flowing Fluid,"
        Trans. ASME, Vol. 77, 1955, pp. 65-68.

170.   Mintzer, D. and B. S. Tanenbaum, "Spatial and Temporal
        Absorption in a Viscous Medium," _Journal of the Acoustical
        Society of America_, Vol. 32, 1960, pp. 67-71.

171.   Moise, J. C., "Pneumatic Transmission Lines," _ISA Trans._,
        Vol. 1, April, 1954, pp. 35-40.

172.   Morgan, G. W. and W. R. Ferrante, "Wave Propagation in
        Elastic Tubes Filled With Streaming Liquid," _Journal of
        Acoustical Society of America_, Vol. 27, July, 1955,
        pp. 715-725.

173.   Morgan, G. W. and J. P. Kiely, "Wave Propagation in Viscous
        Liquid Contained in a Flexible Tube," _Journal of the
        Acoustical Society of America_, Vol. 26, May, 1954, pp.
        323-328.

174.   Oppenheim, A. K. and E. G. Chilton, "Pulsating-Flow
        Measurement - A Literature Survey," _Trans. ASME_, Vol.
        77, February, 1955, pp. 231-248.

Chapter II

175.   Paynter, H. M. and F. D. Ezekiel, "Water Hammer in Nonuniform
        Pipes as an Example of Wave Propagation in Gradually Varying
        Media," Trans. ASME, Vol. 80, 1958, pp. 1585-1595.

176.   Rich, G. R., "Water-Hammer Analysis by the Laplace-Mellin
        Transformation," Trans. ASME, Vol. 67, 1945, pp. 361-376.

177.   Richardson, E. G., and E. Tyler, "The Transverse Velocity
        Gradient Near the Mouths of Pipes in Which an Alternating
        or Continuous Flow of Air is Established," The Proceedings
        of the Physical Society, Vol. 42, No. 231, December, 1929,
        pp. 1-15.

178.   Rohmann, C. P. and E. C. Grogan, "On the Dynamics of Pneu-
        matic Transmission Lines," Trans. ASME, Vol. 79, 1957,
        pp. 853-874.

179.   Rouleau, W. T. and F. J. Young, "Distortion of Short Pulses
        in Tapered Tube Pulse Transformers. Part I - Inviscid
        Liquid," Trans. ASME, 64-WA/FE-11, pp. 1-6.

180.   Rouleau, W. T. and F. J. Young, "Distortion of Short Pulses
        in Tapered Tube Pulse Transformers. Part II - Inviscid
        Liquid," Trans. ASME, Paper No. 64-WA/FE-12, pp. 1-6.

181.   Sabersky, Rolf H., "Effect of Wave Propagation in Feed
        Lines on Low-Frequency Rocket Instability," Jet Propulsion,
        Vol. 24, 1954, pp. 172-174.

182.   Schiesser, Boonshaft and Fuchs, Inc., "The Frequency Response
        of an Actuator Supplied by Two Long Hydraulic Lines,"
        Trans. AIChE, 1964 Joint Automatic Control Conference,
        Stanford University.

183.   Schuder, C. B. and G. C. Blunck, "The Driving Point Impedance
        of Fluid Process Lines," ISA Transactions, January, 1963,
        Vol. 2, Part 1, pp. 39-45.

184.   Sexl, Theodor, "Uber den von E. G. Richardson's entdeckten
        'Annulareffekt'," Z. Phys., Vol. 61, 1930, pp. 349-362.

185.   Sibley, W. A. and W. G. Oakes, "Dynamic Characteristics
        of a Liquid Filled Tube," American Rocket Society Pub-
        lication, November, 1956, pp. 5953-5987.

186.   Skalak, R., "An Extension of the Theory of Water Hammer,"
        Trans. ASME, Vol. 78, 1956, pp. 105-116.

Chapter II

187.   Thomson, W. T., "Transmission of Pressure Waves in Liquid
         Filled Tubes," _Proceedings of First U.S. Congress of
         Applied Mechanics_, pp. 927-933.

188.   Thurston, G. B., "Periodic Fluid Flow Through Circular
         Tubes," _Journal of the Acoustical Society of America_,
         Vol. 24, November, 1952, pp. 653-656.

189.   Uchida, S., "The Pulsating Viscous Flow Superposed on the
         Steady Laminar Motion of Incompressible Fluid in a
         Circular Pipe," _ZAMP_, Vol. VII, 1956, pp. 403-422.

Chapter IV - Cavitation

190.   Ball, J. W., "Cavitation Characteristics of Gate Valves
         and Globe Valves Used as Flow Regulators Under Heads
         Up to About 125 Feet," _Trans. ASME_, Vol. 79, 1957,
         pp. 1275-1283.

191.   Ball, J. W., "Hydraulic Characteristics of Gate Slots,"
         ASCE, _Journal of the Hydraulics Division_, Vol. 85,
         No. HY10, 1959, pp. 81-114.

192.   Briggs, J. L., "The Maximum Superheating of Water as
         a Measure of Negative Pressure," _Journal of Applied
         Physics_, Vol. 26, 1955, pp. 1001-1003.

193.   Briggs, J. L., "Limiting Negative Pressure of Water,"
         Journal of Applied Physics, Vol. 21, 1950, pp. 721-722.

194.   Brown, F. R., "Cavitation in Hydraulic Structures: Problems
         Created by Cavitation Phenomena," _Journal of the Hydraulics
         Division_, ASCE, Vol. 89, January, 1963, pp. 99-115.

195.   "Cavitation in Hydrodynamics," Proc. Symposium Natl. Phys.
         Lab., London, 1956.

196.   "Cavitation in Hydraulic Structures: A Symposium," _Proc.
         Amer. Soc. Civ. Engrs._, Vol. 71, September, 1945, pp.
         999-1068.

197.   "Cavitation in Hydrodynamics," Proceedings, Symposium
         of the National Physical Laboratory, London, September
         14-17, 1955.

Chapter IV - Cavitation

198.   Daily, J. W., "Cavitation Characteristics and Infinite-Aspect - Ratio Characteristics of a Hydrofoil Section," Trans. ASME, Vol. 71, 1949, pp. 269-284.

199.   Dean, R. B., "The Formation of Bubbles," Journal of Applied Physics, Vol. 15, 1944, pp. 446-451.

200.   Eisenberg, P., "Modern Developments in the Mechanics of Cavitation," Applied Mechanics Reviews, Vol. 10, 1957, pp. 85-89.

201.   Eisenberg, P., "Cavitation," International Science and Technology, February, 1963, pp. 72-84.

202.   Eisenberg, P. and M. P. Tulin, "Cavitation," Handbook of Fluid Dynamics, McGraw-Hill Book Company, Inc., 1961.

203.   Fisher, J. C., "The Fracture of Liquids," Journal of Applied Physics, Vol. 19, 1948, pp. 1062-1067.

204.   Fox, F. E. and K. F. Herzfeld, "Gas Bubbles with Organic Skin as Cavitation Nuclei," Journal of the Acoustical Society of American, Vol. 26, 1954, pp. 984-989.

205.   Harvey, E. N., K. W. Cooper, and A. H. Whiteley, "Bubble Formation from Contact of Surfaces," Journal of the American Chemical Society, Vol. 68, Part 2, 1946, pp. 2119-2120.

206.   Harvey, E. N., D. K. Barnes, W. D. McElroy, A. H. Whiteley, D. C. Pease, and K. W. Cooper, "Bubble Formation in Animals," Journal of Cellular and Comparative Physiology, Vol. 24, 1944, pp. 23-44.

207.   Harvey, E. N., D. K. Barnes, W. D. McElroy, A. H. Whiteley, and D. C. Pease, "Removal of Gas Nuclei From Liquids and Surfaces," Journal of the American Chemical Society, Vol. 67, 1945, pp. 156-157.

208.   Hunsaker, J. C., "Cavitation Research," Mechanical Engineering, Vol. 57, 1935, pp. 211-216.

209.   Jakobsen, J. K., "On the Mechanism of Head Breakdown in Cavitating Inducers," Trans. ASME, Series D, Journal of Basic Engineering, Vol. 86, 1964, pp. 291-305.

210.   Jarman, P. D. and K. J. Taylor, "Light Emission from
        Cavitating Water," Brit. Journal of Applied Phys.,
        Vol. 15, 1964, pp. 321-322.

211.   Numachi, F., R. Kobayashi, and S. Kamiyama, "Effect of
        Cavitation on the Accuracy of Herschel - Type Venturi
        Tubes," Trans. ASME, Series D, Journal of Basic Engineering,
        Vol. 84, 1962, pp. 351-362.

212.   Pease, D. C. and L. R. Blinks, "Cavitation From Solid
        Surfaces in the Absence of Gas Nuclei," Journal of Phys.
        Colloid Chem., Vol. 51, 1947, pp. 556-567.

213.   Robertson, J. M., "Water Tunnels for Hydraulic Investigations,"
        Trans. ASME, Vol. 78, 1956, pp. 95-104.

214.   Rouse, H., "Cavitation in the Mixing Zone of a Submerged
        Jet," La-Houille Blanche, 1953, pp. 9-19.

215.   Rouse, H. and J. S. McNown, "Cavitation and Pressure Dis-
        tribution: Head Forms at Zero Angle of Yaw," State Uni-
        versity Iowa Studies in Engr. Bull 32, 1948.

216.   Rouse, H., "Cavitation and Pressure Distribution: Head
        Forms at Angles of Yaw," State University Iowa Studies
        in Engr. Bull. 42, 1962.

217.   Sarosdy, L. R. and A. J. Acosta, "Note on Observations
        of Cavitation in Different Fluids," Trans. ASME, Series
        D, Journal of Basic Engineering, Vol. 83, 1961, pp.
        399-400.

218.   Stahl, H. A. and A. J. Stepanoff, "Thermodynamic Aspects
        of Cavitation in Centrifugal Pumps," Trans. ASME, Vol.
        78, 1956, pp. 1691-1693.

219.   Stepanoff, A. J., "Cavitation Properties of Liquids,"
        Trans. ASME, Series A, Journal of Engineering for Power,
        Vol. 86, 1964, pp. 195-200.

220.   Stiles, G. F., "Cavitation in Control Valves," Instruments
        and Control Systems, Vol. 34, 1961, pp. 2086-2093.

221.   Strasberg, N., "The Influence of Air-Filled Nuclei on
        Cavitation Inception," David W. Taylor Model Basin
        Report 1078, May, 1957.

Chapter IV - Cavitation

222.   Temperley, H. V. N. and L. L. G. Chambers, "The Behavior of
Water Under Hydrostatic Tension," Proc. Physical Society,
(London), Vol. 58, 1946, pp. 420-443.

223.   Thomas, H. A. and E. P. Schuleen, "Cavitation in Outlet
Conduits of High Dams," Trans. of the ASCE, Vol. 107,
1942, pp. 421-493.

224.   Wang, P. K. C. and J. T. S. Ma, "Cavitation in Valve-
Controlled Hydraulic Actuators," Trans. ASME, Series E
Journal of Applied Mechanics, Vol. 85, 1963, pp. 537-
546.

225.   Ziegler, G., "Tensile Stresses in Flowing Water," Cavitation
in Hydrodynamics, (Proc. Nat. Phys. Lab. Symposium), Paper
3, Her Majesty's Stationery Office, London, 1956.

Chapter IV - Ultrasonic Cavitation

226.   Akulichev, V. A. and V. I. Il'ichev, "Spectral Indication
of the Origin of Ultrasonic Cavitation in Water," Soviet
Physics - Acoustics, Vol. 9, 1963, pp. 128-130 (English
Translation).

227.   Bondy, C. and K. Söllner, "On the Mechanism of Emulsification
by Ultrasonic Waves," Trans. Faraday Society, Vol. 31, Part
I, 1935, pp. 835-846.

228.   Brown, B., "Ultrasonic Cavitation in Water," British
Communications and Electronics, Vol. 9, Part 2, 1962,
pp. 918-920.

229.   Connolly, W. and F. E. Fox, "Ultrasonic Cavitation
Thresholds in Water," Journal of the Acoustical Society
of America, Vol. 26, 1954, pp. 843-848.

230.   Gabrielli, I. and G. Iernetti, "Cavitation and Chemical
Effects in Ultrasonic Stationary Fields," Acustica,
Vol. 13, 1963, pp. 165-174.

231.   Gaertner, W., "Frequency Dependence of Ultrasonic
Cavitation," Journal of the Acoustical Society of
America, Vol. 26, 1954, pp. 977-980.

232.   Gallant, H., "Untersuchungen über Kavitationsblasen,"
        Österreichische Ingenieur Zeitschrift, Vol. 5, 1962,
        pp. 74-83.

233.   Galloway, W. J., "An Experimental Study of Acoustically
        Induced Cavitation in Liquids," Journal of the Acoustical
        Society of America, Vol. 26, 1954, pp. 849-857.

234.   Goldsmith, H. A. and R. C. Heim, "New Way to Measure
        Ultrasonic Cavitation Intensity," Metal Engineering
        Quarterly, Vol. 2, No. 1, 1962, pp. 62-66.

235.   Kozyrev, S. P., "Ultrasonic Apparatus for Testing Materials
        for Cavitation - Abrasive Wear," Industrial Laboratory,
        Vol. 29, No. 2, 1963, pp. 216-218.

236.   Mellen, R. H., "Ultrasonic Spectrum of Cavitation Noise
        in Water," Journal of the Acoustical Society of America,
        Vol. 26, 1954, pp. 356-360.

237.   Messino, D., D. Sette, and F. Wanderlingh, "Statistical
        Approach to Ultrasonic Cavitation," Journal of the
        Acoustical Society of America, Vol. 35, 1963, pp.
        1575-1583.

238.   Neppiras, E. A. and B. E. Noltingk, "Cavitation Produced
        by Ultrasonics: Theoretical Conditions for the Onset of
        Cavitation," Proc., Phys. Soc. (B), Vol. 64, 1951,
        pp. 1032-1038.

239.   Numachi, F., "Transitional Phenomena in Ultrasonic Shock
        Waves Emitted by Cavitation on Hydrofoils," Trans. ASME,
        Series D, Journal of Basic Engineering, Vol. 81, 1959,
        pp. 153-166.

240.   Sette, D. and F. Wanderlingh, "Nucleation by Cosmic Rays
        in Ultrasonic Cavitation," Physical Review, Vol. 125
        No. 2, 1962, pp. 409-417.

241.   Weissler, A., "A Chemical Method for Measuring Relative
        Amounts of Cavitation in an Ultrasonic Cleaner," IRE
        International Convention Record, Vol. 10, Part 6, 1962,
        pp. 24-30.

242.   Willard, G. W., "Ultrasonically Induced Cavitation in Water:
        A Step-by-Step Process," Journal of the Acoustical Society
        of America, Vol. 25, 1953, pp. 669-686.

## Chapter IV - Ultrasonic Cavitation

243.   Wilson, R. W., "Influence of Physical Properties of
        Liquids on Severity of Cavitation Damage," Compressed
        Air and Hydraulics, Vol. 27, No. 319, 1962, pp. 382-
        385.

B. Summary of Vector Notation

Given below is a list defining some of the vector notation used in

Chapter II; also given are some of the vector identities. See also

reference 4.

1. i, j and K are the unit vectors in the x, y, and z

directions respectively in a rectangular coordinate system (see Fig.

B.1.).
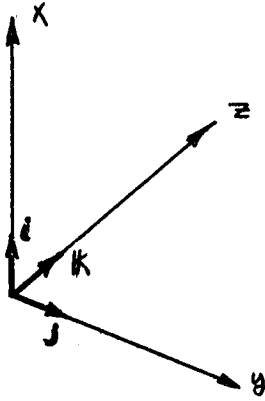
r, Θ and K are the unit vectors in the r, θ and z directions

respectively in a cylindrical coordinate system (see Fig. 1.1).

2. ∇ denotes the vector operator del and is given by

$$\nabla = i \frac{\partial}{\partial x} + j \frac{\partial}{\partial y} + K \frac{\partial}{\partial z} \tag{B.1}$$

in rectangular coordinates.

3. $\nabla \varphi$ denotes the gradient of the scalar φ and is given by

$$\nabla \varphi = i \frac{\partial \varphi}{\partial x} + j \frac{\partial \varphi}{\partial y} + K \frac{\partial \varphi}{\partial z} \tag{B.2}$$

in rectangular coordinates and by

$$\nabla \varphi = \hat{r}\, \frac{\partial \varphi}{\partial r} + \hat{\Theta}\, \frac{1}{r}\, \frac{\partial \varphi}{\partial \theta} + \hat{k}\, \frac{\partial \varphi}{\partial z} \qquad (B.3)$$

in cylindrical coordinates.

4. $\nabla \cdot \mathcal{V}$ denotes the divergence of $\mathcal{V}$. In rectangular coordinates

$$\nabla \cdot \mathcal{V} = \frac{\partial \mathcal{V}_x}{\partial x} + \frac{\partial \mathcal{V}_y}{\partial y} + \frac{\partial \mathcal{V}_z}{\partial z} \qquad (B.4)$$

and in cylindrical coordinates

$$\nabla \cdot \mathcal{V} = \frac{1}{r}\, \frac{\partial}{\partial r} \left(r \mathcal{V}_r \right) + \frac{1}{r}\, \frac{\partial \mathcal{V}_\theta}{\partial \theta} + \frac{\partial \mathcal{V}_z}{\partial z}. \qquad (B.5)$$

5. $\nabla \cdot \nabla = \nabla^2$ denotes the Laplacian operator. The form of this operator depends not only on the coordinate system but also upon the variable being operated upon. In rectangular coordinates ∇^2 is always given by

$$\nabla^2 = \frac{\partial^2}{\partial x^2} + \frac{\partial^2}{\partial y^2} + \frac{\partial^2}{\partial z^2}. \qquad (B.6)$$

In cylindrical coordinates we have, if φ is a scalar quantity,

$$\nabla^2 \varphi = \frac{1}{r}\, \frac{\partial}{\partial r} \left(r\, \frac{\partial \varphi}{\partial r} \right) + \frac{1}{r^2}\, \frac{\partial^2 \varphi}{\partial \theta^2} + \frac{\partial^2 \varphi}{\partial z^2} \qquad (B.7)$$

or if we are operating on a vector such as $\mathcal{V}$, then

$$\nabla^2 \mathcal{V} = \hat{r}\, \left[\nabla^2 \mathcal{V} \right]_r + \hat{\Theta}\, \left[\nabla^2 \mathcal{V} \right]_\theta + \hat{k}\, \left[\nabla^2 \mathcal{V} \right]_z \qquad (B.8)$$

where

$$\left[\nabla^2 \mathcal{V} \right]_r = \frac{\partial}{\partial r} \left\{ \frac{1}{r}\, \frac{\partial}{\partial r} \left(r \mathcal{V}_r \right) \right\} + \frac{1}{r^2}\, \frac{\partial^2 \mathcal{V}_r}{\partial \theta^2} - \frac{2}{r^2}\, \frac{\partial \mathcal{V}_\theta}{\partial \theta} + \frac{\partial^2 \mathcal{V}_r}{\partial z^2} \qquad (B.9)$$

$$\left[\nabla^2 \upsilon\right]_\theta = \frac{\partial}{\partial r}\left\{\frac{1}{r}\frac{\partial}{\partial r}\left(r\upsilon_\theta\right)\right\} + \frac{1}{r^2}\frac{\partial^2 \upsilon_\theta}{\partial \theta^2} + \frac{2}{r^2}\frac{\partial \upsilon_r}{\partial \theta} + \frac{\partial^2 \upsilon_\theta}{\partial z^2} \qquad (B.10)$$

and

$$\left[\nabla^2 \upsilon\right]_z = \frac{1}{r}\frac{\partial}{\partial r}\left(r\frac{\partial \upsilon_z}{\partial r}\right) + \frac{1}{r^2}\frac{\partial^2 \upsilon_z}{\partial \theta^2} + \frac{\partial^2 \upsilon_z}{\partial z^2}. \qquad (B.11)$$

6. $\nabla \times \vec{\upsilon}$ denotes the curl of the vector $\vec{\upsilon}$ and is defined for rectangular coordinates by

$$\nabla \times \vec{\upsilon} = \begin{vmatrix} \vec{i} & \vec{j} & \vec{k} \\ \frac{\partial}{\partial x} & \frac{\partial}{\partial y} & \frac{\partial}{\partial z} \\ \upsilon_x & \upsilon_y & \upsilon_z \end{vmatrix}. \qquad (B.12)$$

7. A list of important vector identities is given below:

a. $\nabla \times (\nabla \varphi) = 0$

b. $\nabla \cdot (\nabla \times \vec{\upsilon}) = 0$

c. $\nabla \times (\nabla \times \vec{\upsilon}) = \nabla (\nabla \cdot \vec{\upsilon}) - \nabla^2 \vec{\upsilon}$.

C. Method of Separation of Variables

Let us review the method of separation of variables to see how Eqs. (2.24) and (2.25) are obtained from (2.22) and (2.23). The equations to be solved are

$$S^2 \hat{\varphi} = \left\{ C_0^2 + \frac{4}{3} \nu_0 s \right\} \nabla^2 \varphi \tag{2.22}$$

and

$$S \hat{\psi} = \nu_0 \nabla^2 \hat{\psi}. \tag{2.23}$$

Both equations are linear partial differential equations, a class of equations to which the separation of variables method may be applied. Considering first Eq. (2.23) we assume a solution of the form

$$\hat{\psi} = \hat{\psi}_r \cdot \hat{\psi}_z \tag{C.1}$$

where $\hat{\psi}_r$ is a function of r only and $\hat{\psi}_z$ is a function of z only. Substitution of (C.1) into (2.23) gives

$$\frac{S}{\nu_0} \hat{\psi}_r \cdot \hat{\psi}_z = \frac{d^2 \hat{\psi}_r}{dr^2} \cdot \hat{\psi}_z + \frac{1}{r} \frac{d \hat{\psi}_r}{dr} \cdot \hat{\psi}_z - \frac{\hat{\psi}_r \cdot \hat{\psi}_z}{r^2} + \frac{d^2 \hat{\psi}_z}{dz^2} \cdot \hat{\psi}_r \tag{C.2}$$

Dividing both sides of (C.2) by $\hat{\psi}$ yields

$$\frac{S}{\nu_0} = \frac{1}{\hat{\psi}_r} \left\{ \frac{d^2 \hat{\psi}_r}{dr^2} + \frac{1}{r} \frac{d \hat{\psi}_r}{dr} - \frac{\hat{\psi}_r}{r^2} \right\} + \frac{1}{\hat{\psi}_z} \frac{d^2 \hat{\psi}_z}{dz^2}. \tag{C.3}$$

Eq. (C.3) may be rewritten as

$$\frac{1}{\hat{\psi}_r} \left\{ \frac{d^2 \hat{\psi}_r}{dr^2} + \frac{1}{r} \frac{d \hat{\psi}_r}{dr} - \frac{\hat{\psi}_r}{r^2} \right\} - \frac{S}{\nu_0} = -\frac{1}{\hat{\psi}_z} \frac{d^2 \hat{\psi}_z}{dz^2}. \tag{C.4}$$

Since the equality defined by Eq. (C.4) must remain true regardless of the values of r and z, thus each side of the equation must be constant or equal to $(-\alpha^2)$ where α denotes the separation constant. We may now write

$$\frac{d^2\hat{\psi_z}}{dz^2} \cdot \frac{1}{\hat{\psi_z}} = \alpha^2 \qquad\qquad (C.5)$$

and

$$\frac{1}{\hat{\psi_r}}\left\{\frac{d^2\hat{\psi_r}}{dr^2} + \frac{1}{r}\frac{d\hat{\psi_r}}{dr} - \frac{\hat{\psi_r}}{r^2}\right\} - \frac{S}{\mathcal{V}_0} = -\alpha^2 \,. \qquad\qquad (C.6)$$

A general solution of (C.5) is

$$\hat{\psi_z} = C_1 e^{\alpha z} + C_2 e^{-\alpha z} \qquad\qquad (C.7)$$

and a physically consistent solution to (C.6) is

$$\hat{\psi_r} = C_3 J_1(kr), \quad k^2 = \alpha^2 - \frac{S}{\mathcal{V}_0}. \qquad\qquad (C.8)$$

From Eqs. (C.1), (C.7) and (C.8) we have

$$\hat{\psi} = C_3 J_1(kr)\left[C_1 e^{\alpha z} + C_2 e^{-\alpha z}\right] \qquad\qquad (C.9)$$

or, keeping in mind that α has a positive and a negative value, we may write for convenience

$$\hat{\psi} = A J_1(kr) e^{\alpha z}. \qquad\qquad (C.10)$$

The solution of Eq. (2.22) will follow in the manner as above except that for this case γ^2 is of a different form so that the solution contains

the zero-order Bessel function, thus

$$\hat{\varphi} = B J_0(\beta r) e^{\alpha z}.$$

(C.11)

In Eq. (C.8), $J_1(Kr)$ represents the first-order Bessel function of the
first kind and $J_0(\beta r)$ from (C.11) is the zero-order Bessel function
of the first kind. (See Fig. 2.2).